MICROARRAY ANALYSIS OF THE EFFECTS OF LIGHT INTENSITY ON HYDROGEN PRODUCTION METABOLISM OF RHODOBACTER CAPSULATUS

A THESIS SUBMITTED TO
THE GRADUATE SCHOOL OF NATURAL AND APPLIED SCIENCES
OF
MIDDLE EAST TECHNICAL UNIVERSITY

BY
MUAZZEZ GÜRGAN ESER

IN PARTIAL FULFILLMENT OF THE REQUIREMENTS
FOR
THE DEGREE OF DOCTOR OF PHILOSOPHY
IN
BIOLOGY

JUNE 2017

Approval of the Thesis;

MICROARRAY ANALYSIS OF THE EFFECTS OF LIGHT INTENSITY ON HYDROGEN PRODUCTION METABOLISM OF RHODOBACTER CAPSULATUS

submitted by **MUAZZEZ GÜRGAN ESER** in partial fulfillment of the requirements for the degree of **Doctor of Philosophy in Biological Sciences Department, Middle East Technical University** by,

Prof. Dr. Gülbin Dural Ünver
Dean, Graduate School of **Natural and Applied Sciences** _____

Prof. Dr. Orhan Adalı
Head of Department, **Biological Sciences** _____

Prof. Dr. Meral Yücel
Supervisor, **Biological Sciences Dept., METU** _____

Assist.Prof. Dr. Harun Koku
Co-Supervisor, **Chemical Engineering Dept., METU** _____

Examining Committee Members:
Prof.Dr. İnci Eroğlu
Chemical Engineering Dept., METU _____

Prof. Dr. Meral Yücel
Biological Sciences Dept., METU _____

Prof. Dr. Ayşe Gül Gözen
Biological Sciences Dept., METU _____

Prof. Dr. Füsun Eyidoğan
Elementary Education Department, Başkent University _____

Assoc. Prof. Dr. Başar Uyar,
Chemical Engineering Dept., Kocaeli Univesity _____

Date: 22.06.2017

I hereby declare that all information in this document has been obtained and presented in accordance with academic rules and ethical conduct. I also declare that, as required by these rules and conduct, I have fully cited and referenced all material and results that are not original to this work.

Name, Last name : Muazzez Gürgan Eser

Signature :

ABSTRACT

MICROARRAY ANALYSIS OF THE EFFECTS OF LIGHT INTENSITY ON HYDROGEN PRODUCTION METABOLISM OF RHODOBACTER CAPSULATUS

Gürgan Eser, Muazzez

Ph.D., Department of Biological Sciences

Supervisor: Prof. Dr. Meral Yücel

Co-Supervisor: Assist. Prof. Dr. Harun Koku

June 2017, 130 pages

Biohydrogen generated by purple non-sulfur bacteria is a clean and renewable method of hydrogen production. It can be achieved in outdoor phototobioreactors using the natural sun light in lab to pilot scales. Light is one of the most important parameter affecting hydrogen production in the outdoor condition. Hydrogen productivity may decrease upon light intensity stress by sun light and the diurnal cycle in outdoor conditions. It is important to understand the metabolic response of these bacteria to varying light and dark periods and high light intensity. For this purpose, the transcriptome of *Rhodobacter capsulatus* was studied using microarray chips.

The experiments were carried out with the wild type *R. capsulatus* (DSM1710) and an uptake hydrogenase deficient mutant of *Rhodobacter capsulatus* (YO3) on 30/2 acetate/glutamate medium at 30°C with cyclic illumination of 12h light/12h dark periods. Hydrogen production experiments were performed under 2000 lux and 7000 lux, separately. The bacterial growth, pH, hydrogen production, bacteriochlorophyll *a*

and organic acid profiles were followed by taking samples at the end of each light and dark periods. Bacterial growth ceased and even decreased in the dark and recovered in the light. Concurrently, hydrogen production stopped in dark periods but resumed when light was available and enhanced by 7000 lux light intensity. High light intensity enhanced molar yield (25.5% and 34% for wild type and 37.6% and 51.4% for mutant bacteria under low and high light intensities, respectively). Moreover, molar productivities were significantly enhanced (0.26 and 0.61 mmol/(Lc.h) for wild type and 0.75 and 1.44 mmol/(Lc.h) for mutant bacteria under low and high light intensities, respectively). High light intensity also accelerated substrate consumption.

In order to understand the metabolic response of *R. capsulatus*, microarray analyses were completed for the conditions of shift to light after a dark period, and exposure of bacteria to a stress causing high light intensity (10,000 lux). The results revealed that a shift to light after a dark period stimulated expressions of photosynthetic apparatus, nitrogenase system and electron transport system genes. Transcription processes were intense in darkness, which triggered stress response. High light intensity further enhanced expression of nitrogenase and electron transport system genes to dissipate excess electrons for redox balance, while down-regulated the photosystem genes in order to protect the photosynthetic membrane from damage.

Keywords: Biohydrogen, *R. capsulatus*, light intensity, transcriptome analysis, microarray

ÖZ

IŞIK ŞİDDETİNİN RHODOBACTER CAPSULATUS BAKTERİSİNİN HİDROJEN ÜRETİM METABOLİZMASI ÜZERİNE ETKİLERİNİN MİKRODİZİN YÖNTEMİ İLE İNCELENMESİ

Gürgan Eser, Muazzez

Doktora, Biyolojik Bilimler Bölümü

Tez Danışmanı: Prof. Dr. Meral Yücel

Ortak Tez Danışmanı: Yrd. Doç. Dr. Harun Koku

Haziran 2017, 130 sayfa

Mor kükürtsüz bakteriler tarafından üretilen biyohidrojen temiz ve yenilenebilir bir hidrojen üretim yöntemidir ve dış ortam fotobiyoreaktörlerde doğal güneş ışığını kullanarak üretilebilir. Işık, dış ortamda hidrojen üretimini etkileyen en önemli faktörlerden biridir. Güneşten gelen ışık şiddetine ve dış ortamda gece-gündüz döngüsüne bağlı olarak hidrojen üretimi azalabilir. Bakterilerin değişken ışık-karanlık periyotlarına ve yüksek ışık şiddetine verdiği metabolik tepkileri anlamak önemlidir. Bu amaçla, *Rhodobacter capsulatus* bakterisinin transkriptomu mikrodizin çipleri kullanılarak analiz edilmiştir.

Deneyler yabanıl tip *R. capsulatus* DSM1710 ve geri-alım hidrojenaz geni eksik olan (*hup*$^-$) mutant *R. capsulatus* (YO3) suşlarıyla 30/2 asetat/glutamat ortamında 30°C'de 2000 lüks ve 7000 lüks ışık şiddetlerinde yapılmıştır. Bakteri büyümesi, pH, hidrojen üretimi, bakterioklorofil *a* ve organic asit profilleri her bir ışık ve karanlık ve

periyotlarının sonunda alınan örneklerle takip edilmiştir. Bakteri büyümesi karanlıkta durmuş hatta azalmıştır ve ışıkta tekrar artmıştır. Bununla birlikte, hidrojen üretimi karanlıkta durmuş ancak ışık mevcudiyetinde yeniden başlamış, hatta 7000 lüks ışık şiddetiyle artmıştır. Yüksek ışık şiddeti molar hidrojen eldesini artırmıştır (sırasıyla düşük ve yüksek ışık şiddetlerinde yabanıl suş için %25.5 ve %34, ve mutant suş için %37.6 ve %51.4). Bununla beraber, hidrojen üretim hızı da yüksek ışık şiddeti ile artmıştır (sırasıyla düşük ve yüksek ışık şiddetlerinde yabanıl tip için 0.26 ve 0.61 mmol/(Lc.h), ve mutant suş için 0.75 ve 1.44 mmol/(Lc.h). Yüksek ışık şiddeti ayrıca subtrat tüketim hızını da artırmıştır.

R. capsulatus bakterisinin metabolik tepkisini öğrenebilmek için karanlıktan ışığa geçişte ve strese sebep olan yüksek bir ışık şiddetinde (10,000 lüks) mikrodizin analizleri yapılmıştır. Sonuçlar, karanlıktan ışığa geçişin fotosentetik sistem, nitrojenaz sistemi ve elektron trasnport sistemi genlerinin ifadesinin arttığını göstermiştir. Karanlıkta transkripsiyon prosesi yoğundur, bu da stres tepkisini tetiklemiştir. Yüksek ışık şiddeti fazla elektronları bertaraf etmek ve redoks dengesini sağlamak için nitrojenaz ve elektron taşıma sisteminin gen ifadelerini artırken, fotosentetik membranı hasardan korumak için fotosentetik sistem genlerinin ifadesini azaltmıştır.

Anahtar kelimeler: Biyohidrojen, *R. capsulatus*, ışık şiddeti, transkriptom analizi, mikrodizin

To my niece Nihal Beyza

ACKNOWLEDGEMENTS

I would like to thank sincerely to my supervisor Prof. Dr. Meral Yücel and my co-supervisor Assist. Prof. Dr. Harun Koku for their guidance, support and suggestions throughout my studies.

I also want to thank to Prof. Dr. İnci Eroğlu and Prof. Dr. Ayşe Gül Gözen for their valuable advices for this study. I also thank to thesis examining members Prof. Dr. Füsun Eyidoğan and Assoc. Dr. Başar Uyar for their precious contributions.

I am grateful to Günce Bayram, Mehmet Gazaloğlu, Nihal Yerli and Kübra Tosun for being understanding and sharing friends about everything in life and for all the fun and laughter.

I am thankful to Melih Can Akman and Engin Koç for their friendship and their great engineering trouble shooting skills, especially for HPLC.

I specially thank to Aysuluu Usubalieva and Rezan Şahinkaya for their endless friendship. Thousands of miles never set a barrier to their support and love.

I want to thank deeply to Jenny, Juna and Tobias Lienen for their friendship and great manner they showed me and help me a lot in Germany. I also want to thank to Geo-Research Center, Potsdam, Germany for the research opportunities and hospitable and respectful environment in the lab.

I also want to thank to METU Central Lab Molecular Biology and Biotechnology R&D Center for microarray, bioanalyzer and RT-qPCR opportunities.

I want to thank my brother Niyazi Mete Gürgan for a great childhood; and him and Rabia Gürgan for their best gift ever, my niece Nihal Beyza Gürgan.

I am greatful to my husband Adem Eser for his patience and love. With him I started to believe there are still conscientious people in the world.

I want to send my thanks to my grandma who supported me very much in my education life. I miss her very much.

I am expressing my deepest love and appreciation to my mother Nihal Gürgan and my father Nurettin Gürgan for everything they offered me in my whole life. They taught the most valuable things: good manners. Without their love and support I would not be the one I am today.

I want to thank to Scientific and Technological Research Council of Turkey (TÜBİTAK-BİDEB) for financial support in the frame of National PhD Fellowship Programme 2211-C.

Finally, I want to thank to Namık Kemal University, Tekirdağ for the opportunity to become a research and teaching assistant. This was really a great contribution to my life.

This study was supported by 6th frame European Union Project "HYVOLUTION", TÜBİTAK 1001 Project 108T455 and METU BAP Project with the number of 07-02-2013-005.

TABLE OF CONTENTS

LIST OF TABLES

LIST OF FIGURES

LIST OF SYMBOLS AND ABBREVIATIONS

A	irradiated area (m^2)
Acetyl-coA	acetyl coenzyme A
ATP	adenosine triphosphate
ATPase	ATP synthase
bchl	bacteriochlorophyll
BP	Biebl and Phennig
bp	base pair
°C	degree Celcius
cDNA	complementary DNA
Cyt bc_1	cytochrome bc_1 complex
Cyt c_2	cytochrome c_2 complex
E. coli	*Escherichia coli*
ETC	Electron transport chain
g	gram
GC	gas chromatography
gdcw	gram dry cell weight
GCOS	GeneChip® Operating System
HPLC	high performance liquid chromatography
I	light intensity (Watt/m^2)

kDa	kilo Dalton
LH	Light harvesting
min	minutes
mL	milliliter
mM	millimolar
mmol	millimole
mRNA	messenger RNA
µL	microliter
nm	nanometer
OD	optical density
PCR	polymerase chain reaction
ρ_{H2}	energy density of hydrogen gas (watt.h/g)
RC	Reaction center
R. capsulatus	*Rhodobacter capsulatus*
R. sphaeroides	*Rhodobacter sphaeroides*
RNA	ribonucleic acid
rRNA	ribosomal RNA
RT-qPCR	real time quantitative polymerase chain reaction
RuBisCo	Ribulose bisphosphate carboxylase
PNSB	purple non-sulfur bacteria
t	time (hour)
TCA	tricarboxylic acid cycle

TE	Tris ethylene diamine tetra-acetic acid
tRNA	transfer RNA
V	volume (mL or L)

CHAPTER 1

INTRODUCTION

The change in the climate patterns is believed to be a consequence of global warming due to excessive consumption of fossil fuels. About $6x10^9$ tons of carbon is added to the atmosphere in the form of CO_2 by combustion of fossil fuels (IPCC, 2006). This urges scientists and politicians to find alternative energy sources and take solid steps against carbon based fuels.

Several environmentally friendly alternative energy sources involve solar, wind, wave, geothermal and nuclear sources (Androga et al., 2012). Besides these, hydrogen energy is universally accepted as one of the most promising alternatives to fossil fuels. Among all fuels, hydrogen has the highest gravimetric density and the combustion of hydrogen yields only water (Levin et al., 2004).

Hydrogen can be generated from steam reforming of the natural gas, gasification of coal and electrolysis of water. These conventional methods are not sustainable since they utilize non-renewable energy sources. One inevitable solution lies in the microbial world. Biohydrogen production using microorganisms is advantageous over conventional hydrogen production methods, as it utilizes renewable sources such as agricultural waste materials, and can be operated under mild conditions at ambient temperatures and atmospheric pressure, which makes it less energy intensive (Basak & Das, 2007).

1.1 Biohydrogen

Microorganisms generate hydrogen to either dispose of excess reducing equivalents, or to fix nitrogen through which hydrogen is produced as a byproduct (Kotay & Das, 2008).

Biological routes for generation of hydrogen are categorized into four groups (Chandrasekhar et al., 2015; Das & Veziroglu, 2001) :

1) Enzymatic and microbial electrolysis by algae and cyanobacteria
2) Anaerobic fermentation of organic compounds
3) Photobiological fermentation
4) Hybrid systems using fermentative and photosynthetic bacteria

The biological hydrogen production processes can further be classified according to light dependency: light independent (dark) fermentation and light dependent photosynthetic processes. Anaerobic fermentation is light independent, while biophotolysis and photofermentation are light dependent. These processes are carried out by different types of microorganisms. The diversity of hydrogen producing microorganisms is represented in Figure 1.1.

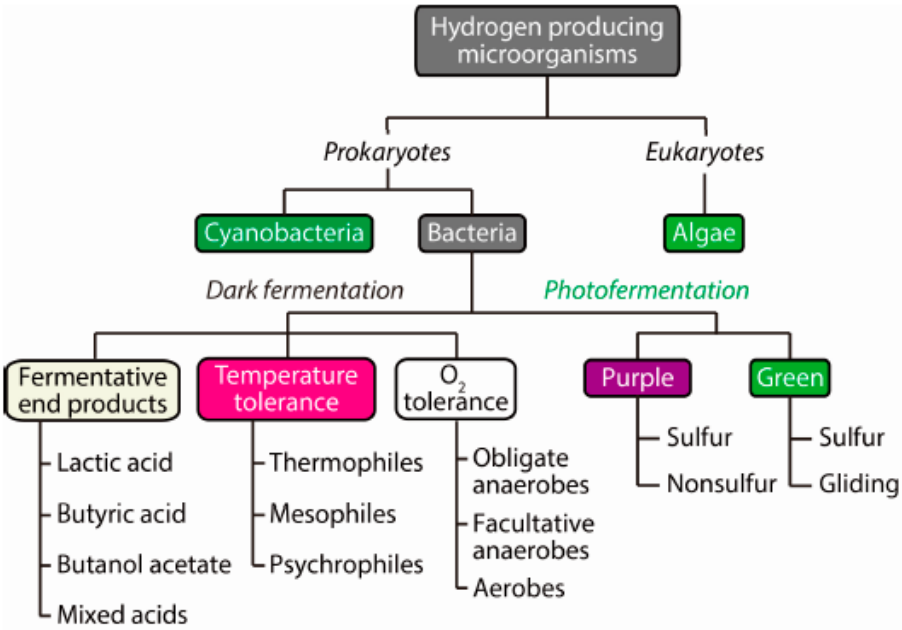

Figure 1. 1 Schematic representation of diversity of hydrogen producing microoranisms (Chandrasekhar et al., 2015)

1.1.1 Biophotolysis

Microalgae and cyanobacteria decompose water into hydrogen and oxygen in biophotolysis of water. A (FeFe)-hydrogenase in green algae drives the evolution of H_2, whereas nitrogenase is responsible for this process in heterocystous cyanobacteria. The process is categorized into two types: direct biophotolysis and indirect biophotolysis.

In direct biophotolysis, light is captured by photosynthetic apparatus and the derived electrons are transferred to ferredoxins which then reduce hydrogenase enzyme which is responsible for hydrogen production (Patrick C. Hallenbeck & Benemann, 2002). The net reaction of direct biophotolysis is as follows:

$$4H_2O + \text{“light energy”} \rightarrow 2O_2 + 4H_2 \quad (1.1)$$

In indirect biophotolysis, on the other hand, light energy is converted to chemical energy in the form of a carbohydrate which is reused to produce H_2 as in the below reactions:

$$6H_2O + 6CO_2 + \text{“light energy”} \rightarrow C_6H_{12}O_6 + 6O_2 \quad (1.2)$$

$$C_6H_{12}O_6 + 6H_2O + \text{“light energy”} \rightarrow 12H_2 + 6CO_2 \quad (1.3)$$

This process is carried out by cyanobacteria which are gram positive bacteria which have the same type of photosynthesis as higher plants. They also possess hydrogenase and nitrogenase for nitrogen fixation and can perform biophotolysis of water (D Das & Veziroglu, 2001).

The nitrogenase enzyme which is highly O_2-sensitive is protected in cyanobacteria because oxygenic photosynthesis (Eq. 1.2) occurs in vegetative cell while H_2 production (Eq. 1.3) takes place in heterocyst. Thus nitrogenase can operate the following reaction in cyanobacteria to generate H_2:

$$N_2 + 8e^- + 8H^+ + 16ATP \rightarrow 2NH_3 + H_2 + 16ADP + 16P_i \quad (1.4)$$

The maximum efficiency of biophotolysis by green algae is predicted to be 12.2% and 4.1% by heterocystous cyanobacteria (Hallenbeck, 2011).

1.1.2 Dark Fermentation

Fermentation is an anaerobic process which can occur at mesophilic, thermophilic or hyperthermophilic temperatures and usually a mixed biogas containing H_2 and CO_2 is produced. *Clostridium, Bacillus* and *Enterobacter* species can produce hydrogen through dark fermentation. The preferred substrates for hydrogen production by dark fermentation are carbohydrates like glucose, isomers of hexoses or polysaccharides like starch, which are eventually converted to glucose. Glucose is converted to pyruvate by glycolytic pathways. The fate of pyruvate depends on the organism and metabolic pathways, where a variety of enzymes and hydrogenase can participate. The net result is the production of one mole of hydrogen per mole of pyruvate. The oxidation of pyruvate yields acetyl-CoA which is used to from a variety of liquid fermentation products, acetate, acetone, ethanol, butanol, butyrate, etc. (Das & Veziroglu, 2008; Hallenbeck, 2014). The yield of hydrogen decreases when the end product is propionate, alcohol or lactic acid, which contain hydrogen not liberated as gas, thus bacteria should be directed away from lactate and alcohols, but towards volatile fatty acids (Levin et al., 2004).

1.1.3 Photofermentation

Photosynthetic bacteria, particularly purple non sulfur bacteria (PNSB) produce hydrogen anaerobically in the presence of light from a wide variety of substrates through the following photofermentation reaction:

$$CH_3COOH + 2H_2O + \text{“light energy”} \rightarrow 4H_2 + 2CO_2 \qquad (1.5)$$

Photofermentation, among other hydrogen production methods, offers some advantages (Basak & Das, 2007; Kars et al., 2008):

- The produced hydrogen is of high purity.
- The theoretical substrate conversion efficiency is high.
- No contaminating O_2 is evolved by PNS bacteria which would inhibit the nitrogenase enzyme responsible for hydrogen production. Nitrogenase is also

not inhibited by certain pressures of hydrogen gas unlike the hydrogenase system.

- A wide variety of organic substrates such as organic acids, sugars, fatty acids or waste products of factories can be utilized by PNS bacteria.
- PNS bacteria can show great metabolic diversity so that they can survive in very different physiological conditions
- PNS bacteria can trap light energy over a wide spectrum range.

The maximum efficiency of hydrogen production through photofermentation of organic substrates by photosynthetic bacteria can be predicted to be 8.5% (Hallenbeck, 2011).

1.1.4 Integrated Systems

Several studies showed that single-stage processes do not allow obtaining high hydrogen yield, since only part of the substrate is converted to hydrogen. Dark fermentation can only yield a theoretical maximum hydrogen yield of 4 mol H_2 per mol of glucose (Gómez et al., 2011). The effluents of dark fermentation are mainly composed of volatile fatty acids (VFAs) such as acetate, propionate, malate and butyrate. These VFAs can be utilized by PNS bacteria during photofermentation for additional hydrogen production. Therefore, integration of these two processes maximizes the overall H_2 yield and substrate conversion efficiency and theoretically yields 12 mol of H_2 per 1 mol of glucose (Kotay & Das, 2008; Ren et al., 2011).

The EU 6th framework integrated project HYVOLUTION, non-thermal production of pure hydrogen from biomass, was a good example for the integrated systems. It was aimed to produce cost effective pure hydrogen using multiple biomass feedstocks in a two stage process (Claassen et al., 2010). Thermophilic bacteria were employed in the first stage to convert several feedstocks (such as sugar beet molasses, potato steam peel, miscanthus and thick juice) into H_2, CO_2 and organic acids by dark fermentation. In the following step, organic acids from the first stage were further converted into hydrogen and CO_2 by photofermentation. The METU Biohydrogen group was the

coordinator of a work package which focused on the second stage of this integrated system and aimed to produce hydrogen from organic acids to increased yield and construct large scale photobioreactors.

Besides integration of dark and photofermentations, there are studies for integration of microbial electrolysis cells (MECs) and dark fermentation since the development of MECs in 2005 (Liu et al., 2005). MECs allow the oxidation of organic substances by microorganisms with the aid of an external circuit containing a power supply. Organic materials are oxidized at anode resulting in protons, CO_2 and electrons. Electrons then are transported through the external circuit to the cathode and combine with protons at the cathode and produce H_2 gas (Jeremiasse et al., 2009).

1.2 Purple Non Sulfur Bacteria (PNSB)

Purple nonsulfur bacteria (PNSB) are anoxygenic phototrophic bacteria which are capable of performing photosynthesis under anoxic conditions. They belong to *α-proteobacteria* and *β-proteobacteria* groups (18 and 3 genera have been recognized for each group (Madigan & Jung, 2009). The α-proteobacteria are further divided into three subgroups: α-1 for *Rhodospirillum* and relatives, α-2 for *Rhodopseudomonas* and relatives and finally α-3 for *Rhodobacter* and relatives (Imhoff, 2006). This group is very diverse in terms of morphology, internal membrane structure, carotenoid composition, utilization of carbon sources and electron donors, cytochrome c structures, lipid composition, quinone composition, lipopolysaccharide structure, and fatty acid composition (Imhoff, 1995).

PNSB are motile by polar flagella, and have a shape of ovoid to rod, and multiply by binary fission. They occupy anoxic parts of waters and sediments where they receive enough light for phototrophic growth. The color of the cell suspensions is determined by the carotenoids and photosynthetic pigments (bacteriochlorophyll *a* or *b*). The photosynthetic pigment-protein complexes are located in the cell membrane and intracytoplasmic membrane system whose formation is triggered by lowered oxygen tension (McEwan, 1994). The α-proteobacteria have extraordinary metabolic versatility as shown in Table 1.1.

Photoheterotrophy is both the preferred mode of growth and the only mode resulting hydrogen production (Koku et al.,2002). The optimum temperature for growth is 25-35°C and optimum pH range is 6-9 (Sasikala et al., 1991). These bacteria need vitamins, especially thiamin, biotin and niacin in the growth medium.

One of the bacteria belonging to α-proteobacteria is *Rhodobacter capsulatus*, which is a gram negative bacterium with a rod shape and a diameter of 0.5-1.2 μm. It produces slime and capsule and can store poly-β-hydroxybutyric acid as a storage material (Imhoff, 1995). The microscopic image of this bacterium is shown in Figure 1.2.

Table 1. 1 Various growth modes of PNSB

Growth mode	**C-source**	**Energy source**	**Notes**
Photoheterotrophy	Organic carbon	Light	Only mode that results in H2 production
Photoautotrophy	CO	Light	CO_2 fixation occurs. H_2 is used as electron donor
Aerobic respiration	Organic carbon	Organic carbon	O_2 is the terminal acceptor
Anaerobic respiration/chemoheterotrophy	Organic carbon	Organic carbon	Requires a terminal electron acceptor other than O_2 (N_2 , H_2S or H_2)
Fermentation/anaerobic, dark	Organic carbon	Organic carbon	

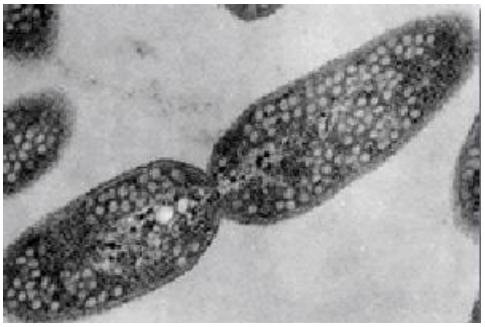

Figure 1. 2 The microscopic image of *R. capsulatus.* (https://www.ncbi.nlm.nih.gov/genome/?term=rhodobacter+capsulatus Last access date: April 12, 2017)

R. capsulatus can easily be mutated by classical procedures, thus offers good opportunities for biochemical and genetic approaches. It has been frequently studied for its versatile metabolism, nitrogen fixation and hydrogen production (Weaver et al., 1975). It is shown to perform an efficient hydrogen production on acetate, which is the primary organic acid in dark fermentation effluents of several feedstocks (Barbosa et al., 2001; Afşar et al., 2009; Özgür et al., 2010). This bacterium was mutated to achieve higher hydrogen production (Kars et al., 2008; Ozturk et al., 2006; Öztürk et al., 2012). The genome of this bacterium is composed of a circular chromosome and a plasmid (Strnad et al., 2010). The genome is GC rich (66%) composed of 3531 open reading frames on the chromosome and 154 open reading frame on the plasmid. GenBank accession numbers of *R. capsulatus* chromosome and plasmid are CP001312 and CP001313, respectively.

1.3 Hydrogen production metabolism of PNSB

1.3.1 Nitrogenase

Two classes of enzymes produce hydrogen: hydrogenase and nitrogenase. Hydrogen is primarily produced by nitrogenase in PNSB. Although nitrogenase is better known for NH_3 production from atmospheric N_2, H_2 is an obligate product of nitrogenase

reaction, but when the atmosphere is lacking N_2, the enzyme acts like a hydrogenase and H_2 becomes the sole product (Eq. 1.6 & 1.7, respectively).

$$N_2 + 8H^+ + 8e^- \ 16\ ATP \ \rightarrow \ 2\ NH_3 + H_2 + 16\ ADP + 16P_i \quad (1.6)$$

$$8H^+ + 8e^- \ 16\ ATP \ \rightarrow \ 4\ H_2 + 16\ ADP + 16P_i \quad (1.7)$$

As seen in the above reactions, nitrogenase requires ATP, unlike hydrogenase, which simply requires an electron donor (Eq. 1.8).

$$2H^+ + 2e^- \leftrightarrow H_2 \quad (1.8)$$

The high ATP requirement of nitrogenase is not a barrier to H_2 production of PNSB, since they can produce ATP abundantly via cyclic photophosphorylation as long as they are illuminated (McKinlay, 2014).

The nitrogenase of *Rhodobacter capsulatus* is a molybdenum-dependent nitrogenase which is a two-protein complex (Figure 1.4). It is composed of a dinitrogenase (known as MoFe protein) and a dinitrogenase reductase (known as Fe protein). The former, encoded by *nifDK*, contains Fe and Mo as cofactors, and its molecular weight is 250 kDa, while the latter, encoded by *nifH*, contains Fe, and has weight of 70 kDa. The dinitrogenase component contains two types of metal clusters, the M-cluster (FeMo cofactor), which represents the site of substrate reduction, and the P-cluster that transfer electrons and protons to the FeMo cofactor. Electron donors, such as ferredoxins reduce the Fe protein, then a single electron is transferred to from Fe protein to MoFe protein; this step requires MgATP hydrolysis. Finally, an internal electron is transferred by the P cluster to FeMo cofactor substrate-binding site (Peters, 1995).

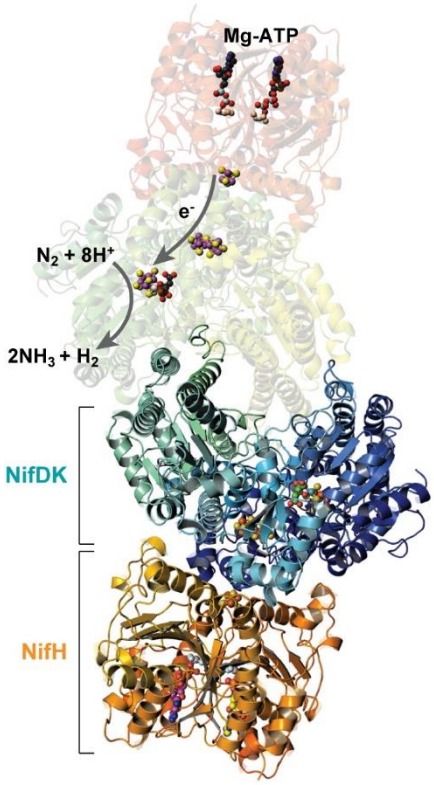

Figure 1. 3 Structure of the molybdenum nitrogenase enzyme complex (Rubio & Ludden, 2008)

R. capsulatus has also an alternative nitrogenase, an iron-only nitrogenase (Fe-nitrogenase). It does not contain any heterometal in the active site and it is encoded by *anf* genes (Dixon & Kahn, 2004). Mo-nitrogenase and Fe-nitrogenase of *R. capsulatus* have overlapping transcriptional control mechanisms with regard to the presence of fixed nitrogen source, oxygen, and molybdenum. *R. capsulatus* has more than 50 nitrogen fixation related genes which are clustered into 4 unlinked regions of the chromosome: *nif* region A,B,C and D (ref). **Region A** contains genes involved in electron supply to nitrogenase (*rnfABCDGEH*, *rnfF* and *fdxN*), FeMo cofactor biosynthesis (*nifEN*, *nifQ*, *nifSV*, and *nifB2*), and nitrogen regulation (*nifA*). **Region B** contains structural genes of Mo-nitrogenase (*nifHDK*), the nitrogen regulatory genes *rpoN* and *nifA2*, FeMo cofactor biosynthesis gene *nifB2*, gene involved in molybdenum uptake (*modABC*), and two molybdenum regulatory genes (*mopA* and *mopB*). **Region C** contains genes coding for a two-component system which acts on

top of the nitrogen regulatory cascade (*ntrBC*). Finally, **Region D** contains the nitrogen regulatory *anfA* gene and the structural genes of Fe-nitrogenase, *anfHDGK*.

Mo-nitrogenase is the most common and the most efficient nitrogenase for the reaction (1.6), Fe nitrogenase is only synthesized in absence of Mo (Oda et al., 2005). Fe-nitrogenase does not support efficient hydrogen production alone, but co-expression of Mo-nitrogenase and Fe-nitrogenase enhanced hydrogen production by disrupting *mopAB*, which does not affect activity of Mo-nitrogenase while derepresses Fe-nitrogenase expression (Yang et al., 2015). Nitrogenase synthesis and nitrogenase activity can be inhibited irreversibly by molecular oxygen (Goldberg et al., 1987).

1.3.2 Hydrogenase

The other enzyme responsible for hydrogen production in PNS bacteria is hydrogenase. It is a metalloenzyme which catalyzes the following reaction

$$H_2 \leftrightarrow 2H^+ + 2e^- \quad (1.9)$$

In the presence of H_2, this enzyme works as an hydrogen uptake enzyme and converts hydrogen molecule into protons and electrons (Kars & Gündüz, 2010). It is a membrane bound enzyme encoded by *hup* and *hyp* genes in *R. capsulatus* (Colbeau et al., 1993). Because of the hydrogen uptake role of hydrogenase, elimination of the genes of hydrogenase would increase the hydrogen yield in PNS. In fact, Ozturk et al. (2006) deleted *hup* gene in *R. capsulatus* by interposon mutagenesis using gentamycin casette. The uptake hydrogenase mutant strain *hup*-, also called YO3 yielded more hydrogen than the wild type strain. Similarly, the uptake hydrogenase deficient *R. sphaeroides* was a more efficient hydrogen producer than its wild type strain (Kars et al., 2008).

1.3.3 Ferredoxin

The electrons from the electron pool are carried to the nitrogenase by the electron carrier ferredoxins. *R. capsulatus* synthesizes six soluble ferredoxins, which are divided into two classes depending on the number of [2Fe-2S] clusters. FdI, FdII and

FdIII has the group of dicluster ferredoxins, while FdIV, FdV and FdVI contain a single [2Fe-2S] cluster. FdI has been shown to serve as physiological electron donor to nitrogenase (Jouanneau et al., 1995) and it is encoded by *fdxN* gene in *R. capsulatus*.

1.3.4 Anoxygenic Photosynthesis

The reaction nitrogenase catalyzes is an energy expensive reaction – it requires high ATP consumption (Eq. 1.7). Besides 4 molecules of ATP for 1 molecule of H_2, an additional number of ATP molecules is needed for reducing the ferredoxins that serve as electron donor to nitrogenase. During photofermentation, ATP is formed via anoxygenic photosynthesis while the reducing power is derived from the catabolism of organic substrates (Figure 1.4)

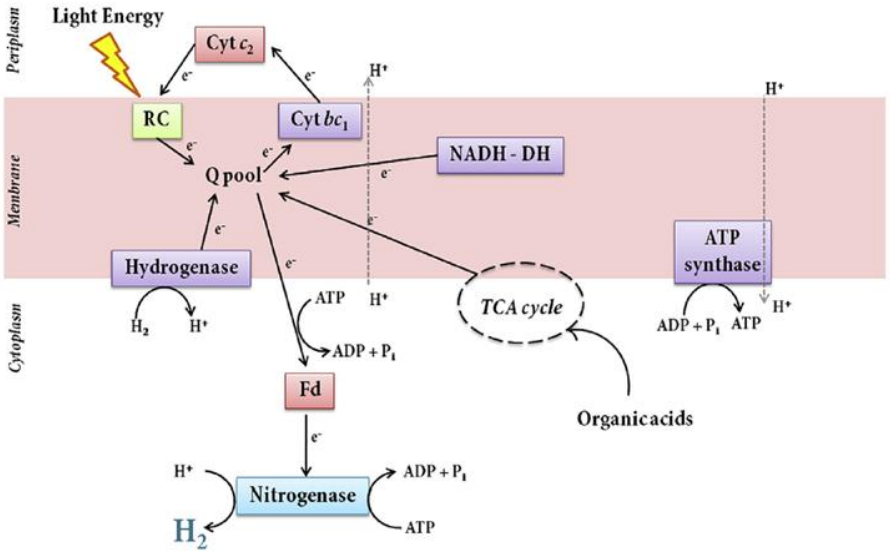

Figure 1. 4 General scheme of hydrogen production and related metabolism in PNS bacteria (Adessi & De Philippis, 2014)

Hydrogen production in PNSB is directly related to photosynthesis. Light dependent hydrogen production by PNSB was first observed by Gest & Kamen (1949). Photosynthesis of PNSB is anoxygenic. Electrons are not obtained from water and O_2 is not produced, unlike oxygenic cyanobacteria, algae and plants. They possess a single

photosystem resembling photosystem II but are incapable of oxidizing water, thus no O_2 is produced. PNSB utilize organic carbons as both source of carbon and electrons during photosynthetic growth. Electrons from the electron donor are energized by photosystem using light and channeled through a H+ pumping electron transfer chain resulting in a proton motive force. ATP synthase uses this proton motive force to produce ATP, or this force powers other energy requiring processes (Figure 1.4). Electron can be donated to NADP+ to generate NAPH for biosynthesis, or they can alternatively be energized repeatedly through cyclic electron transport chain. This cycling is called cyclic photophosphorylation and it allows maintenance of the proton motive force and ATP pools. Cyclic photophosphorylation is advantageous under starvation conditions as cycling a few electrons can generate usable energy for cell repair and maintenance (McKinlay, 2014).

Photosynthesis is carried out by pigment-protein complexes of the photosynthetic membrane. There are two of these complexes: the reaction center and the light harvesting complexes. In the photosynthetic membrane there is a downhill flow of energy from the light-harvesting (LH) proteins to the reaction centers (RC). Light harvesting complexes collect solar energy and deliver it to reaction center. In purple bacteria, LH2 absorbs radiation at a shorter wavelength than LH1 and therefore delivers its energy to LH1, which in turn passes it on to the reaction center (Kühlbrandt, 1995). Pigments are noncovalently bound to these complexes. LH1 and LH2 are structurally different. LH1 is closely associated to the RC, and often referred to as the "core" or "primary" complex. LH2, on the other hand, is distant from the RC and called as the "secondary" complex (Figure 1.5). LH1 is encoded by *pufA* and *pufB*, and LH2 is encoded by *puc* operon. Both light harvesting antenna complexes bind to two bacteriochlorophylls (bchl) and one or two carotenoids. LH1 contains bchls which absorb light at about 880 nm, while LH2 binds bchls absorbing light at 800 and 850 nm. One other type of pigment in the photosynthetic unit is the carotenoid. Carotenoids function both to harvest light energy and to protect cell from stress caused by light. They absorb green light at 450-550 nm. By these pigments, the absorption spectrum of purple bacteria is very wide and covers the two ends of the visible spectrum (Figure 1.6).

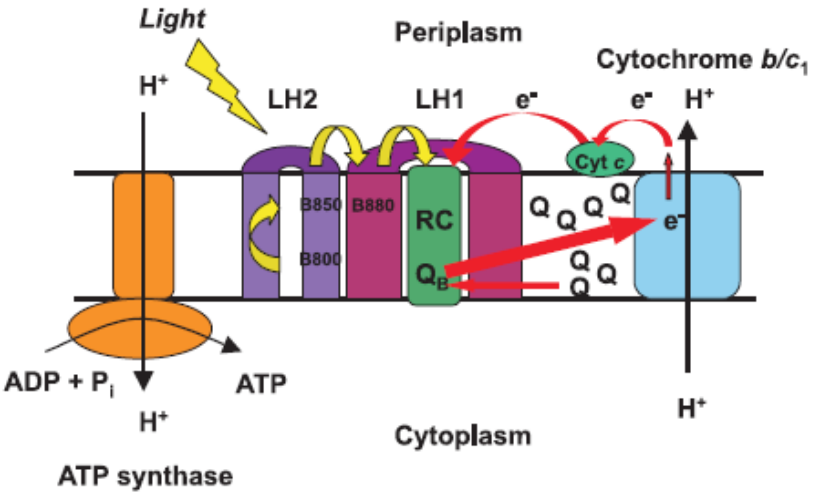

Figure 1. 5 The photosynthetic apparatus (Law et al., 2004)

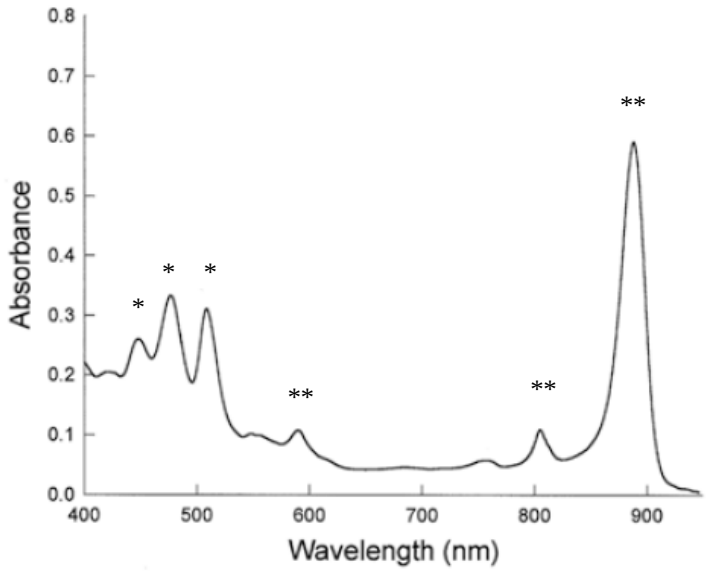

Figure 1. 6 Absorption spectrum typical for PNSB. Absorption maxima indicated with * are due to carotenoids, while ** indicate the absorption maxima due to bacteriochlorophylls. Peak wavelengths slightly vary among species (Adessi & De Philippis, 2012)

The reaction center is an integral membrane protein complex composed of L, M, and H subunits. The L and M subunits compose the core of RC, H subunit provides structure stability. The L subunit is encoded by *pufL* gene, M subunit by *pufM* and L

subunit is encoded by *puhH* gene. The prosthetic groups bind to L and M subunits. Those are two bchls (special pair), two accessory bchls in close proximity to the special pair, two bacteriopheophytins (bchl lacking the central Mg+2), and a pair of quinones (QA, QB), a non heme iron and a carotenoid.

A photon is absorbed by the LH2 and transferred to LH1 and then trapped by bacteriochlorophylls in the RC and charge separation occurs, starting the electron transport chain (ETC). This energy releases an electron which reduces the quinone Q (Adessi & De Philippis, 2013). In purple bacteria, reducing equivalents are exported in pair from the RC, and reduced quinol (QH2) is the molecule migrating from the RC to the other membrane proteins. Two electrons are needed to reduce quinone to quinol. Once quinone is doubly reduced, it picks up protons from the cytoplasmic space and translocate through the membrane to reach the cytochrome bc_1 (Cyt *bc*1) complex (Figure 1.7).

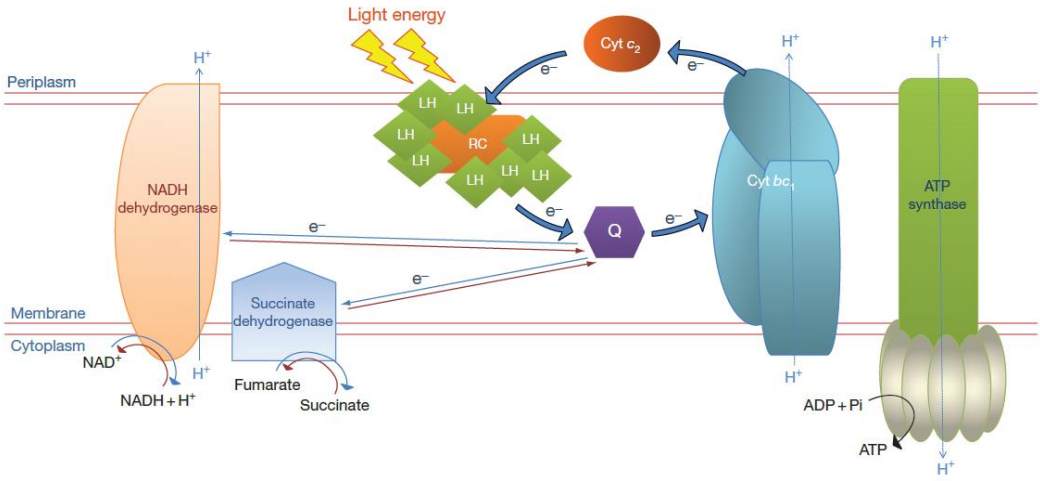

Figure 1. 7 Schematic representation of the photosynthetic ETC. The photosynthetic electron cycle is indicated by the blue bold arrows. The Δp-driven reversed electron transport is indicated by the thin blue arrows; the red arrows indicate the oxidation of NADH and succinate and the reduction of quinones. The dotted arrows indicate the steps for proton translocation. (Adessi & De Philippis, 2013)

From Cyt bc_1, electrons are sent to cytochrome c_2 (Cyt c_2), and the protons are released to the periplasmic space. Cyt c_2 becomes ready to reduce primary electron donors in RC and closing the cycle. During this process protons accumulate in the periplasm and generate an electrochemical gradient which is utilized by ATP synthase to generate ATP.

Doubly reduced quinone (QH2) is lipophilic enough to freely move throughout the membrane, thus it transports its reducing power to different membrane-bound enzymes. It can reach not only the cytochrome bc1 complex but also NADH dehydrogenase (NADH quinone oxidoreductase) and succinate dehydrogenase, thus opening the cyclic photosynthetic process with the 'reversed electron flow' in photosynthesis. The reverse action of the NADH dehydrogenase is necessary to refurnish the cell of NADH (Adessi & De Philippis, 2013).

The quinone pool has a very important role in recognizing the signal from cell's redox state, which changes depending on the metabolic conditions. Different metabolic behaviors are controlled by RegA/RegB system accordingly, which regulates photosynthesis, nitrogen fixation, carbon fixation and respiration.

As seen in Figure 1.4, tricarboxylic acid (TCA) cycle and the photosynthetic apparatus work in parallel. Photoheterotrophic conditions can cause over-reduction of the photosynthetic electron transport chain. Therefore, excess electrons must be dissipated, and this is achieved by hydrogen production, CO_2 fixation (Calvin cycle) or polyhydroxybutyrate (PHB) synthesis. During exponential growth, the Calvin cycle utilizes most of the excess electrons via reduction of CO_2 into biosynthetic intermediates. Only a small portion of electrons generated from organic substrate oxidation is used for hydrogen production. However, in the stationary phase, biosynthesis almost stops, majority of organic carbon is oxidized into CO_2 and most of the electrons are directed toward hydrogen production (Golomysova et al., 2010; Koku et al., 2002).

1.4 Factors affecting photofermentative hydrogen production

Hydrogen production by PNSB depends on several factors such as temperature, pH, light intensity, bacterial strain, carbon and nitrogen sources, mode of operation, presence of oxygen and presence of different metals (e.g. Mo, Fe, V). These parameters are of great importance for the scale up and sustainable hydrogen production in an industrial scale. The ultimate goal of photofermentative hydrogen production is indeed to carry out the process in large scale photobioreactors at outdoor conditions under natural sunlight (Androga et al., 2012b).

1.4.1 Effect of temperature and pH

Since hydrogen production is an enzymatic reaction, one of the most important parameters is temperature. While low temperatures slow down or stop the process, higher temperatures than optimal can cause more severe results, such as bacterial death. The optimum temperature range for hydrogen production is 30-35°C, and the most efficient hydrogen production was observed at 30°C (Sasikala et al., 1991; Sevinç, 2010). The optimum temperature for nitrogenase was found to be 35°C (Rainbird et al., 1983). A sudden increase in temperature from 30°C to 42°C results both in immediate termination of hydrogen production and death of bacteria (Gürgan et al., 2015). Under outdoor condition, the daily fluctuation in the temperature also results in decreased hydrogen production (Özgür et al., 2010). Another parameter important in enzymatic reactions is the pH of the environment. The optimum pH for bacterial growth was found to be 6.5-7.5, while the optimum range for hydrogen production is 6-9 (Sasikala et al., 1991; Holt et al., 1994)

1.4.2 Effect of carbon and nitrogen sources

Carbon and nitrogen sources are also parameters to be considered for efficient hydrogen production. Nitrogenase enzyme catalyzes the reaction of fixation of

nitrogen to ammonia and its synthesis is reversibly repressed by the presence of ammonia. Thus already fixed nitrogen sources are of choice for hydrogen production.

Glutamate is thus a good nitrogen source for hydrogen production of PNSB (Hillmer & Gest, 1977). The concentration of glutamate is also important. Increase in the concentration of glutamate results in increase in biomass yield. A glutamate concentration of 1-2 mM yields the highest hydrogen (Uyar et al., 2012).

Although a wide range of substrates can be used for bacterial growth, only a portion of them can be used for hydrogen production. Organic acids, such as acetate, lactate, malate, butyrate, etc. are good sources for hydrogen production and *Rhodopseudomonas sp*. performed better hydrogen production on acetate (Barbosa et al., 2001). 30 mM of acetate was found to be the best concentration for hydrogen production of H_2 by *R. capsulatus* (Özgür et al., 2010).

Agricultural wastes and dark fermenter effluents of agricultural wastes can also be used for hydrogen production (Afşar et al., 2009; Androga et al., 2012a; Avcioglu et al., 2011; Boran et al., 2012; Özgür & Peksel, 2013; Uyar et al., 2015).

1.4.3 Effect of bacterial species

The species of bacteria significantly affect the hydrogen productivity. They can show different performances upon different substrates. *R. capsulatus*, for example, can produce more hydrogen on media containing acetate as the sole or primary carbon source. *R. sphaeroides*, on the other hand, can produce hydrogen more efficiently when the substrate contain glucose. (Afsar et al., 2011; Özgür et al., 2010). Even different strains of bacterial species can differ in hydrogen productivity (Asada et al., 2008).

The mode of operation is another important parameter. Continuous operations can be stable for months, while batch operations can be stable for only few days to a few weeks, depending on the volume of the photobioreactor. For a long term industrial scale, continuous operation is of importance. In METU Biohydrogen group, several

research studies have been carried out on the design and operation of outdoor photobioreactors (Avcioglu et al., 2011; Androga et al., 2012; Boran et al., 2012).

1.4.4 Effect of light

Light is another significant parameter because ATP is only synthesized by photosynthesis and many molecules are consumed while nitrogenase is active. Therefore, parameters related to light and photosynthesis are of crucial importance for the nitrogenase-mediated hydrogen production process in PNSB. For this reason in recent years a large amount of research was conducted to optimize illumination protocols to increase photosynthesis efficiency (Adessi & Philippis, 2014). Light intensity and illumination protocols are the primary light-related parameters. Light intensity should be in an optimal range. The optimum light intensity for the most efficient hydrogen production by *R. capsulatus* was found to be 4000 lux under continuous illumination (Akman et al., 2014). When the illumination mode was cyclic light/dark periods, however, 4000 lux (270 W/m^2) light intensity was found to be point of saturation by *R. sphaeroides* (Uyar et al., 2007). Another study with *R. sphaeroides* also showed that optimum light intensity for photofermentative hydrogen production was 352 W/m2. In the same study, the effect of light sources was also examined and

halogen lamps were found to be the most effective while tungsten was comparable with halogen and yielded more hydrogen than sunlight, fluorescent and infrared lamps (Argun & Kargi, 2010). The emission spectrum of tungsten lamps cover the spectrum of PNSB therefore, tungsten and tungsten-halogen lamps were frequently used in other studies too (Afşar et al., 2009; Argun, Kargi, & Kapdan, 2009; Boran et al., 2010; B. Uyar et al., 2015) .

A light intensity higher than optimum is known to cause photo-inhibition because of excessive light energy. Short intermittent light/dark cycles increased the efficiency of hydrogen production while longer intermittent periods decreased it (Wakayama et al., 2000). Bacteria do not produce hydrogen in dark periods, however they survive and continue to produce hydrogen when the illumination is restored (Li et al., 2011; Uyar

et al., 2007). This is due to increased photosystem synthesis due to light. Synthesis of photosystem elements are enhanced when there is light which allows cells to capture more light energy.

Most of the studies about light stress were focused on stress caused by reactive oxygen species which are generated by aerobic photosynthetic activity in purple non-sulfur bacteria (Berghoff & Klug, 2016; Ziegelhoffer & Donohue, 2009). However, genetic studies on light intensity effect on PNSB in anaerobic mode is very limited, although physiological studies have been carried out more frequently as mentioned above (Uyar et al., 2007; Adessi & De Philippis, 2014; Akman et al., 2014). Therefore, there is a need for understanding the metabolism of the effect of light.

Since the ultimate goal is to produce hydrogen in large scale in outdoor conditions, research on light/dark cycles can be more informative than studies with continuous illumination. Therefore it is important to learn the genetic and molecular basis of reasons underlying the reduction of H_2 production efficiency in 12-h light/12-h dark diurnal cycles and the case of light intensity stress. This can be achieved by high throughput gene expression studies using microarray technology.

1.5 Microarray Technology

Microarrays are miniaturized assays of ordered arrangements which are used to study biological materials located at certain position on a solid support. While the biological materials vary and can be DNA, proteins or carbohydrates, the principle is the same. A mixture of biological molecules, called target, are hybridized with the probes, which are immobilized on a solid surface. The interactions between biological materials can be studied this way. While traditional molecular biology tools allow the study of a single gene or a small set of genes, microarrays allow the study of a large set of genes and facilitate discovery of totally novel and unexpected functional roles of genes (Slonim & Yanai, 2009).

DNA microarrays are perhaps the most successful and mature methodologies for high-throughput and large-scale genomic analyses and frequently used for analyzing gene

expression of thousands of genes at the same time. The leading manufacturer of DNA microarrays is Affymetrix (Santa Clara, CA, USA, http://www.affymetrix.com) (Trevino et al., 2007). The GeneChip®s manufactured by Affymetrix contain very high feature densities that having 400,000 features on a single array is typical. The 25 residues long oligonucleotides (probes) are synthesized chemically directly on the quartz surface by photolithography (Figure 1.8).

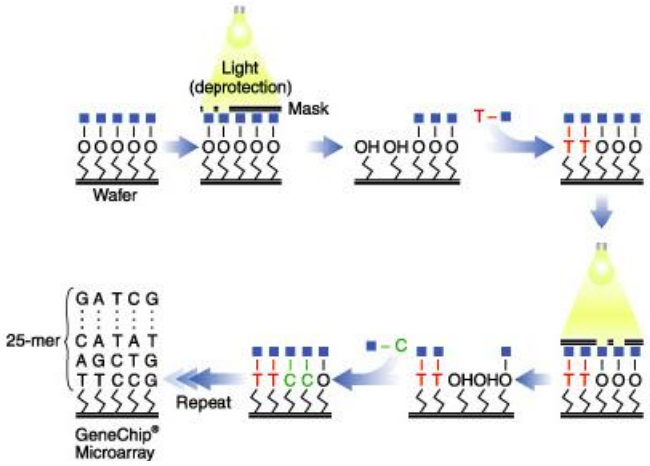

Figure 1. 8 Photolithography used for Affymetrix GeneChip® manufacturing (German Cancer Research Center, https://www.dkfz.de/gpcf/affymetrix_genechips.html. Last access: May 16, 2017)

Each probe is called "match" and has a negative control which has a single differing base in the middle of the probe which is called "mismatch probe". Match and mismatch probes together make a "probe pair". A single gene is represented by a 11-15 set of probe pairs. Probe pairs are used to detect and eliminate the cross hybridizations.

For transcriptome analysis with microarrays, the target is prepared by purifying the total RNA from the cells. For eukaryotic organisms, the mRNA is converted into cDNA using 3' end polyA tails. For prokaryotic organisms total RNA is isolated and mRNA is converted into cDNA using random primers. Affymetrix GeneChip® are advantageous when the starting material is limited. Only 50-100 ng RNA is usually enough. Targets are labelled using biotin and hybridizations are detected streptavidin-phycoerythrin. This method eliminated dye effects and eases experimental design and

statistical analysis (Ehrenreich, 2006). The labelled cDNAs are hybridized with the arrays by incubating overnight, then washing to remove non-specific hybrids. A laser excites the fluorescent dye to produce light which is detected by a scanner and a digital image is generated. This image is further processed by a software and transforms the image into numerical reading for each spot on the array. The intensities inside the defined spots are integrated. Surrounding background noise is subtracted from the integrated signal. This final reading is a value proportional to the concentration of that sequence in the sample. Relative quantitation method together with statistical analyses are performed then to detect the significantly differentially expressed genes among different samples (Trevino et al., 2007).

The microarray assay is a complex one and array results can be influenced by each step from manufacturing to sample preparation and image analysis. That is why the genes with strong hybridization signal and at least two fold difference should be validated by an alternative method. Real time quantitative PCR is well-suited to validate DNA array results because it is quantitative, rapid and required much less starting RNA (Rajeevan et al., 2001).

1.5.1 Real Time Quantitative PCR for Validation of Microarray

Real time quantitative PCR (RT-qPCR) is a gold standard for validation of microarray based gene expression studies (VanGuilder, et al., 2008). Microarrays are preferred for large scale discovery experiments, while qPCR is a method of choice for analyzing gene expression of moderate number of genes.

Quantitative PCR has three phases: exponential phase, linear phase and plateau phase. In the exponential phase, the reagents are not limited yet and the product increases exponentially. The linear increase of the product characterizes the linear phase where the PCR reagents begins to become limited. As some reagents become depleted, the reaction reaches a plateau phase where the product amount does not change. Real time PCR is based on the fact that the quantity of the PCR products in exponential phase is in proportion to the quantity of initial template. During the exponential phase the amount of products double during each cycle, if the efficiency of the reaction is 100%.

Real time qPCR technology offers quantification of PCR products during the PCR cycle thanks to the fluorescent detector molecule, which can be a probe sequence (e.g. Taqman) or intercalating dye. The use of probe sequences results in a highly sensitive detection, however they are quite expensive and sequence specific. On the other hand, intercalating dyes are inexpensive, simple to use as they are not sequence specific and can be used for any reaction. SYBR Green, an example of intercalating dyes, fluoresces upon binding to double stranded DNA, but not single stranded DNA and emits a strong fluorescent signal at 530 nm that is easily detected. The fluorescent signal from the product is correlated to the amount of PCR product in the reaction. Data on PCR product concentration is thus collected online from every cycle by the instrument. The reproducibility of SYBR Green real time PCR and its concordance with microarrays in terms of fold-change correlation was found to be high. The results of SYBR Green real time PCR was highly comparable with microarrays. (Arikawa et al., 2008). One drawback of choosing SYBR Green chemistry as the detection method is the need of high specificity as SYBR Green can bind to all double strand DNA, thus primer-dimers and non-specific bindings may give false positive results. In order to detect any non-specific signal, a melting curve analysis can be performed after the reaction is completed.

1.5.2 Melting Curve Analysis

Melting Curve analysis with SYBR Green is used for product characterization, i.e., to determine whether the desired PCR product is free of nonspecific by-products. PCR products can be characterized by melting curve analysis because each double-stranded DNA molecule has a characteristic melting temperature (Tm), at which 50% of the DNA is double-stranded and 50% is melted, i.e., single-stranded. During a melting curve run, the reaction mixture is slowly heated to 95°C, which causes dsDNA to melt. A sharp decrease in SYBR Green I fluorescence occurs when the temperature reaches Tm of a PCR product present in the reaction. Melting curve graph fluorescence (F) vs Temperature (T) displays this.

The Tm of a PCR product in the reaction can be estimated from the inflection point of the melting curve. However, to make the Tm easier to see, the software plots a derivative melting curve (-dF/dT) in which the center of a melting curve analysis will show only one melting peak. If primer-dimers or other non-specific products are present, they will be shown as additional melting peaks. Checking the Tm of a PCR product can thus be compared to analyzing the length of a PCR product by gel electrophoresis (Roche PCR Applications Manual, Roche Diagnostics GmbH, Mannheim, Germany).

In the analysis of real time qPCR data, either absolute or relative quantification methods are used. In absolute quantification number of copies of a specific RNA per sample is determined by constructing an RNA standard curve of the gene of interest. Relative quantification, on the other hand, uses the relative levels of RNA samples. The latter method is adopted by the majority of the analyses and used to validate microarray results.

The most common method for relative quantification is comparative Ct method, also known as 2-ΔΔCT method (Livak & Schmittgen, 2001). The CT (threshold cycle), also called Cq (quantification cycle), is the cycle number when a significant increase in fluorescent signal is detected above the background fluorescence (Figure 1.9). CT are logarithmic and can be used directly in comparative CT method. Relative quantification with comparative CT method involves the calculation of gene expression levels as the target/reference ratio of gene of interest from each treated sample divided by the target/reference ratio of the control sample. Reference gene (also called as endogenous control gene) is a housekeeping gene whose expression level does not show a difference in all experimental conditions and in all samples (such as 16srRNA in bacteria). Normalization to a reference gene results in the correction of sample to sample variations caused by differences in the initial quality and quantity of the nucleic acid (Roche Applied Science Technical Note No. LC 13/2001). The detailed calculation of relative gene expression by comparative Ct method is provided in 2.6.4.3.

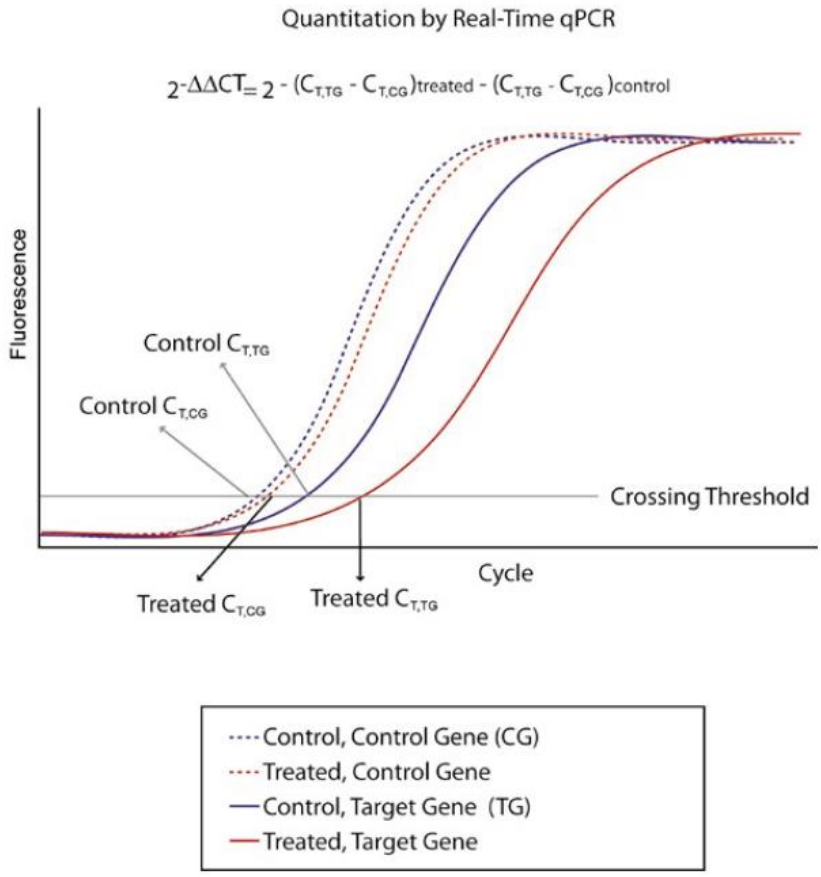

Figure 1. 9 Mathematical basis of the $2^{-\Delta\Delta CT}$ method (VanGuilder, Heather D., Vrana, Kent E., Freeman, 2008)

1.6 Aim of This Study

The ultimate goal of photofermentative hydrogen production is to produce hydrogen in a large scale in outdoor photobioreactors by using natural sunlight as the light source. Under the sunlight, hydrogen production is highly affected by the intensity of the light and the diurnal cycle of illumination, and can be reduced upon high light intensities. Therefore, it is important to learn the genetics and molecular basis of underlying the reduction of hydrogen production under light intensity stress. The aim of this study is to reveal a whole genome expression profile of *R. capsulatus* under low and high light intensities where the illumination is light/dark cycles. For this purpose we evaluated the physiological changes (pH, H_2 production, specific growth rate, molar hydrogen yield, molar productivity, light conversion efficiency and product yield factor) under

low and high light intensities and cyclic illumination in a 150 mL photobioreactor. Then, we carried out microarray analysis to understand the transcriptome of *R. capsulatus* under low and high light intensities. Finally, microarray results were validated with real time qPCR analysis

CHAPTER 2

MATERIALS AND METHODS

2.1 Materials

2.1.1 Bacterial strains

Rhodobacter capsulatus DSM1710 was obtained from German Collection of Microorganisms and Cell Cultures (DSMZ, Braunsweig, Germany). *Rhodobacter capsulatus* YO3 developed by Dr. Yavuz Öztürk by deletion of uptake hydrogenease enzyme via incorporation of gentamycin cassette (Ozturk et al., 2006).

2.1.2 Solid Medium

The bacteria from stock were activated on 1.5% (g/v) agar medium at 30℃. The composition of MPYE medium is given in Appendix A.

2.1.3 Liquid Media

Bacteria were grown at 30 ℃ in minimal (Biebl & Pfennig, 1981) medium with some minor modifications. Growth medium contained 20 mM acetate as carbon source and 10 mM glutamate as nitrogen source, while hydrogen production medium contained 30 mM acetate and 2 mM glutamate. Iron citrate and trace elements were added to the medium before sterilization at 121 ℃ for 20 minutes. Filter sterilized vitamin solution was added to the medium after sterilization. The pH of the media were adjusted to 6.4 with 5 M NaOH. The composition of liquid media, iron citrate, trace element and vitamin solutions were given in Appendix A.

2.2 Methods

2.2.1 Experimental Set-up

Sterile glass photobioreactors (150 mL volume) were used in this study. Bacteria were inoculated into either growth or hydrogen production media to make the inital OD660nm 0.25 in total volume of 150 mL. After inoculation, reactor bottles were

sealed with sterile rubber stoppers. Anaerobic environment was provided by flushing argon gas into the cultures. All the steam sterilizations were carried out in an autoclave (Nüve OT 32, Turkey). The bacterial cultures were kept at 30℃ in a cooling incubator (Nüve ES 250, Turkey) throughout the experiments. The inner culture temperatures were measured by digital thermometer (Maxi T, Amarell Electronic, Germany). Illuminations were done by 100 Watt incandescent lamps and light intensity was adjusted to 2000 lux for growth, and to 2000, 3500, 7000 and 10,000 lux for different experiments using a lux meter (Extech HD400, Boston, USA). Water displacement method (Uyar et al., 2007) was used to measure the volume of the evolved gas. Gas collection tubes were filled with distilled water and closed with a rubber tap, and connected to the reactor bottles via plastic tubings with needles at each end. The diagram of the experimental set up is given in Figure 2.1.

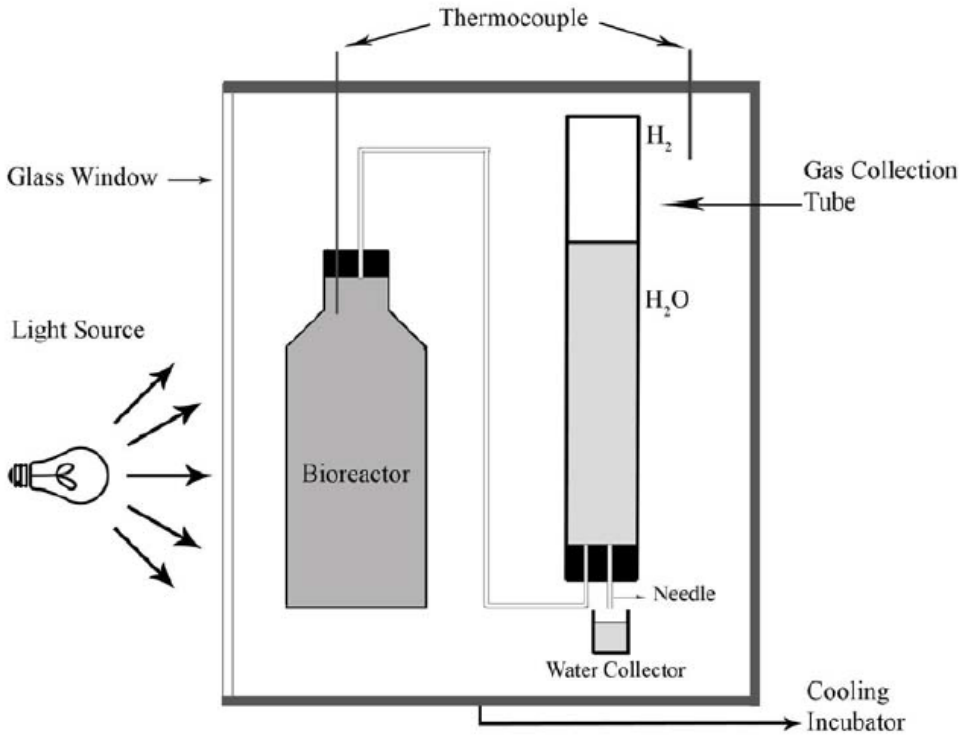

Figure 2. 1 Schematic diagram of the experimental set-up (Uyar, 2008)

2.3 Experimental Designs

2.3.1 Effect of light intensity on physiology of bacteria-1

R. capsulatus DSM1710 were inoculated into hydrogen production medium and were exposed to 13 cycles of 12h/12h light/dark periods. The experiment was started by a light period directly after the inoculation of the bacteria. The illumination in the light periods were one of three different light intensities: 2000, 3500 and 5000 lux. The experiment was carried out in duplicate bioreactors with 150 mL working volume.

2.3.2 Effect of light intensity on physiology of bacteria-2

R. capsulatus DSM1710 and *R. capsulatus* YO3 were inoculated into hydrogen production medium (30mM acetate / 2 mM glutamate) and were exposed to 13 cycles

of light and dark periods. The experiment was started with a light period directly after the inoculation of the bacteria. The illumination in the light periods were 2000 and 7000 lux in parallel runs. The experiment was carried out in duplicate bioreactors of 150 mL.

2.3.3 Physiological Analyses

Liquid samples (1.5 mL) were removed from triplicate reactor bottles at the end of light and dark periods, i.e. every 12 hours. The same amount of sterile distilled water was injected into the bioreactors to eliminate pressure differences. Bacterial growth, pH of the culture, organic acid consumption, and bacteriochlorophyll a concentration were measured from the liquid samples. The volume of the produced gas was determined volumetrically by water displacement method, and the composition of the gas samples was determined from the gas sample drawn from the top of the bioreactors.

2.3.4 Bacterial growth

Bacterial growth was monitored spectrophotometrically at 660 nm with a

spectrophotometer (Shimadzu UV-1201, Kyoto, Japan). Ten times dilution with distilled water was done for every measurement and distilled water was used as blank. The calibration curves given in Appendix B were used to determine the dry cell weight values (Öztürk, 2005; Uyar et al., 2007).

Bacterial dry cell weight at the end of light and dark periods was determined by centrifugation of 6 mL of bacteria suspension at 13,400 rpm for 10 minutes in a bench-top centrifuge (Eppendorf MiniSpin, Hamburg, Germany), drying the sample overnight at 80°C in a heat sterilizer (Electro-mag, M3025P, Istanbul, Turkey) and then weighing it on an analytical balance (Kern ABJ 220-4NM, Kern & Sohn GmbH, Balingen, Germany).

Bacterial cell numbers were determined by colony count after serial dilutions at the end of light and dark periods for 9 cycles. 1mL sample was taken and diluted in 9 mL of MPYE medium. The final dilution was 10^{-5} after 5 serial dilutions. 100 µL of sample was taken from the last dilution and cultivated on MPYE agar plates by spread plate method. The colony forming unit (CFU)/mL was calculated by first dividing the number of colonies on the plate to 0.1 mL (100 µL) then multiplying it with the dilution factor (10^{-5}).

2.3.5 pH analysis

A pH meter (Ezdo MP-103, GonDO Electronic, Taipei, Taiwan) was used for analysis of the pH of the cultures. It was calibrated with pH standard solutions at pH 7 and pH 4 before use. The pH of the liquid samples was recorderd using a pH meter every 12 hours during bacterial growth and hydrogen production.

2.3.6 Gas analysis

The gas sample was drawn from the top of the bioreactor by a gas tight syringe (Hamilton, 22 GA 500 µL-No. 1750, Bonaduz, Switzerland) and analyzed by a gas chromatograph (GC) (Agilent Technologies 6890N, Santa Clara, CA, USA) with the column SupelcoCarboxen 1010 (Sigma-Aldrich, St. Louis, MO, USA). Argon was the carrier gas with a flow rate of 26 mL/min. The oven, injector and detector temperatures were 140℃, 160℃ and 170℃, respectively. The software used was Agilent Chemstation ver.B.01.01 (Agilent Technologies, Santa Clara, CA, USA). A sample gas chromatogram is given in Appendix C. The millimoles of the produced hydrogen was calculated from the ideal gas equation (PV=nRT). P is the atmospheric pressure taken as 1 atm, V is the volume of the produced hydrogen gas in L, n is the mole of the produced hydrogen, R is the gas constant which is 8.31441 J K-1 mol-1. Finally, T is the temperature in Kelvin, it is 303.15 Kelvin for 30℃.

2.3.7 Organic acid analysis

Liquid bacterial culture samples taken at the end of each light and dark periods were centrifuged at 13,600 rpm for 10 min in a bench-top centrifuge (Eppendorf MiniSpin, Hamburg, Germany). The supernatant was filtered through 45 μm nylon filters (Merck Millipore 13mm, Darmstadt, Germany) and analyzed by High Performance Liquid

Chromatography (HPLC) equipped with Alltech IOA-1000 (300mm ×7.8 mm) column (Fisher Scientific, Waltham, MA, USA) . An auto-sampler (Shimadzu SIL-20AC, Kyoto, Japan) injected 10 μL sample and UV/VIS detector (Shimadzu SPD-20A, Kyoto, Japan) detected the organic acids at 210 nm. The mobile phase was 0.085 M H_2SO_4 with a flow rate of 0.4 mL/min with a low gradient pump (Schimadzu LC-20AT, Kyoto, Japan). The oven (Schimadzu CTO-10AS VP, Kyoto, Japan) temperature was set to 66 ℃. Calibration curves were used to determine the concentration of the analyzed organic acids. The calibration curves for acetic and formic acid are given in Appendix D.

2.3.8 Bacteriochlorophyll *a* analysis

A sample of 1 mL was taken from the photobioreactors at the end of each dark and light periods and centrifuged for 10 minutes at 10,000 rpm (Eppendorf MiniSpin, Hamburg, Germany). The supernatant was discarded and 1 mL of 7:2 (v/v) acetone: methanol was added to the pellet for the extraction of bacteriochlorophyll *a*.

The mixture was homogenized by vortexing for 1 minute. The mixture was centrifuged for 10 minutes at 10,000 rpm in order to remove the proteins. The supernatant was separated and the absorbance of it was measured at 770 nm by a spectrophotometer (Shimadzu UV-1201, Kyoto, Japan). The bacteriochlorophyll *a* content was calculated from the Beer Lambert's Law with the following equation:

$$A = \varepsilon C l \quad (1)$$

where A is the absorbance, ε is the extinction coefficient (mM^{-1} cm^{-1}), C is the concentration in mM and l is the length of the path light follows in the

spectrophotometer cuvette. From this formula the concentration of the bacteriochlorophyll becomes:

$$bchl\ a\ concentration = \left(\frac{Absorbance\ at\ 770nm}{76\ mM{-}1\ cm{-}1x\ 1\ cm}\right)\ x\ (911.5\ g/mol) \qquad (2)$$

As the extinction coefficient ε is 76 mM^{-1} cm^{-1}, l is 1 cm and the molecular weight of bacteriochlorophyll *a* ($C_{55}H_{74}N_4O_6Mg$) is 911.5 g/mol

2.3.9 Data analysis

The important parameters for hydrogen production evaluation are molar hydrogen yield, molar productivity, product yield factor, and light conversion efficiency.

Molar hydrogen yield is calculated as the percentage of produced hydrogen in moles in relation to the moles of hydrogen that can be theoretically produced with the utilization of the organic acids. When the major carbon source is acetate for 1 mole of acetate 4 mole of H_2 is produced theoretically by the following equation:

$$C_2H_4O_2 + 2H_2O \rightarrow 4H_2 + 2CO_2 \qquad (3)$$

Molar productivity Q_{H2} (mmol/Lc.h) was calculated by the following equation:

$$Q_{H2} = N_{H2} / (V_c \cdot t) \qquad (4)$$

where N_{H2} is the number of millimoles of the produced hydrogen, Vc is the volume of the bioreactor (L), and t is the duration of hydrogen production (h).

The duration of light periods were taken into account in the calculations of light conversion efficiency and the molar productivity since hydrogen production stops in dark periods.

Specific growth rate, μ.($h^{-}1$), was calculated during exponential growth phase according to the following equation:

$$\mu = \ln(X/X_0) / (t\text{-}t_0) \qquad (5)$$

where, X_0 is the initial cell concentration (gdcw/Lc) at time t_0 and X is the cell concentration at time *t*.

Product yield factor was calculated by dividing the cumulative hydrogen produced (mmol) by maximum dry cell weight (g). An optical density of 1 at 660nm corresponds to a concentration of 0.55 g dry cell weight per liter of culture (gdcw/L) for *R. capsulatus* DSM1710.

Light conversion efficiency is determined as the ratio of obtained total energy to the total energy input to the photobioreactor by light radiation. It is calculated by the following equation:

$$\eta = ((33.6 \cdot \rho_{H2} \cdot V_{H2}) / (I \cdot A \cdot t)) \cdot 100 \quad (6)$$

where η is the light conversion efficiency in %, 33.6 is the energy density of the hydrogen gas (Watt.h/g), ρ_{H2} is the density of hydrogen gas (g/L), V_{H2} is the volume of the produced gas (L), *I* is the light intensity (Watt/m^2), *A* is the irradiated area (m^2) and *t* is the duration of hydrogen production (h). In this study, 2000 lux was equal to 114 W/m^2, while 3500 lux is 200 W/m^2, 5000 lux is 285.7 W/m^2, 7000 lux is 400 Watt/m^2 and 10,000 lux to 571.4 Watt/m^2. The conversion factor was determined as 1W/m^2 = 17.5 lux (Uyar, 2008). Irradiated area of 150 mL cylindrical glass bottle photobioreactor is 0.011 m^2.

In order to compare the hydrogen production assessment parameters of different conditions statistically, two-sample t-tests were applied using Minitab 13.0 Software.

2.4 Transcriptome Analysis

The expression analysis of *R. capsulatus* DSM1710 was carried out at both gene-level by RT-qPCR and at whole genome level by microarray. The bacteria were exposed to three light and dark periods where the light intensity was 2000 lux. In order to mimic the outdoor conditions, where bacteria can be exposed to a low light intensity by the sunrise and a higher light intensity at noon, in the middle of the third light period (6^{th}

hour) light intensity was increased to 10,000 lux. Samples were taken at the end of the third dark period, 15 min and 1 hour after exposure to light period (2000 lux) and 15 min and 1 hour after exposure to 10,000 lux. Total RNA was isolated from each sample to be the starting material for transcriptome analyses.

2.4.1 RNA isolation

Total RNA was isolated from $1.5x10^9$ bacterial cells which were grown under indicated conditions and taken into sterile microcentrifuge tubes. Modified protocol of Chomczynski and Sacchi (1987) was followed during RNA isolation. Bacteria were centrifuged at 12,000 g for 15 min at 4 ℃. The cells in the pellet were lysed by 200 µL 5 mg/mL lysozyme (Sigma-Aldrich, activity ≥ 40,000 units/mg protein, Taufkirchen, Germany) which was prepared in 1X Tris EDTA (TE) buffer (10mM Tris, 1mM EDTA, pH 8.0). The composition of the TE buffer is given in Appendix E. The samples were incubated at 37 ℃ for 10 min in a heater block (WTW-CR 3200, Weilheim, Germany). After that, 3 mg/mL proteinase K (AppliChem, activity 37.5 m Anson U, Darmstadt, Germany) was added in 20 µL on lysed cells and incubated at 60 ℃ for 10 min. Then, 1 mL of TRIzol® Reagent (Invitrogen, Carlsbad, CA, USA) was added, the mixture was vortexed for 1 min and incubated at room temperature for 5 min. 200 µL of chloroform (Merck, Darmstadt, Germany) was added onto the mixture and mixed by vigorous shaking for 15 seconds, let at room temperature for 6 min and centrifuged at 12,000 g for 15 min at 4 ℃. Three phases appear after this step: the upper most clear phase containing RNA, the middle phase containing DNA and the bottom phase containing cell debris, proteins and TRIzol® Reagent. 650 µL of the upper phase was taken into a new sterile microcentrifuge tube onto which 500 µL cold isopropanol was added. The mixture was mixed 40 times by inverting and kept at room temperature for 10 min, then centrifuged at 17,000 g for 10 min at 4 ℃. Supernatant was removed and RNA pellet was washed with 1 mL of 80% ethanol (Merck, Darmstadt, Germany) by centrifugation at 20,000 g for 10 min at 4 ℃. The supernatant was removed and the

pellet was air dried and dissolved in 20 µL of sterile ultrapure water and incubated at 60 ℃ for 10 min for better dissolution . The RNA solution was then kept at -80 ℃ for later use.

2.4.1.1 Concentration of RNA

For prokaryotic microarray chips, the total RNA concentration must be high. The concentration of the isolated RNA was determined by Multiskan™ GO Microplate Spectrophotometer (ThermoFisher Scientific, Waltham, MA, USA). 1µL of RNA sample was used for the measurement as sterile ultrapure water was used as blank. The software used was SkanIt™ microplate reader software. Absorption at 260 nm gives the concentration of nucleic acids and an absorbance of 1.0 at 260 nm correlates to 40 µg/µL RNA. Absorption at 280 nm gives idea about the contamination of proteins since proteins give absorbance at this wavelength. Protein contamination in RNA samples would be problematic in microarray and qPCR experiments, thus absorbance at 280 nm is important and the ratio of 260/280 should be between 1.8-2.1 (Dumur et al., 2004).

2.4.1.2 Integrity of RNA

In order to detect the integrity of the isolated total RNA samples, Agilent 2100 Bioanalyzer was used (Agilent, Santa Clara, CA, USA) with 1 µL of total RNA loaded into the gel based RNA 6000 NanoChip. Sample Bioanalyzer electrophoresis gel image for *R. capsulatus* and related electropherogram are given in Appendix F.

2.4.2 Microarray Analysis

Affymetrix Expression Analysis Technical Manual for Prokaryotic Target Preparation was followed for protocols from preparation of cDNA from total RNA to hybridization of cDNA onto custom designed microarray chips, and to scan the chips. The protocol is given in detail by Gürgan (2011). The protocol is basically shown in Figure 2.2.

The custom designed microarray chips for *Rhodobacter capsulatus* was designed according to GeneChip® Custom Expression Array Design Guide. The DNA of *R. capsulatus* was sequenced by Strnad et al (2010). The chip was named as Affymetrix.GeneChip®.TR_RCH2a520699F. It was a prokaryoric antisense DNA array. The feature size was 11 micron and the chip format was 100-3660. The probes were selected from 600 bases from 3' end of the gene and intergenic region sequences. 13 probe pairs were produced for each sequence by match/mismatch probe strategy, i.e. a mismatch probe having a single base mismatch in its center was generated. All sequences were pruned against all other sequences. Totally 4052 probe sets were present on the array.

2.4.3 Reverse transcription for microarray analysis

The starting material was 10 µg total RNA which was mixed with 10 µl of 100 ng/µl random primers (Invitrogen, Waltham, MA, USA) in an RNase free microcentrifuge tube. Poly-A RNA controls containing polyadenylated trasncripts of *B. subtilis* genes and nuclease free water was added to make the volume 30 µL. For the reverse transcription reaction, RNA/primer mix was incubated at 70 ℃ for 10 min and 25 ℃ for 10 min, then chilled to 4 ℃. Then onto this mix, 7.5 µL 200U/µL SuperScriptII™ Reverse Transcriptase, 12 µL first strand buffer (Invitrogen), 6 µL 100 mM DTT (Affymetrix, Waltham, MA, USA), 3 µL 10 mM dNTP (Invitrogen) and 1.5 µL 20U/ µL SUPERase•In™ (ThermoFisher Scientific, Waltham, MA, USA) was added. The 60 µL mix was incubated at 25 ℃ for 10 min, 37 ℃ for 60 min, 42 ℃ for 60 min and 70 ℃ for 10 min, and chilled to 4 ℃.

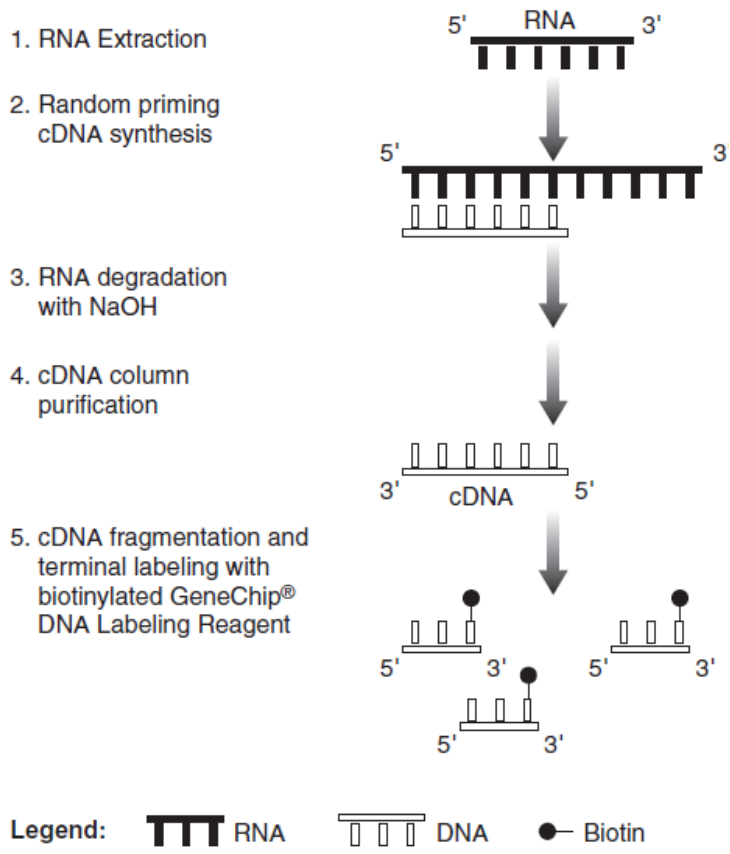

Figure 2. 2 Target labeling for prokaryotic GeneChip® antisense arrays (Affymetrix expression analysis technical manual)

2.4.3.1 Removal of RNA, Purification and Quantification of cDNA

The RNA was degraded by addition of 20 µL 1N NaOH (Merck, Darmstadt, Germany) and incubation at 65 ℃ for 30 min. Then, 20 µL 1N HCl (Merck, Darmstadt, Germany) was used to neutralize NaOH.

Purification Beads of GeneChip® 3' IVT PLUS Reagent Kit (Affymetrix, Waltham, MA, USA) was used to purify the cDNA from the mixture above. 100 µL magnetic beads were mixed with 60 µL cDNA sample by pipetting up and down in 2 mL U-bottom microcentrifuge tube and incubated for 10 min. The samples were moved to a magnetic stand and let for 10 min so that the Purification Beads are captured by the

magnetic stand. The supernatant was discarded carefully without disturbing the Purification Beads. Then 800 µL 80% ethanol was added, let for 20 seconds.

The ethanol solution was discarded with care and air-dried for 5 min at room temperature. Then the samples were removed from the magnetic stand and 12 µL nuclease free water was added onto the beads and mixed by pipetting. The tubes were placed to the magnetic stand for about 5 min to capture the Purification Beads. The supernatant containing the eluted cDNA was removed carefully. The concentration of the cDNA in 1 µl was measured by in-tip micro-volume spectrophotometer (AlphaSpec™, Alpha Innotech, San Leandro, CA, USA) at 260nm. At least 1.5 µg cDNA was needed to continue to the next step and to obtain sufficient amount of material to hybridize onto the microarray chip.

2.4.3.2 Fragmentation of cDNA

Fragmentation of 10 µL cDNA was carried out by addition of 2 µL 10X Dnase Buffer (Ambion, Waltham, MA, USA), Dnase I (Ambion, 2U/µL, Waltham, MA, USA) and nuclease free water (Affymetrix, USA). The amount of Dnase I was calculated to be 0.6 U Dnase I for 1 µg of cDNA. The reaction mix was incubated at 37 °C for 10 minutes. Then Dnase I was inactivated at 98 ^{0}C for 10 minutes.

2.4.3.3 Labeling of cDNA

The fragmented cDNA was then labelled by biotin at the 3' termini. 20 µL fragmented cDNA was mixed with 2 µL 7.5 mM GeneChip® DNA Labelling Reagent (Affymetrix, USA), 2 µL Terminal Deoxynucleotidy Transferase (Promega, 30 U/µL, Madison, WI, USA) and 10 µL its reaction buffer 5X Reaction Buffer, and 16 µL nuclease free water (Affymetrix, USA). The reaction mix was incubated at 37 ^{0}C for 60 min. After that the reaction was stopped by adding 2 µL 0.5M EDTA (Invitrogen, pH 8, Waltham, MA, USA).

2.4.3.4 Hybridization

The microarray chips to be used were previously custom designed in our laboratory (Gürgan, 2011) and manufactured by Affymetrix. They were named as Affymetrix.GeneChip®.TR_RCH2a520699F. They are 100 format chips, thus the hybridization coctail for the hybridization of fragmented and labelled cDNA was prepared in 130 µL. The cDNA used for hybridization was 1.5 µg. It was mixed with 2.2 µL 3 nM Control Oligo B2, 65 µL 2X hybridization mix, 10.2 µL DMSO and 6.5 µL 20X Hybridization Control and an amount of water (volume determined according to the volume of cDNA) from GeneChip® Hybridization, Wash and Stain Kit (Affymetrix, USA). This mixture was loaded into the arrays carefully as shown in the manual. The chips were incubated at 50 ^{0}C for 16 hours in the GeneChip® Hybridization Oven 640 (Affymetrix, USA) where the rotation was at 60 rpm.

2.4.3.5 Washing, Staining and Scanning

After the hybridizaiton step, the arrays were washed and stained at GeneChip® Fluidics Station 450 (Affymetrix, USA) operated by GeneChip® Operating Software (GCOS) in METU Central Lab Molecular Biology and Biotechnology R&D Center. The fluidics protocol was Flex FS450_0002. Wash A, Wash B and distilled water were used fo washing; and Stain Coctail 1 (600 µL), Stain cocktail 2 (600 µL) and Array Holding Buffer (800 µL) of the kit were used for staining the arrays.

After washing and staining was complete, the chips were scanned using GeneChip® Scanner 3000 (Affymetrix, USA) operated by GCOS. Chip image after the scanning was provided as a .DAT file. It was inspected for any image artifacts. A sample .DAT image of the is given in Figure 2.3.

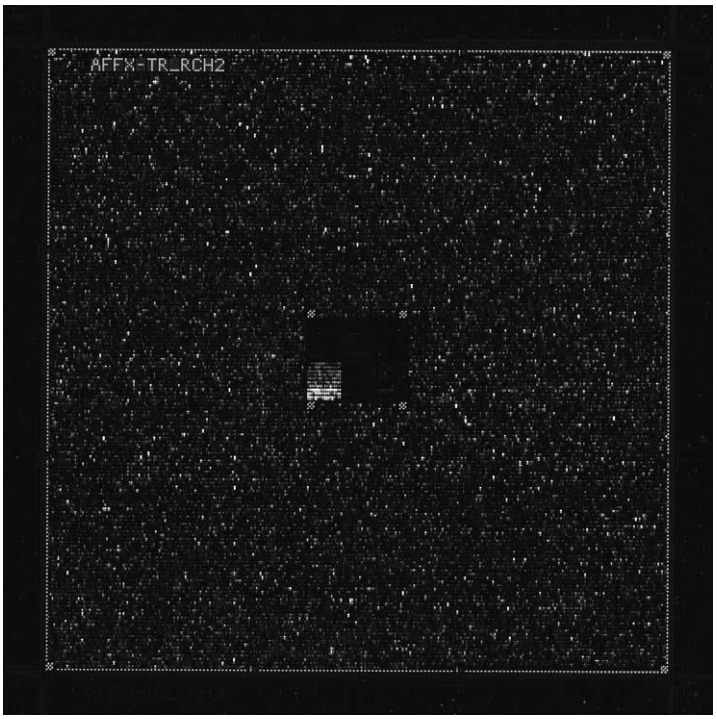

Figure 2. 3 The Affymetrix GeneChip® scan image of custom design array *R.capsulatus* DSM1710

2.4.3.6 Microarray Data Analysis

The .CEL files provided by GCOS were processed in BRB Array Tools (Simon et al., 2007). Quality control analysis on samples were carried out in this software with correlation and principal component analysis. The raw data was normalized using Robust Multiarray Analysis (RMA). The resulting data were then filtered with the fold change analysis. The genes showing more than 2.0 fold change were subjected to statistical analysis with one way ANOVA followed by Benjamini-Hochberg correction with GeneSpring GX 14.8 software. The entities that satisfied the significance analysis ($p \leq 0.05$) were then classified into appropriate metabolisms.

2.4.4 Real time qPCR

In order to validate the microarray results, real time qPCR was performed on selected genes related to hydrogen production and energy metabolism. The primers for the

selected genes were designed with Primer 3 software (Untergasser et al., 2012). The list, functions and the primer designs of the selected gene are given in Table 2.1

Table 2. 1 Primer sequences of the genes used in real time qPCR

Gene	Gene Function	Forward primer (5'>3')	Reverse primer (3'>5')
16s rRNA	Ribosomal RNA	GCTAGTAATCGCGTAACAGCA	CAGTCACTGAGCCTACCGT
atpF	ATP synthase subunit b	CAGAAGATCCTGGCGAGCTA	GATCCTTGACGTCCTTCAGC
pucA	Light-harvesting protein B-800/850 alpha chain	AAAATCTGGACCGTCGTCAA	GGTTGCCGTTCCAGTAGTTC
pufL	Reaction center protein L chain	CTGCGTGAAGTCGAAATCTG	GAGGTGCGTCCAGATACCAT
pufM	Reaction center protein M chain	AAATGGGCCTCAAGGAAGAC	AGAACAGATCCCGCATGAAG
nifH	Nitrogenase iron protein 1	ACGTCGTGAAAATCGGCTAC	TAGATTTCCTGCGCCTTGTT
fdxN	Ferredoxin 1	TGAAGATCGATCCCGAACTC	GTTGATGCAGTTGTCGGTCA
idi	Isopentenyl-diphosphate delta isomerase 1	ATGATCGAGCATGAGGTGGT	GTTGAGCCATTTCGAGAACC

2.4.4.1 Reverse Transcription for RT-qPCR analysis

The gene expression analysis by real time qPCR begins with reverse transcription of total RNA to cDNA. This was achieved by Transcriptor High Fidelity cDNA Synthesis Kit (Roche, Mannheim, Germany). Into a sterile microcentrifuge tube, 1 µg of total RNA was added together with 2 µL of random hexamer and PCR grade water to make the volume 11.4 µL. This primer-template mixture was heated at 65 ℃ for 10 min in a thermal cycler (Applied Biosystems, 96-well GeneAmp® PCR System 9700, ThermoFisher Scientific, Waltham, MA, USA) to denature RNA secondary structures.

Then, 4 µL 5X Transcriptor High Fidelity Transcriptase Reaction buffer, 0.5 µL Protector Rnase Inhibitor, 2 µL Deoxynucleotide mix (10mM each), 1 µL DTT, 1.1 µL Transcriptor High Fidelity Reverse Transcriptase were added to the tube and incubated at 29 ℃ for 20 min, 48 ℃ for 60 min and 85 ℃ for 5 min.

2.4.4.2 Real time qPCR protocol

LightCycler 480 (Roche, Manheim, Germany) in METU Central Lab Molecular Biology and Biotechnology R&D Center was used as real time qPCR instrument for amplification and detection of the quantitative PCR reactions in this study. SYBR Green I was used as the fluorescent dye to bind to the nucleic acids to detect the amplification. The reaction set up and the reaction protocol are given in Table 2.2 and Table 2.3.

Table 2. 2 Reaction set up for RT qPCR

Reagent	**Final Concentration**	**Volume (µL) / one reaction**
Water		1.0
Primer – Forward (5 µM Stock)	0.5 µM	2.0
Primer – Reverse (5 µM Stock)	0.5 µM	2.0
LightCycler® 480 SYBR Green I Master	1x	10.0
Template DNA		5
	Total	15.0

2.4.4.3 Real time qPCR data analysis

Melting curve analysis was performed to determine whether the desired PCR product is free of nonspecific by-products. The reaction mixture was slowly heated to 95°C, which causes the double stranded DNA to melt. The software plots a derivate melting curve to detect the melting temperature ™. The melt curve analysis for *nifH1* gene is given as an example in Figure 2.4.

Table 2. 3 Real time qPCR protocol

Program		Temperature	Time	Cycle
Preincubation		95°C	5 min	1
Amplification	Denaturation	95°C	10 sec	45
	Annealing	58°C	5 sec	
	Extension	72°C	Product [bp]/25s*	
Melting Curve		95°C	5 sec	
		65°C	1 min	1
		97°C		
Cooling		40°C	10 sec	1

*16srRNA: 146/25=5.84 Extention time: 6
afpF: 205/25= 8.2 Extention time: 8
fdxN: 179/25= 7.16 Extention time: 7
idi: 162/25= 6.48 Extention time: 7
nifH1: 220/25= 8.8 Extention time: 9
pucA: 133/25= 5.32 Extention time: 6
pufM: 219/25= 8.76 Extention time: 9
pufL: 159/25=6.36 Extention time: 7

Quantification cycle (Cq) is the output of RT-qPCR by LightCycler 480. They were detected and used for the analysis of differential gene expression for each 9 genes. The normality of the Cq values for each gene was checked with Shapiro-Wilk test using the R software. After that, comparison of light application conditions with the control condition (dark) for each gene was performed using paired t-test as the samples were from the same bacterial cultures.

Relative quantification method was adopted for the data analysis. The endogenous control or the reference gene used for the normalization of sample to sample differences was 16s rRNA. Relative quantification was accomplished using E-Method of Roche, which is based on the comparative Ct method, also known as ΔΔCt method (Livak & Schmittgen, 2001; Tellmann, 2006).

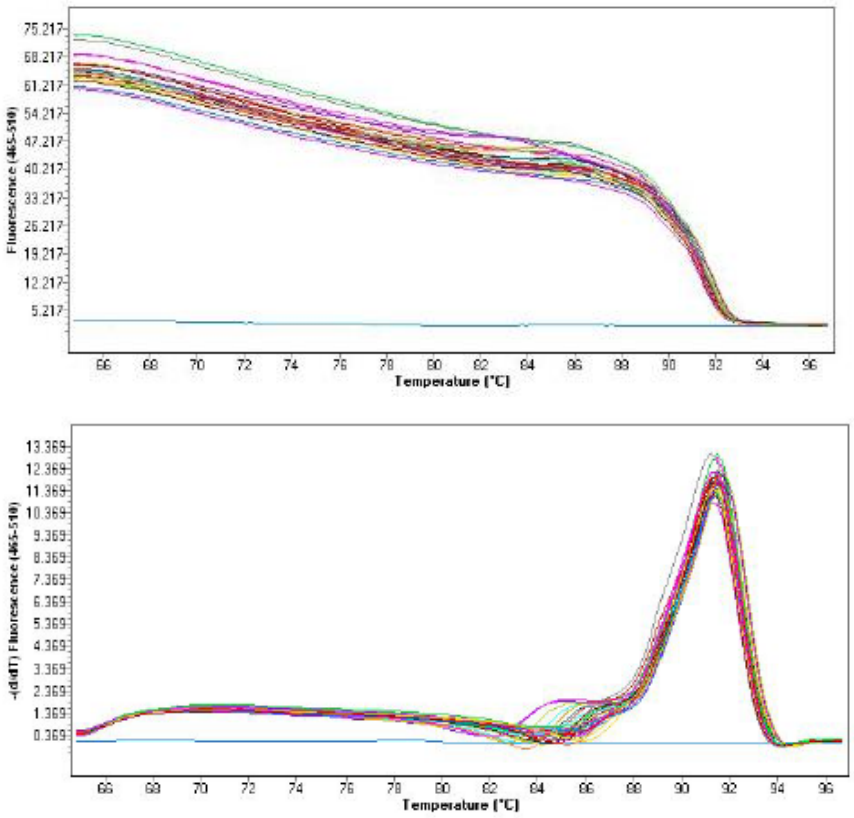

Figure 2. 4 Melting curve analysis for *nifH1* gene

The amount of target normalized to endogenous reference and relative to calibrator, so the fold change difference, was calculated as:

$$\text{Amount of target} = 2^{-\Delta\Delta Ct} \quad (7)$$

where

$$\Delta Ct = Ct \text{ (a target gene)} - Ct \text{ (a reference gene)}$$

$$\Delta\Delta Ct = \Delta Ct \text{ (a target sample)} - \Delta Ct \text{ (a reference sample)}$$

In this study, the reference gene was selected to be 16s rRNA, thus Ct values of this reference gene was subtracted from the corresponding Ct values of the target genes. The reference sample, called the control in this study, was the sample taken at the end

of dark period. The ΔCt of the target samples, i.e. 15 minutes and 1 hour of low light intensity (2000 lux) application, and 15 minutes and 1 hour of high light intensity (10,000 lux) applications.

CHAPTER 3

RESULTS AND DISCUSSION

In this study the effects of light intensity on the physiology and the transcriptome of *Rhodobacter capsulatus* were assessed. Growth, hydrogen production, organic acid consumption and production, and bacteriochlorophyll *a* contents of *Rhodobacter capsulatus* wild type and uptake hydrogenase deficient mutant (*hup*$^-$) strain were measured at dark and under different light intensities. In order to understand the metabolic changes at gene level, gene expression analysis at the same conditions were analyzed by microarray and real time quantitative PCR.**Effect of Light Intensity on Physiology**

The hydrogen production rate and yield are known to be dependent on changes in temperature and light intensity (Androga et al., 2014) At first, *Rhodobacter capsulatus* was exposed to three different light intensities in order to determine a light intensity which might cause a stress. The optimum light intensity for *R. capsulatus* for hydrogen production under continuous illumination was determined to be 4000 lux (Akman et.al., 2014) and over 270 W/m^2 (around 4725 lux), hydrogen production of *R. sphaeroides* O.U.001 was shown to decrease significantly (Basar Uyar et al., 2007). Therefore, the low light intensity in this set of experiment was set as 2000 lux (114.3 W/m^2) and high light intensity was chosen to be 5000 lux (285.7 W/m^2). An intermediate light intensity (3500 lux, 200 W/m^2) was also tested to see the transition from 2000 to 5000 lux. The growth of the bacteria, hydrogen production and bacteriochlorophyll *a* concentrations measured at the end of each light and dark cycles (after each 12 hours) are shown in Figure 3.1 and the hydrogen production assessment parameters are given in Table 3.1.

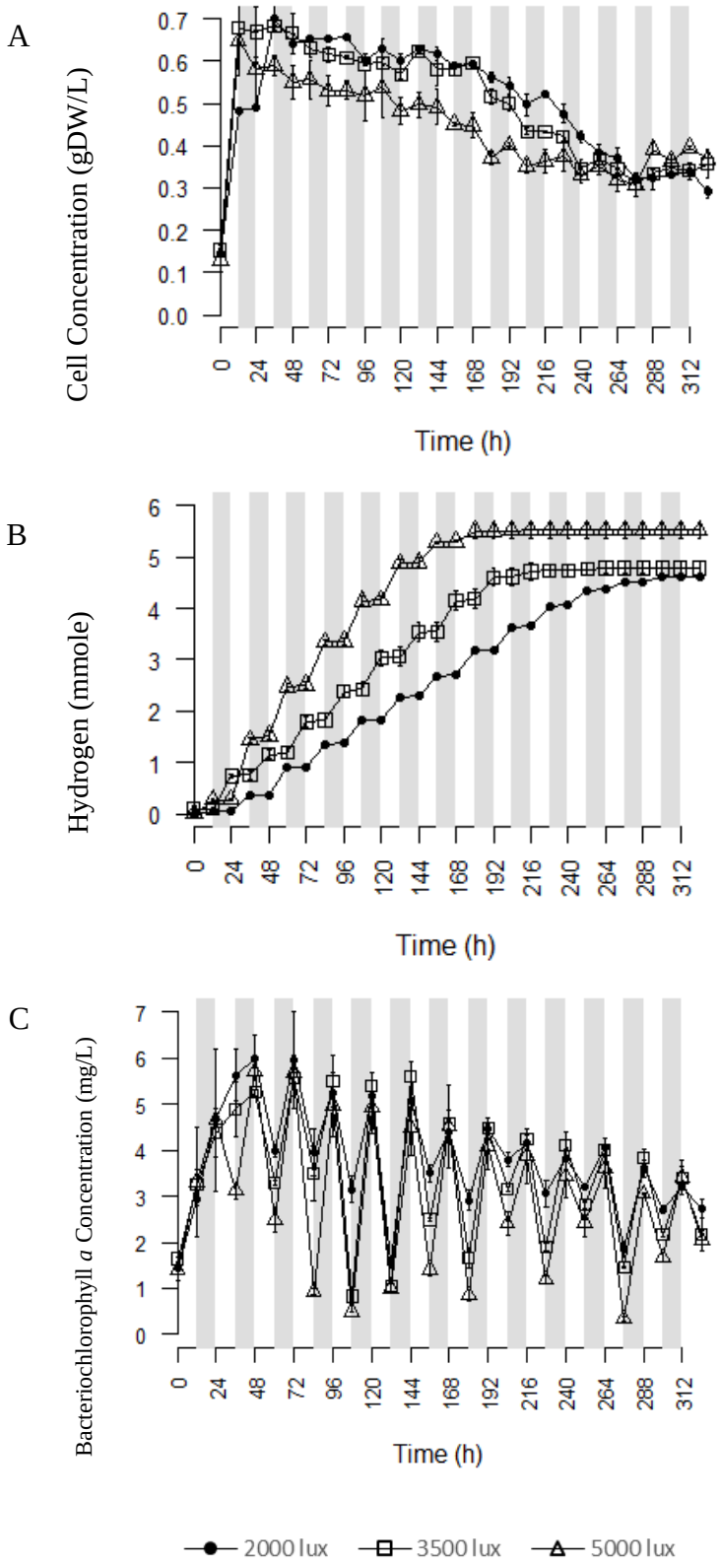

Figure 3. 1 Bacterial growth (A), hydrogen production (B) and bacteriochlorophyll *a* content (C) of *R. capsulatus* wild type under different light intensities. The shaded bands indicate the dark periods. Data are shown as mean ± SEM, n=3.

Molar hydrogen productivity of *R. capsulatus* DSM1710 was similar under 2000 and 3500 lux, but higher under 5000 lux (Table 3.1). The higher light intensity also decreased cell concentration which suggests that under cyclic illumination 5000 lux did not inhibit but enhanced hydrogen production of *R. capsulatus*. Bacteriochlorophyll *a* concentration varied inversely with the presence of light and its intensity (Figure 3.1 C). It is the photsynthetic pigment responsible for light harvesting. In the dark periods, more bchl *a* was produced, and concentration decreased in the presence of light, since bacteria were in shortage of energy in dark and in order to gather more light they synthesized bchl *a*. However in the light periods, the higher the light intensity, the lower the bchl a concentration. This was for the protection of the photosynthetic system from damage that can happen due to high light intensity.

Table 3. 1 Hydrogen production assessment parameters for *R. capsulatus* DSM1710

	Max. dry cell weight (gdcw/Lc)	Specific Growth Rate, μ (h^{-1})	Product yield factor (mmol/g)	Molar QH_2 (mmol/(Lc.h))	Molar yield of H_2 (%)	Light Conversion Efficiency (%)
2000 lux	0.70±0.03	0.096±0.002	44.1±0.03	0.22±0.24	25.4±0.03	0.095±0.001
3500 lux	0.68±0.03	0.12±0.001	47.0±0.12	0.23±0.03	25.3±0.24	0.061±0.003
5000 lux	0.65±0.02	0.14±0.004	56.6±0.16	0.33±0.08	29.8±0.08	0.068±0.002

The lowest bacterial growth was observed at 5000 lux. In contrast, hydrogen production not only did not stop, but was enhanced at 5000 lux light intensity. Hence, an even higher light intensity should have been selected to provoke a stress response in the bacteria. In lab scale experiments, in temperature controlled incubators where the illumination was supplied by tungsten lamps, increasing the light intensity was not feasible as a high number of lamps are needed. Furthermore, over 7000 lux light intensity, the temperature of the cultures caused by light radiation exceeded the capacity of incubators to cool reactor bottle. Thus, it was impossible to keep the cultures at 30°C for a long time. The physiological experiments were thus decided to

be carried out at 2000 and 7000 lux light intensities in a second run.

The uptake hydrogenase deficient mutant of *Rhodobacter capsulatus* (YO3) was also tested and compared with the wild type under these light intensities. Similarly, growth, hydrogen production, pH of the medium, bacteriochlorophyll a content, and additionally, organic acid consumption and production were determined. The experiment was conducted until hydrogen production stopped by slowest hydrogen producing condition. The pH of the media in both experimental runs were in the range of 6.7-7.4, which is in the optimum range for hydrogen production (Sasikala et.al, 1991). The parameters used to evaluate hydrogen production are summarized in Table 3.2.

Table 3. 2 Hydrogen production assessment parameters for *R. capsulatus* DSM1710 and *R. capsulatus* YO3

		Max. dry cell weight (gdcw/Lc)	Specific Growth Rate, μ (h^{-1})	Product yield factor (mmol/g)	Molar QH_2 (mmol/(Lc.h))	Molar yield of H_2 (%)	Light Conversion Efficiency (%)
Wild DSM 1710	Low light (2000 lux)	0.71±0.007	0.06±0.008	42.7±0.47	0.26±0.01	25.5±0.28	0.1±0.001
	High light (7000 lux)	0.68±0.0005	0.065±0.01	57.7±1.3	0.61±0.01	34.0±1.08	0.04±0.001
Mutant YO3	Low light (2000 lux)	0.79±0.003	0.039±0.003	57.4±0.18	0.75±0.02	37.6±0.16	0.19±0.001
	High light (7000 lux)	0.74±0.0005	0.059±0.02	86.0±0.32	1.44±0.03	51.4±0.73	0.09±0.001

2.1.1 Effect of Light Intensity on Bacterial Growth

Bacterial cell concentration of both the wild type (DSM1710) and the mutant (hup^-, also called YO3) *Rhodobacter capsulatus* was followed by light absarbance at 660nm (Figure 3.2). The OD values increased during the light periods, and decreased during

the dark periods until the growth curve entered the death phase. The maximum dry cell weights wild type *R. capsulatus* under high light intensity was lower than low light intensity ($p=0.023$) (Table 3.2). The mutant bacteria have a higher specific growth rate under high light intensity, although the maximum dry cell weight under high light was lower than low light intensity ($p=0.003$). Bacterial dry cell weights were calculated using the calibration constants (Appendix B). During dark periods, polyhydroxybutyrate in the cells could have been used which might have caused a decrease in the cell size. This was suspected to be a reason of decreased optical density. Therefore, dry cell weight and colony count were performed. All the results showed that the trend of bacterial absorption decrease in dark periods corresponded to a decrease in bacterial dry cell weight and also cell number, as demonstrated in Figure 3.3. When the illumination was off, lack of ATP energy primarily produced by photofermentation might have caused lysis of some bacteria until the metabolism of shift to dark fermentation and adapt to non-light condition. *R. capsulatus* has diverse metabolic routes, and dark fermentation mode is activated during dark periods. This result is supported by acetate production in the dark, discussed in section 3.1.3.

Higher product yield factor values under high light intensities (Table 3.2) is a result of increased hydrogen production under high light intensity by both of the bacterial strains. Therefore, light intensity of at least 7000 lux is suggested for more efficient hydrogen production when the illumination mode is light/dark cycles.

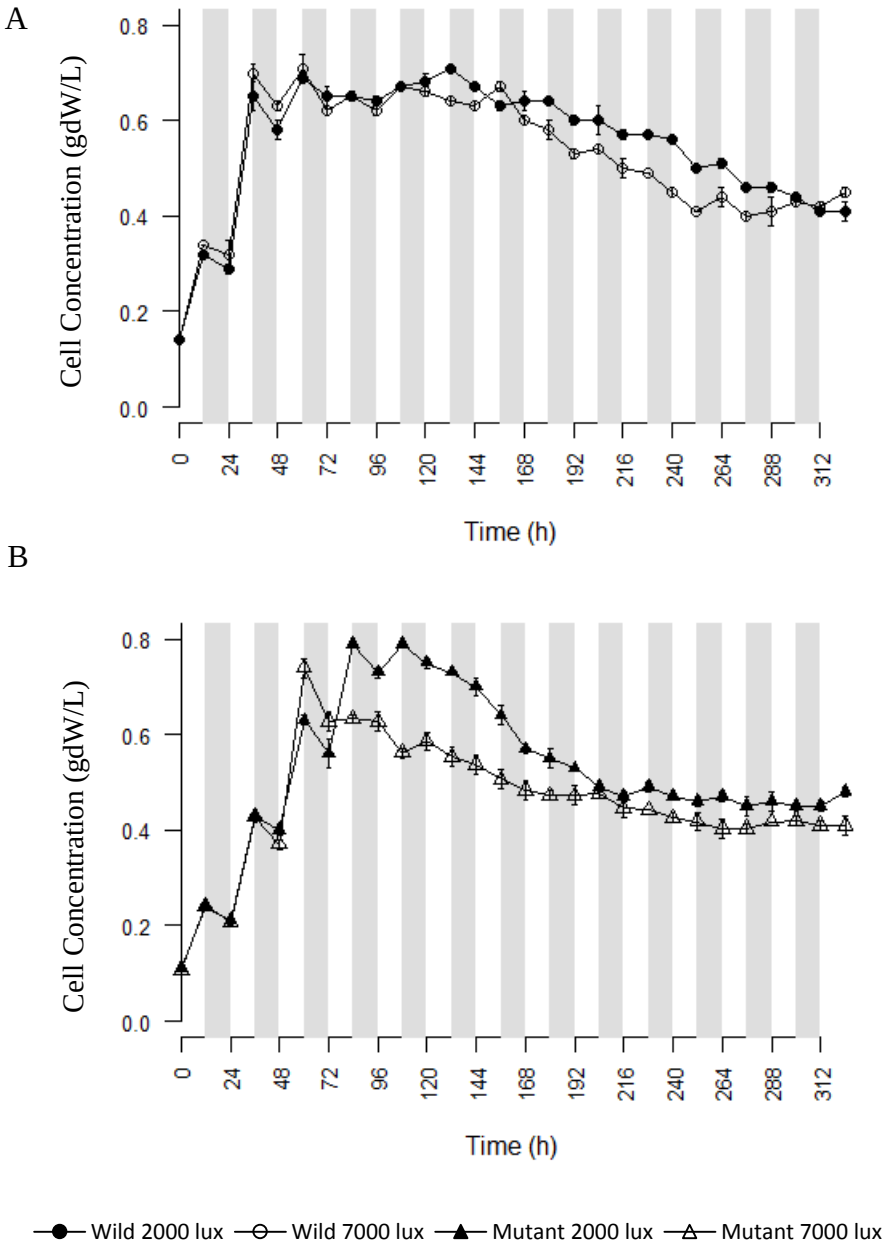

Figure 3. 2 Growth of *Rhodobacter capsulatus* wild type (A) and YO3 (B) under low (2000 lux) and high (7000 lux) light intensities. The shaded bands indicate the dark periods. Data are shown as mean ± SEM, n=3.

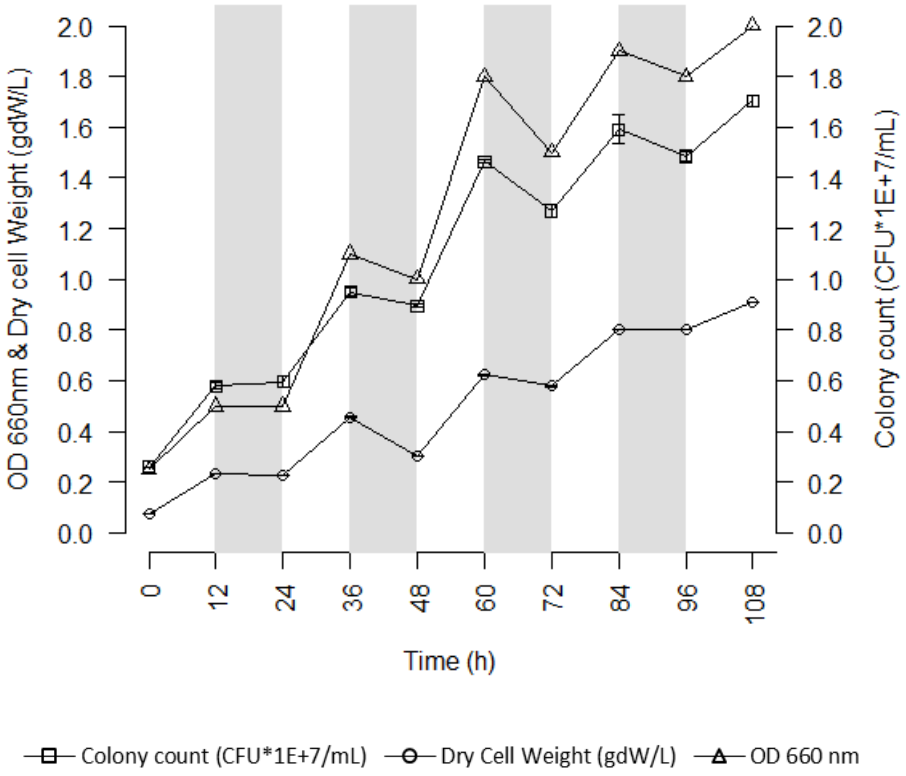

Figure 3. 3 Comparison of optical density with bacterial dry cell weight and cell number of wild type *R. capsulatus* under light/dark periods. The shaded bands indicate the dark periods. Data are shown as mean ± SEM, n=3 (n=2 for colony count).

2.1.2 Effect of Light Intensity on Hydrogen Production

The produced gas was composed of about 85% H_2 and about 15% CO_2 throughout the experiments. Hydrogen production by both bacterial strains stopped in the dark periods, as expected (Figure 3.4). In PNSB hydrogen production by nitrogenase depends on photosynthesis, therefore in dark periods, nitrogenase cannot mediate the hydrogen production reaction due to the absence of light energy and photosynthesis. Hydrogen production started once illumination was resumed, consistent with the literature (Li et al., 2011).

The duration of the slowest hydrogen producer was wild type *R. capsulatus* under low light intensity in this study and it was 312 h. High light intensity increased the rate of hydrogen production by *R. capsulatus* DSM1710 and YO3 significantly (p=0.009 and

p=0.002, respectively). Similarly, molar hydrogen yields of wild and mutant strains were also increased by high light intensity (p=0.008 and p=0.001), respectively.

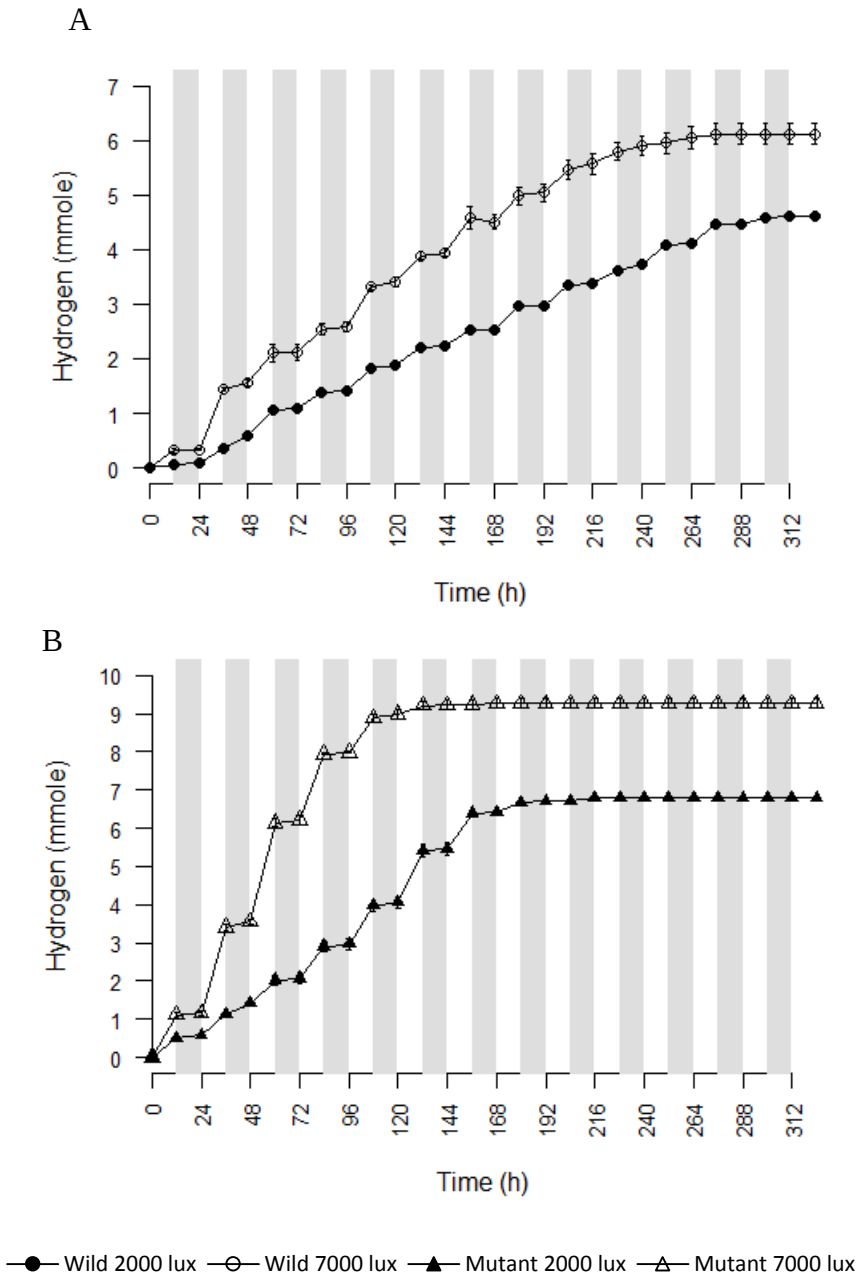

Figure 3. 4 Hydrogen production of *Rhodobacter capsulatus* wild type (A) and YO3 under low (2000 lux) and high (7000 lux) light intensities. The shaded bands indicate the dark periods. Data are shown as mean ± SEM, n=3.

In two previous studies, maximum hydrogen production rate of *R. capsulatus* was 0.56 mmol/Lc.h and it decreased above 280 W/m2 (about 4900 lux) under continuous illumination (Androga et al., 2014), and above 5000 lux, hydrogen production of *R. sphaeroides* stopped (Uyar et al., 2007) when the illumination protocol was light/dark cycles. On contrary to those studies, 7000 lux was not inhibitory but enhanced hydrogen production of *R. capsulatus* when the illumination protocol was cyclic (12h/12h) light/dark periods. Enhanced hydrogen production by high light intensity can be explained by the action of nitrogenase enzyme to dissipate excess reducing power in the cell (Adessi & De Philippis, 2013).

It is known that higher light intensities decrease light conversion efficiency of PNSB (Hoekema et al., 2006; Androga et al., 2012). In this study the light conversion efficiency was significantly lower (more than twice) for high light intensity for both stains (p=0.000 for both) (Table 3.2).

2.1.3 Effect of Light Intensity on Organic Acid Consumption and Production

In this study acetate was used as carbon source because most of the dark fermenter effluents contain acetate as the main by-product and they are used for photofermentation in integrated system to enhance hydrogen production (Afsar et al., 2011; Afşar et al., 2009; Özgür & Peksel, 2013; Basar Uyar et al., 2015) The initial 30 mM of acetate was completely consumed under all conditions (Figure 3.5). Mutant strain consumed all the substrate after 156 h under low light intensity, and 108 h under high light intensity, which means the rate of substrate consumption of mutant *R. capsulatus* increased by increasing light intensity. The consumption of substrate and hydrogen production were in parallel - hydrogen production of *hup*$^{-}$ *R. capsulatus* ceased at almost the same time of consumption of substrate. On the other hand, increasing light intensity did not enhance the rate of acetate consumption of wild type *R. capsulatus*, the rates of acetate consumption were not significantly different.

Production of acetate under some dark periods is worth mentioning. This could be because of the metabolic shift of *R. capsulatus* from photofermentation to dark

fermentation in the lack of light. Under anaerobic dark conditions Pta-Ack (phosphotransacetylase - acetate kinase) pathway was activated where acetyl-CoA is converted to acetylphosphate by phosphotransacetylase (Pta) first, then acetylphosphate is converted to acetate by the action of acetate kinase (Ack) (Bock et al., 1999). *Rhodobacter capsulatus* carry the genes of the Pta-Ack pathway, thus it can produce acetate via this pathway in the dark periods.

In a previous study, *R. sphaeroides* produced butyrate in dark cycles (Eroglu et al., 2008). In this study no considerable amount of butyrate but significant amount of formate was produced by both wild and mutant strains (Figure 3.6). The continuous illumination did not result in production of formate by wild type *R. capsulatus* on acetate (Uyar et al., 2015), however cyclic illumination did, as in this study. The difference between the formate production and utilization of bacterial strains and the light intensities is interesting. Mutant strain produced only about 1 mM formate under low light intensity, and 2 mM formate under high light intensity and utilized about half of it. On the other hand, wild type strain produced about 2 mM under low light and about 7 mM under high light intensity but did not utilize significantly, so formate was accumulated in the culture. Formate is produced either by cleavage of pyruvate or enzymatic reduction of CO_2 in an NADH or ferredoxin dependent manner (Crable et al., 2011). When the carbon source is lactate or malate, the oxidation of them to pyruvate can result in formate production under anaerobic fermentative mode by pyruvate formate lyase enzyme. In this study, however, since the carbon source is only acetate, the formate production should have occurred via reversible NAD+ dependent formate dehydrogenase of Wood-Ljungdhal pathway (Wood et.al., 1986). This enzyme reduces NAD^+ to NADH and leads formate oxidation (Eq. (10)) to CO_2 and the enzyme is expressed by the *fds* operon in *R. capsulatus.* When the products of *fds* operon are present, NAD+ dependent formate dehydrogenase encoded by *fdhA* can be transcribed (Hartmann & Leimkühler, 2013). In fact, the microarray data have shown up-regulation of formate dehydrogenase gene *fdhA* by shift to light intensity which is consistent with formate production in the light periods (Appendix G).

$$CO_2 + NAD(P)H \leftrightarrow HCOO- + NAD(P)+ \quad (10)$$

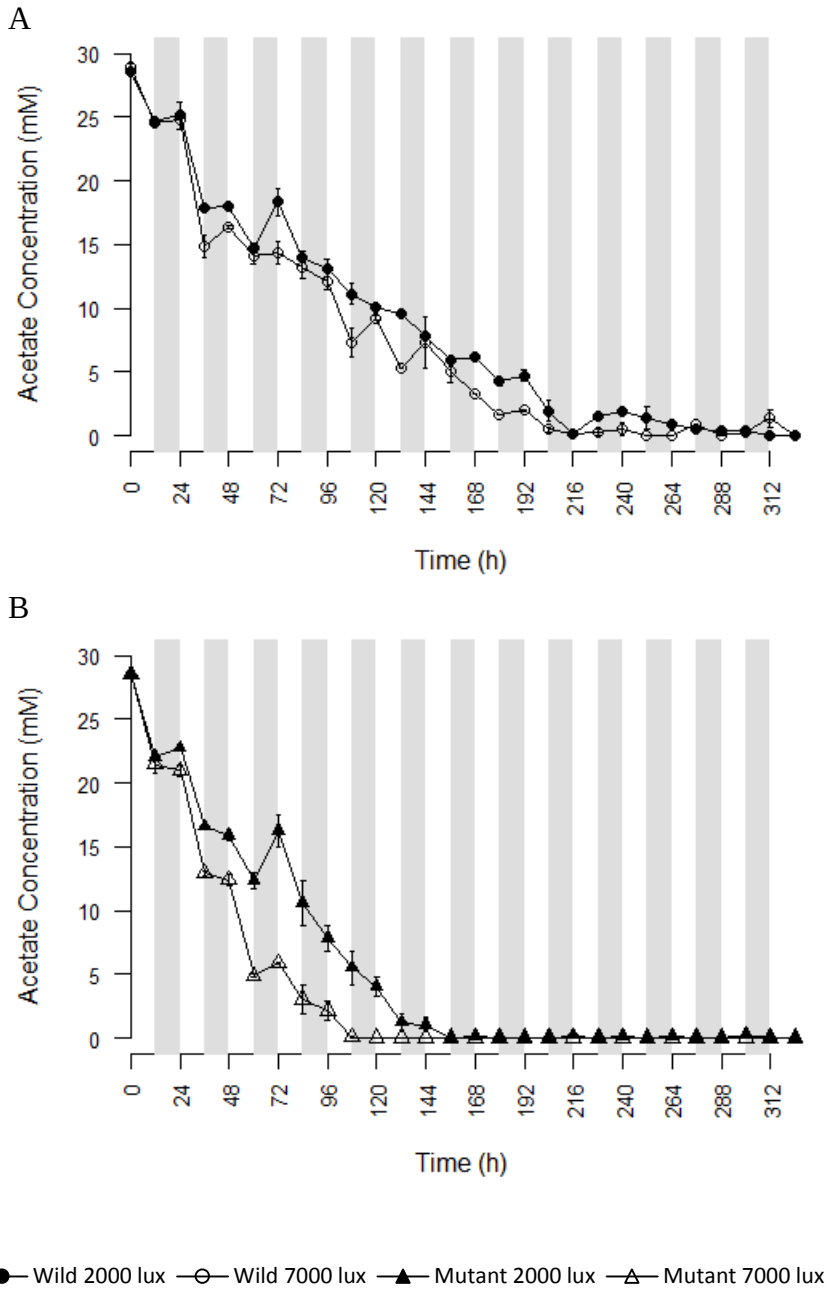

Figure 3. 5 Acetate concentration of *Rhodobacter capsulatus* wild type (A) and YO3 (B) cultures under low (2000 lux) and high (7000 lux) light intensities. The shaded bands indicate the dark periods. Data are shown as mean ± SEM, n=3

Carbon fixations are suggested to be used to balance the redox potential of the cell during photoheterotrophic growth and CO_2 is the preferred electron acceptor (Tichi & Tabita, 2000). The high reducing power caused by high light intensity in this study explains the formation of formate as a redox balancing way together with hydrogen production.

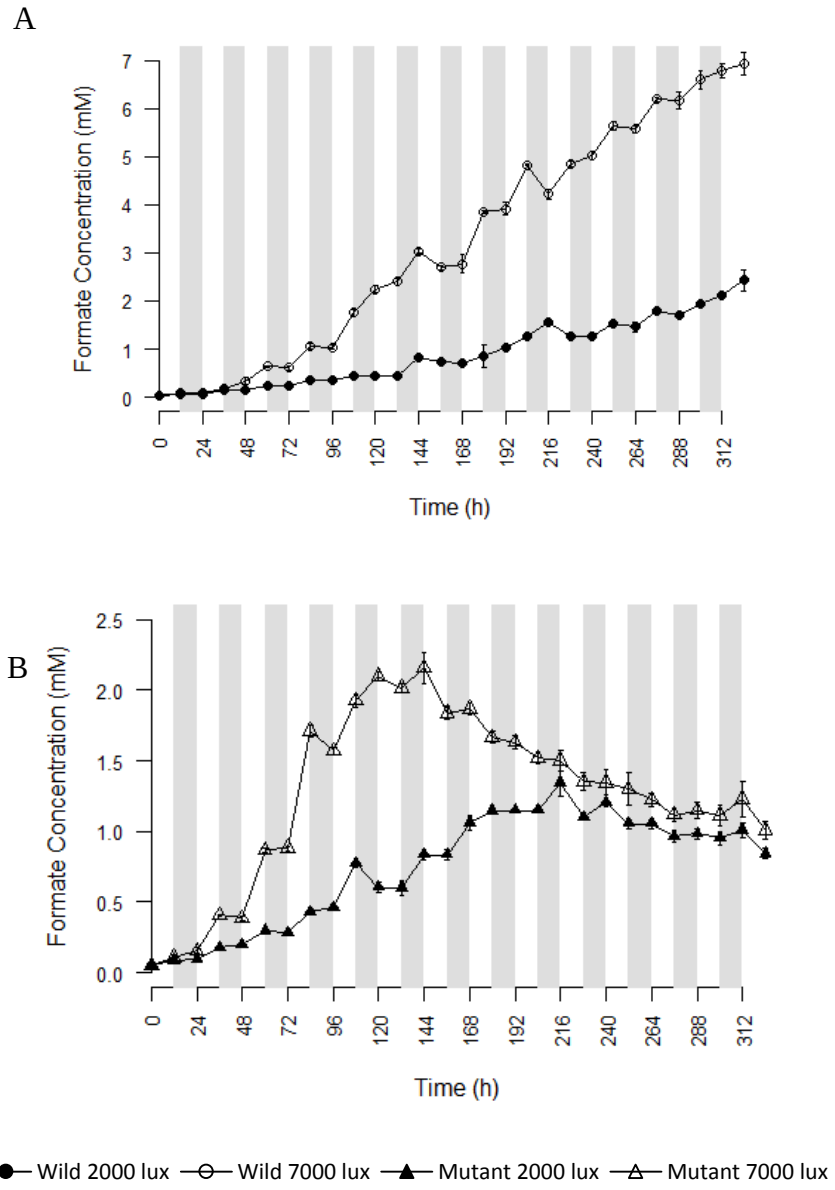

Figure 3. 6 Formate concentration of *Rhodobacter capsulatus* wild type (A) and YO3 (B) cultures under low (2000 lux) and high (7000 lux) light intensities. The shaded bands indicate the dark periods. Data are shown as mean ± SEM, n=3.

2.1.4 Effect of Light Intensity on Bacteriochlorophyll *a* Concentration

The bacteriochlorophyll *a* (bchl *a*) is a photosynthetic pigment responsible for collecting light and transfer the energy to the reaction center (J. P. Allen & Williams, 1998), thus it is very important in the operation of anoxygenic photosynthesis. The maximum absorption of bchl *a* is located near infrared region. For this reason, tungsten lamps were used in this study as their emission spectrum covers the whole absorption spectrum of *Rhodobacter capsulatus* (Adessi & De Philippis, 2014). Figure 3.7 clearly displays the effect of light and dark on bchl *a* content of the cells. The bchl *a* content varied inversely with the presence of light and its intensity. Hydrogen cannot be produced in the lack of ATP. Hence, bchl *a* concentration and hydrogen production profiles of this study are consistent.

The mutant strain's bchl *a* concentration profiles were similar under low and high light intensities. Wild type *R. capsulatus* synthesized clearly more bchl *a* under low light intensity when compared to high light intensity. Under low light intensity the production increased up to 3 times of dark periods, as the bacteria are in need of energy for growth and maintenance and produce more bacteriochlorophyll a to overcome the shortage of energy.

3.2. Microarray Analysis

The transcriptome profile of *R. capsulatus* as response to light after dark and to high light intensity was analyzed using microarray chips. The first step of microarray analysis is quality control of arrays. The arrays that do not meet the quality control parameters should be eliminated and not considered for further analysis. Immediately after scanning the chips by GCOS software, the chip images were inspected for any artifacts and abnormalities. Alternating intensity pattern on the borders, checkerboards on the corners and the array names were adequate for two of three replicates. Therefore the analyses were carried out with two replicates for each groups. Report files were generated by Expression Console software (ThermoFisher Scientific, Waltham, MA, USA). The average background, noise, percent present values, poly-A and

hybridization controls were all checked according to Yilmaz et al. (2008). The results are given in Table 3.3. Target preparation controls are all present on each chip, while hybridization controls are absent. The hybridization control kit might have been expired. Since they are absent in all of the chips, and since the analysis is relative, this absence will not affect the results.

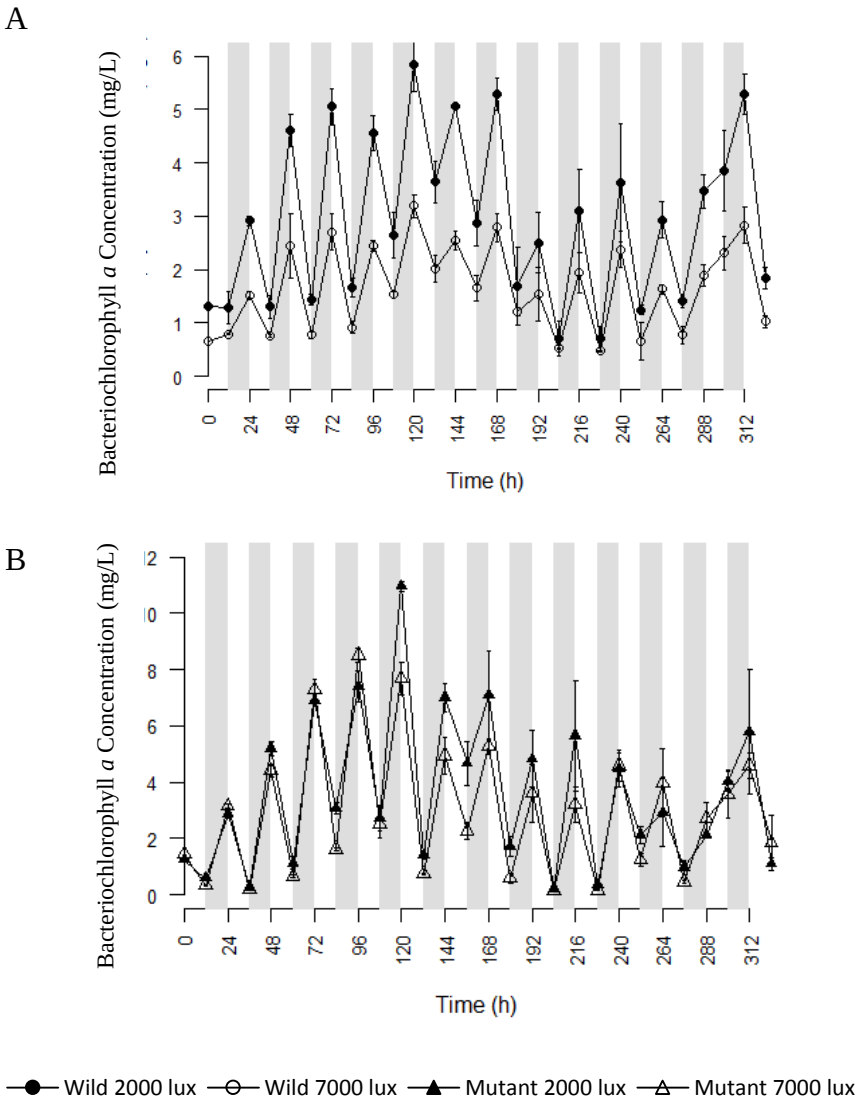

Figure 3. 7 Bacteriochlorophyll *a* concentration of *Rhodobacter capsulatus* wild type (A) and YO3 (B) cultures under low (2000 lux) and high (7000 lux) light intensities. The shaded bands indicate the dark periods. Data are shown as mean ± SEM, n=3.

Table 3. 3 The values of the quality control criteria probe sets of selected chips

	Average Back ground	Noise	AFF XDap Sig	AFF XLys Sig	AFF XPhe Sig	AFF XThr Sig	AFF XBio B Sig	AFF XBio C Sig	AFF XBio D Sig	AFF Xcre Sig	% Present
2	31.35	1.29	P (1.15)	P (1.01)	P (0.43)	P (1.19)	A	A	A	A	84.7
3	33.36	1.19	P (1.51)	P (0.7)	P (0.45)	P (1.17)	A	A	A	A	81.6
5	32.14	1.14	P (0.95)	P (1.91)	P (0.2)	P (0.82)	A	A	A	A	56.0
6	33.68	1.27	P (0.97)	P (1.37)	P (0.26)	P (1.28)	A	A	A	A	71.4
8	34.63	1.17	P (1.13)	P (1.81)	P (0.10)	P (0.91)	A	A	A	A	54.2
9	31.01	1.02	P (1.37)	P (1.64)	P (0.13)	P (1.11)	A	A	A	A	49.9
11	30.4	1.11	P (1.09)	P (1.13)	P (0.19)	P (0.78)	A	A	A	A	49.6
12	30.12	1.03	P (1.15)	P (1.01)	P (0.43)	P (1.19)	A	A	A	A	52.1
13	31.76	1.11	P (1.15)	P (1.01)	P (0.43)	P (1.19)	A	A	A	A	48.0
14	34.72	1.27	P (1.15)	P (1.01)	P (0.43)	P (1.19)	A	A	A	A	57.0

After deciding the arrays to continue, data from the scanned chips were grouped. The dark sample is the sample at the end of the third dark period (72 h), 2K 15min and 2K 1h groups are the samples after 15 minute and 1hour exposure to 2000 lux after the dark period. The light intensity was increased to 10,000 lux after 6 hours of exposure to 2000 lux. Similarly, 10K 15 min and 10K 1h groups are the ones after 15 minute and 1 hour exposure to 10,000 lux. The sampling times were chosen to be 15 minutes and 1 hour. In our previous studies, temperature stress was applied on *R. capsulatus* and samples were analysed after 2 and 6 hours (Gürgan et al., 2015). Expression of some stress response genes could not be observed after this time so it was thought that these time points were late for bacterial expression analysis. Moreover, expression analysis studies with *E. coli* were mostly carried out after 15 minutes of exposure to

certain stress factors (Allen et al., 2010; Pfaffl et al., 2001; Wei et al., 2001; Worden et al., 2009). In order to observe the expression of genes that may show a late response 1 hour was chosen to be another time point. The replicate arrays were inspected in terms of other quality control criteria. Pearson correlation analysis and principal component analysis after RMA normalization were carried out. The results are given in Figure 3.9 and Figure 3.10.

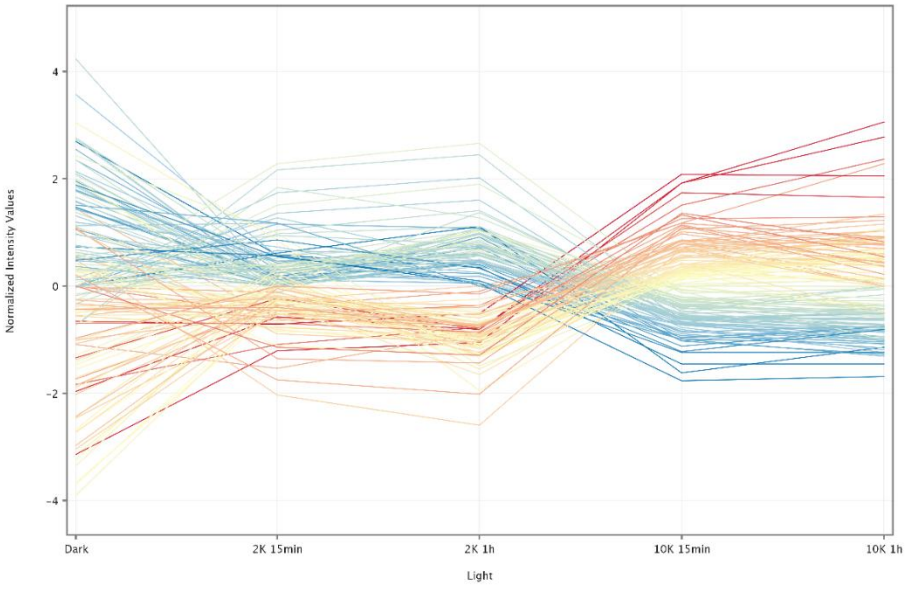

Figure 3. 8 Profile plot of experimental groups after normalization

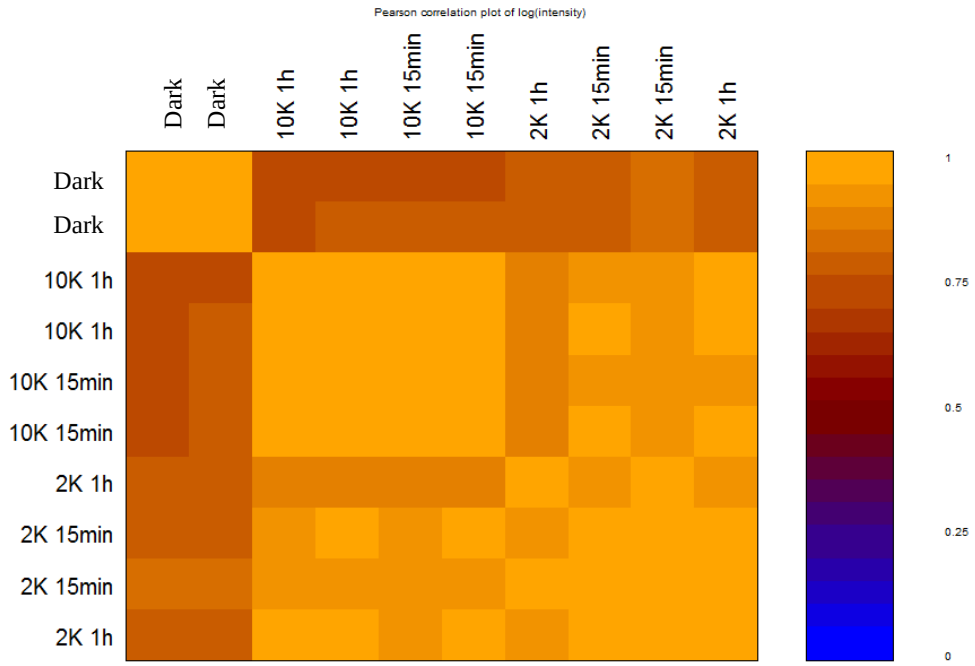

Figure 3. 9 Correlation plot after normalization

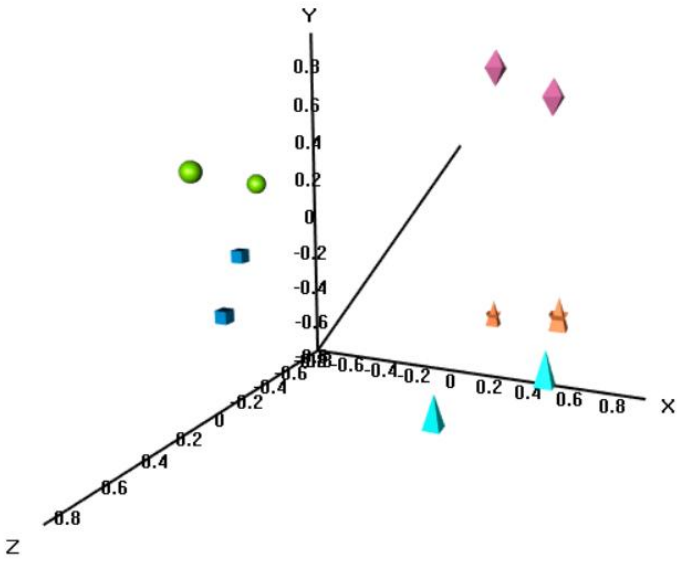

Figure 3. 10 Principal Component Analysis. Pink: Dark, orange: 2K 15min, turquoise: 2K 1h, green: 10K 15min, blue: 10K 1h

The correlation plot of Pearson correlation analysis indicates that the correlation within and among the arrays are high. The dark sample arrays have slightly different

expression levels, but two arrays of the dark sample are highly correlated and there are no outlier samples. Together with the correlation plot, principal component analysis shows that replicates of arrays are highly correlated and close to each other. This indicated that gene expression values resulted from biological experimental conditions not during RNA isolation, cDNA synthesis, fragmentation, labelling or hybridization. This also suggests that the experiments were carried out in a controlled way.

The changes in intensity values between the conditions are shown with profile plot. The change between dark and low light intensity is very different. High light intensity seem to change the intensity values of the probe sets, but not as a high change as entering light period after dark. However, change between 15 min and 1 hour of each light intensity applications does not seem to be very high. But profile of the lines at 1 hour of each light intensity application get more scattered. This suggests that the fold change of up- and down- regulated genes increase after 1 hour and for some genes bacterial response to light applications might become clearer after 1 hour. Because of this reason, the fold change and statistical analyses were carried out using 1 h samples.

The effect of light exposure after dark was inspected by comparing 2000 lux 1h sample. The effect of high light intensity was inspected by comparing 10,000 lux 1 h sample with 2000 lux 1h sample (LL). In order to find the differentially expressed gene, first a fold change analysis (≥ 2.0) was performed, then moderated t-test (α=0.05) followed by Benjamini-Hochberg correction was performed for both cases (Benjamini & Hochberg, 1995). Moderated t-test is similar to Student's t-test, and it is used to compare the means of gene expression values two groups of replicates for a given gene (Smyth, 2004). In the scope of MicroArray Quality Control (MAQC) Project Shi et al. (2008) inspected the reproducibility of microarray data and concluded when the ranking criterion is fold change with a non-stringent p-value cut-off, the gene lists become more reproducible. That is why in the present study fold change ≥ 2.0 followed by a significance analysis with p-value cut-off 0.05 were chosen. Entering light period after a long dark period caused change in the expression of 914 genes, while expression of only 145 genes changed upon high light intensity. Scatter plots in Figure 3.11 show the distribution of up and down regulated genes.

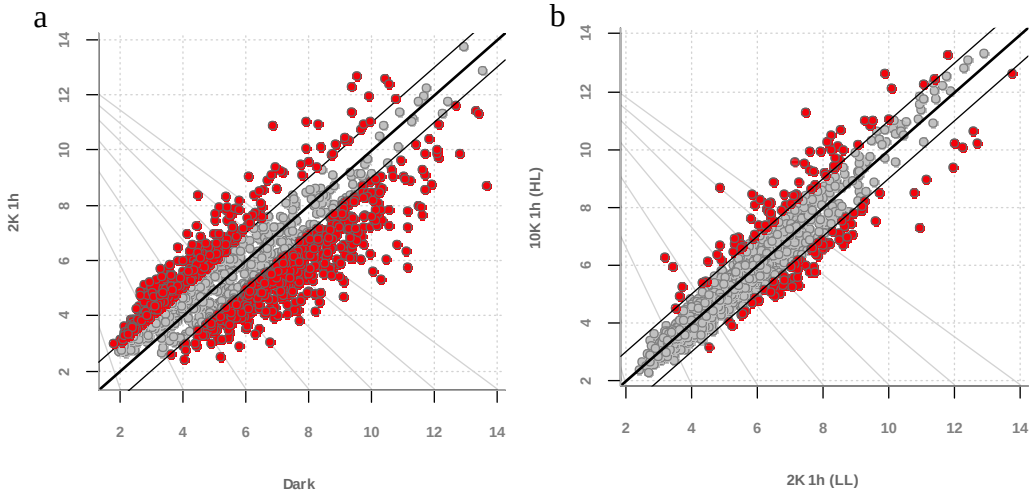

Figure 3. 11 Scatter plots of light applications after dark (a) and high light intensity (b).

The genes that show significant change were classified into different groups depending on their metabolic functions. Gene groupings were accomplished depending on the classifications of Strnad et al. (2010) and Onder et al. (2010), and the information on the online databates www.ncbi.nlm.nih.gov and www.kegg.jp. The pie charts in Figure 3.12 and Figure 3.13 show the distribution of genes into corresponding metabolisms. The annotation of *R. capsulatus* genes is not complete yet, that is why a high proportion of the genes are either proteins of unknown function or hypothetical proteins. The scope of this study, hydrogen production, makes nitrogen metabolism, photosynthesis and electron transport are of high importance. The genes belonging to these metabolisms will be discussed in the following sections.

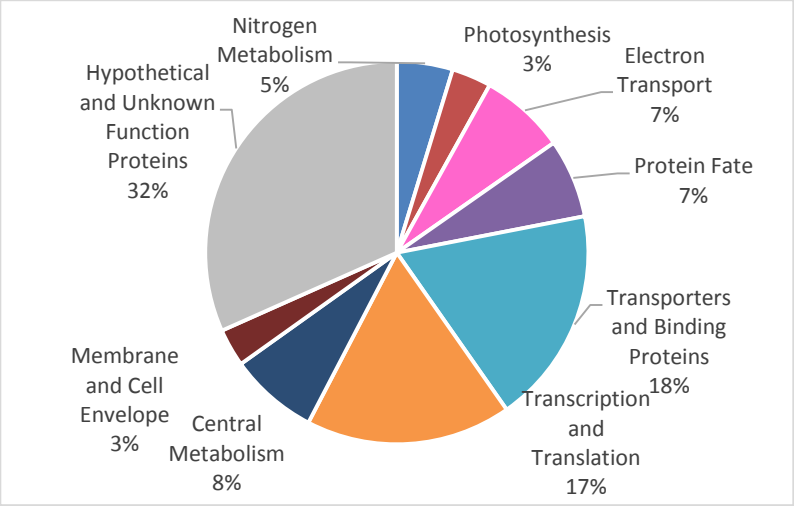

Figure 3. 12 Metabolic distributions of the differentially expressed genes by shift to light period.

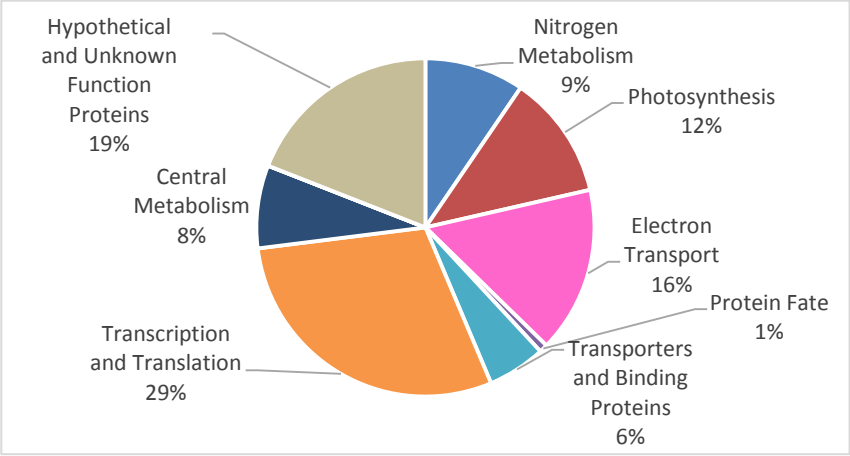

Figure 3. 13 Metabolic distributions of the differentially expressed genes affected by high light intensity

2.2.1 Effect of Light on Nitrogen Metabolism

Hydrogen production in PNSB is primarily connected with nitrogen metabolism since hydrogen production is catalyzed by the nitrogenase enzyme. Table 3.4 shows some important genes related to nitrogen metabolism whose expression were significantly changed by light application after dark period. Figure 3.4 shows that hydrogen

production stopped in dark periods and resumed in the availability of light. Nitrogenase genes were expected to be up regulated when the bacteria enter light period as expected. Jouanneau et al. (1985) found that activity of nitrogenase depends on light intensity. A high light intensity of 7000 lux doubled the nitrogenase activity. We found that 7000 lux increases hydrogen production (Figure 3.4). Indeed, 11 *nif* genes and 3 *anf* genes were up-regulated by the presence of light after a dark period. Also, hydrogenase expression/formation protein was up-regulated. Together with the nitrogenase genes, this suggest that bacteria would start to produce hydrogen in the presence of mild light intensity. Moreover, bacterial growth stopped in dark periods, and in light periods bacteria started to grow up again (Figure 3.3). Up-regulation of *glnA* and *glnB* genes show the resume of bacterial growth since these genes are involved in glutamine synthesis and required for growth. They are cotranscribed from *glnAB* operon (Zinchenko et al., 1994). *glnB* also activates the *nif* genes under nitrogen limited condition (Kranz et al., 1990), such as the condition in this study, which is also suitable for hydrogen production. Besides *glnAB*, *ure* and *modABCD* operons are activated in nitrogen starvation condition (Masepohl et al., 2001). *modABC* operon codes for high affinity molybdate uptake system, and *ure* codes for urease. In this study, 4 urease genes were up regulated by light exposure after dark. The increase in the urease genes in the absence of urea in the medium is intriguing and could not be explained with the results of this study. Although many genes in nitrogen metabolism are up regulated, *gltD* and *nifA*, which is the activator of other *nif* genes are down regulated. This can be a false negative result of microarray analysis since thousands of statistical tests applied can come with some false positive and false negative results, in spite of stringent statistical criteria (Gerling et al., 2003).

Table 3. 4 Changes of important genes of nitrogen metabolism by shift to light period

	Probe set ID	Gene symbol	Description	Fold change (LL/dark)	P value
Nitrogen Metabolism	RCAP_rcc00571_at	*nifD*	nitrogenase molybdenum-iron protein alpha chain	+5.54	0.001
	RCAP_rcc00572_at	*nifH*	nitrogenase iron protein	+3.36	0.026
	RCAP_rcc01728_at	*nifJ*	pyruvate-flavodoxin oxidoreductase	+3.24	0.002
	RCAP_rcc00570_at	*nifK*	nitrogenase molybdenum-iron protein beta chain	+4.51	0.011
	RCAP_rcc03263_at	*nifT*	NifT/FixU family protein	+6.39	0.0006
	RCAP_rcc03264_at	*nifZ*	NifZ family protein	+8.05	0.0003
	RCAP_rcc03268_at	*nifW*	nitrogen fixation protein NifW	+2.05	0.005
	RCAP_rcc03269_at	*nifV*	homocitrate synthase	+2.57	0.002
	RCAP_rcc03274_at	*nifQ*	NifQ family protein	+2.35	0.007
	RCAP_rcc03278_at	*nifX*	nitrogen fixation protein NifX	+2.79	0.002
	RCAP_rcc03279_at	*nifN*	nitrogenase molybdenum-iron cofactor biosynthesis protein NifN	+6.24	0.0006
	RCAP_rcc00585_at	*anfH*	nitrogenase iron protein	+3.83	0.005
	RCAP_rcc00587_at	*anfG*	nitrogenase iron-iron protein, delta subunit	+2.62	0.007
	RCAP_rcc00588_at	*anfK*	nitrogenase iron-iron protein, beta subunit	+3.10	0.004
	RCAP_rcc01674_at	*glnA*	glutamine synthetase	+2.57	0.003
	RCAP_rcc01673_at	*glnB*	nitrogen regulatory protein P-II	+2.28	0.002
	RCAP_rcc03387_at	*glnB*	nitrogen regulatory protein P-II	+2.60	0.001
	RCAP_rcc00163_at	*gltD*	glutamate synthase (NADPH), beta subunit	-6.85	0.002
	RCAP_rcc00567_at	*nifA*	Nif-specific regulatory protein	-2.43	0.009
	RCAP_rcc01217_at	*ureD*	urease accessory protein UreD	+2.19	0.004
	RCAP_rcc01218_at	*ureA*	urease, gamma subunit	+2.06	0.004
	RCAP_rcc01226_at	*urtB*	urea ABC transporter, urea binding protein UrtB	+3.72	0.0005
	RCAP_rcc01223_at	*ureF*	urease accessory protein UreF	+2.02	0.005

2.2.2 Effect of Light on Photosynthesis

Photosynthesis is the most important light-induced process on our planet and it allows plants, algae, cyanobacteria, and anoxygenic photosynthetic bacteria to convert energy harvested from light into a chemical form (Blankenship, 2008). *R. capsulatus* is one of the anoxygenic photosynthetic bacteria capable of energy production through photosynthesis. As shown in Figure 1.5, photosynthetic membrane is made up of two pigment-protein complexes: reaction center and light harvesting complexes. Light harvesting complex first capture the light energy and transfer it to the reaction center (Kühlbrandt, 1995). When oxygen is absent and light is available, these bacteria respond by synthesizing an extensive system of light-capturing intracytoplasmic membranes (Hädicke et al., 2011). The expression of photosynthetic reaction center and light harvesting complex genes encoded by *puf* and *puc* operons increased in this study upon light exposure after a dark period (Table 3.5). Moreover, biosynthesis genes of bacteriochlorophylls which are pigments that bind to light harvesting complexes and absorb light are up-regulated. The regulation of all these genes are consistent with bacterial growth and hydrogen production in the light periods. One other gene found to be up regulated in this condition is *idi* encoding isopentenyl-diphosphate delta-isomerase. It is the final enzyme in the non-mevalonate pathway that contributes to the biosynthesis of isoprenoids, which have vital roles in carotenoid and chlorophyll synthesis thus the photosynthesis (Hahn et al., 1996). Its up-regulation is consistent with up-regulation of bacteriochlorophyll genes.

Table 3. 5 Changes of important genes of photosynthesis by shift to light period

	Probe Set ID	Gene Symbol	Description	Fold Change	P value
Photosynthesis	RCAP_rcc00672_at	*pucC*	PUCC family protein	+2.18	0.005
	RCAP_rcc02532_at	*pucC*	protein PucC	+2.72	0.005
	RCAP_rcc02533_at	*pucDE*	light-harvesting protein B-800/850, gamma chain	+4.48	0.001
	RCAP_rcc00693_at	*pufL*	photosynthetic reaction center, L subunit	+8.98	5.7E-4

Table 3.5 (continued)

Photosynthesis	RCAP_rcc00694_at	*pufM*	photosynthetic reaction center, M subunit	+4.04	0.002
	RCAP_rcc00695_at	*pufX*	intrinsic membrane protein PufX	+3.02	0.003
	RCAP_rcc00662_at	*bchL*	light-independent protochlorophyllide reductase, iron-sulfur ATP-binding protein	+2.69	0.003
	RCAP_rcc00663_at	*bchH*	magnesium chelatase, H subunit	+2.04	0.029
	RCAP_rcc00671_at	*bchG*	bacteriochlorophyll synthase	+2.44	0.003
	RCAP_rcc00674_at	*idi*	isopentenyl-diphosphate delta-isomerase	+3.00	0.004

2.2.3 Effect of Light on Electron Transport

The electron transport chain and its role in hydrogen production was discussed in Introduction section (Figure 1.4 and Figure 1.7). Excited electrons in the reaction center can either be donated to NADP+ to generate NADPH for biosynthesis or alternatively be energized repeatedly through cyclic electron transport chain. This cyclic photophosphorylation allows maintenance of proton motive force and ATP pools. Hydrogenase enzyme, NADH dehydrogenase (NADH quinone oxidoreductase) and succinate dehydrogenase can feed the electron pool, but can be reduced by the electron pool, too. The reverse electron flow to NADH dehydrogenase is necessary to refurnish the cell of NADH (Adessi & De Philippis, 2013). The quinone pool in the electron transport chain recognizes the signal from cell's redox state and thus regulates photosynthesis, nitrogen fixation, carbon fixation and respiration. In this concept, photosynthetic apparatus and electron transport chain work in parallel with TCA cycle and Calvin cycle.

In this study, four NADH dehydrogenase (also called NADH quinone oxidoreductase) genes were up-regulated by light exposure which suggests its electron feed to the quinone pool by light exposure. Similarly, hydrogenase gene expression increase

suggest a similar effect on quinone pool. Light exposure starts hydrogen production which is the substrate for hydrogenase, therefore up-regulation of this enzyme genes is consistent with the physiological data. However, succinate dehydrogenase gene expression together with succinyl-CoA synthetase genes were down regulated. Succinate dehydrogenase is the only enzyme participating both in TCA cycle and electron transport chain (Oyedotun & Lemire, 2004) and it oxidizes succinate to fumarate and reduces ubiquinone to ubiquinol. Succinyl-CoA synthethase genes are operated with the same promoter of succinate dehydrogenase. Succinate comes from the TCA cycle which must be active in dark for the bacteria to maintain the ATP need and intermediary products for biosynthesis. However, light exposure stimulates a high electron pool in the photosynthetic membrane which triggers more ATP production by proton motive force and ATPase. Thefore, need for succinate oxidation is decreased and succinate dehydrogenase is down regulated.

Among the genes of electron transport system the electron transport complex genes of *rnf* operon were up-regulated. The product of this operon, electron transport complex can use the electrochemical ion potential produced by photosynthetic system to drive reverse electron flow to reduce ferredoxin and serves as ultimate donor to dinitrogenase reductase (Biegel et al., 2011). It was found that overexpression of Rnf products enhance nitrogenase activity (Jeong & Jouanneau, 2000). Indeed, they are components of nitrogen reducing machinery and named after *Rhodobacter* as *Rhodobacter* nitrogen fixation (Rnf) since it was first discovered in *R. capsulatus*. Increased expression of these genes is consistent with the up-regulation of nitrogenase genes in this study. Ferredoxins and flavodoxins are other important electron donors to nitrogenase, ferredoxin I encoded by *fdxN* being the main electron donor to nitrogenase (Jouanneau et al., 1995). Their up regulation is also consistent with increased nitrogenase gene expressions and resumed hydrogen production in the light periods.

Dimethyl sulfoxide reductase subunit genes were also up-regulated by light exposure, although dimethyl sulfoxide (DMSO) was not present in the medium in this study. It was found that when pyruvate was replaced with malate and in the absence of DMSO, low light condition ($16W/m^2$) activated DMSO reductase activity 10 fold higher than

cells grown on pyruvate (Kappler et al., 2002). The increased expression of DMSO reductase in this study can be related with the carbon source being acetate and exposure to a relatively low light intensity after dark period.

Table 3. 6 Changes of important genes of electron by shift to light period

	Probe Set ID	Gene Symbol	Description	Fold Change	P value
Electron transport	RCAP_rcc03275_at	*fdxB*	ferredoxin III	+5.30	0.022
	RCAP_rcc03284_at	*fdxN*	ferredoxin I	+3.35	0.030
	RCAP_rcc03285_at	*fdxC*	ferredoxin IV	+4.44	0.004
	RCAP_rcc03289_at	*rnfC*	electron transport complex protein RnfC	+6.46	0.008
	RCAP_rcc03291_at	*rnfG*	electron transport complex protein RnfG	+4.74	0.008
	RCAP_rcc03292_at	*rnfE*	electron transport complex protein RnfE	+7.07	0.007
	RCAP_rcc00766_at	*hypF*	hydrogenase maturation protein HypF	+3.51	0.002
	RCAP_rcc00773_at	*hupH*	hydrogenase expression/formation protein HupH	+2.05	0.011
	RCAP_rcc00768_at	*hypE*	hydrogenase expression/formation protein HypE	+2.39	0.004
	RCAP_rcc01533_at	*nuoJ*	NADH-quinone oxidoreductase, J subunit	+2.93	0.002
	RCAP_rcc01535_at	*nuoL*	NADH-quinone oxidoreductase, L subunit	+2.78	0.012
	RCAP_rcc01536_at	*nuoM*	NADH-quinone oxidoreductase, M subunit	+2.89	0.002
	RCAP_rcc01537_at	*nuoN*	NADH-quinone oxidoreductase, N subunit	+3.46	0.003
	RCAP_rcc02279_at	*dmsC*	dimethyl sulfoxide reductase, C subunit	+2.49	0.003
	RCAP_rcc02280_at	*dmsB*	dimethyl sulfoxide reductase, B subunit	+3.62	0.004
	RCAP_rcc02281_at	*dmsA*	dimethyl sulfoxide reductase, A subunit	+2.14	0.004

Table 3.6 (continued)

Electron transport	RCAP_rcc00720_at	*sucC*	succinyl-CoA synthetase (ADP-forming), beta subunit	-2.60	0.005
	RCAP_rcc00721_at	*sucD*	succinyl-CoA synthetase (ADP-forming), alpha subunit	-3.13	0.010
	RCAP_rcc00731_at	*sdhC*	succinate dehydrogenase, cytochrome b556 subunit	-7.57	6.7E-4
	RCAP_rcc00732_at	*sdhD*	succinate dehydrogenase, hydrophobic membrane anchor protein	-2.10	0.012
	RCAP_rcc00733_at	*sdhA*	succinate dehydrogenase, flavoprotein subunit	-4.06	0.003

2.2.4 Effect of Light on Transporters and Binding Proteins

Rhodobacter capsulatus have two types of nitrogenases: 1) a molybdenum-dependent nitrogenase which is composed of dinitrogenase (known as MoFe protein) and a dinitrogenase reductase (known as Fe protein); 2) an iron-only nitrogenase (Fe-nitrogenase). Molybdenum and iron are cofactors in nitrogenases. The growth and hydrogen production media in this study contain molybdenum as trace element, and iron as one of the main ingredients, since they are cofactors of nitrogenases. Increase in the expression of nitrogenases brought about the increase in the molybdenum and iron need in the cell. Therefore, genes for molybdenum ABC transporter, molybdate-binding protein, molybdenum cofactor biosynthesis proteins and 10 iron related transporters were up-regulated (Table 3.7). Cobalt is another element that functions as cofactor in central metabolic reactions. It is incorporated in vitamin B12 which is coenzyme of several essential enzymes of DNA synthesis, fatty acid and amino acid metabolism. Cobalt itself can be associated directly with cobalt-dependent enzymes. Bacteria have high affinity uptake transporters in order to take cobalt in sufficient

amounts (Cheng et al., 2011). With the growth trend of bacteria, the cobalt ABC transporter genes were up-regulated.

Urease genes were also found to be up-regulated, and urea transporters were consistently up regulated. Besides these genes, 5 spermidine/putrescine genes were up-regulated. Spermidine and putrescines are polyamines and serve vital role in cell survival. They stimulate RNA and protein synthesis, stabilize secondary structures of nucleic acids, and stabilize the cell membrane (Raina & Jänne, 1975; Tabor & Tabor, 1976). These functions define the inevitable roles of polyamines in the cell. Growth resume by light exposure after dark result in increased expression of genes whose products are necessary for growth. One of these genes is the thiamine ABC transporter. Thiamin, also called vitamin B1, are very important as its phosphate derivatives are involved in many cellular processes, such as amino acid biosynthesis and central metabolism (Schauer et al., 2009). Therefore, it is needed for growth of bacteria which stimulates the transcription of thiamine ABC transporter (Table 3.7) and thiamine biosynthesis lipoprotein gene *apbE* (Table 3.8). Thiamine is also supplied in the growth and hydrogen production media.

Glutamate/aspartate transporters were found to be overexpressed, too. They take glutamate and aspartate from the extracellular space. They provide the cell with the compounds that can be used as carbon, nitrogen or energy source. This up-regulation of 3 glutamate/aspartate transporter is because the bacteria are in growth phase in the light period.

Table 3. 7 Changes of important genes of transporters and binding proteins by shift to light period

	Probe Set ID	Gene Symbol	Description	Fold Change	P value
Transporters and Binding Proteins	RCAP_rcc00562_at	*modA*	molybdenum ABC transporter, periplasmic molybdenum-binding protein ModA	+2.58	0.007
	RCAP_rcc00564_at	*modC*	molybdenum ABC transporter, ATP-binding protein ModC	+2.03	0.009

Table 3.7 (continued)

Transporters and Binding Proteins	RCAP_rcp00088_at		molybdate-binding protein	+2.36	0.004
	RCAP_rcc02840_at	*moaC*	molybdenum cofactor biosynthesis protein C	+2.21	0.003
	RCAP_rcc02843_at	*moaA*	molybdenum cofactor biosynthesis protein A	+2.89	0.005
	RCAP_rcc00105_at	*fhuC*	ferrichrome ABC transporter, ATP-binding protein FhuC	+4.66	0.001
	RCAP_rcc00107_at	*fhuB*	ferrichrome ABC transporter, permease protein FhuB	+4.53	0.002
	RCAP_rcc00113_at	*fhuB*	ferrichrome ABC transporter, permease protein FhuB	-2.46	0.005
	RCAP_rcc01030_at		iron siderophore/cobalamin ABC transporter, permease protein	+2.90	0.003
	RCAP_rcc01031_at		iron siderophore/cobalamin ABC transporter, ATP-binding protein	+2.56	0.004
	RCAP_rcc03360_at		iron siderophore/cobalamin ABC transporter, permease protein	+2.69	0.003
	RCAP_rcp00044_at		iron siderophore/cobalamin ABC transporter, ATP-binding protein	+2.92	0.004
	RCAP_rcc01786_at	*ccmB*	heme exporter protein B	+3.18	0.008
	RCAP_rcc01787_at	*ccmC*	heme exporter protein C	-2.63	0.002
	RCAP_rcc01788_at	*ccmD*	heme exporter protein D	+2.25	0.004
	RCAP_rcc00336_at	*bztB*	glutamate/aspartate ABC transporter, permease protein BztB	+2.34	0.009

Table 3.7 (continued)

Transporters and Binding Proteins	RCAP_rcc00337_at	*bztC*	glutamate/aspartate ABC transporter, permease protein BztC	+2.38	0.008
	RCAP_rcc00338_at	*bztD*	glutamate/aspartate ABC transporter, ATP-binding protein BztD	+2.12	0.016
	RCAP_rcc01032_at	*cbiO*	cobalt ABC transporter, ATP-binding protein CbiO	+2.18	0.004
	RCAP_rcc01051_at	*cbiO*	cobalt ABC transporter, ATP-binding protein CbiO	+2.04	0.007
	RCAP_rcc01188_at	*phnD*	phosphonate ABC transporter, periplasmic phosphonate-binding protein PhnD	+5.15	0.001
	RCAP_rcc01198_at	*phnK*	phosphonates transport ATP-binding protein PhnK	+2.03	0.005
	RCAP_rcc01228_at	*urtC*	urea ABC transporter, permease protein UrtC	+3.78	0.002
	RCAP_rcc01230_at	*urtE*	urea ABC transporter, ATP-binding protein UrtE	+2.56	0.002
	RCAP_rcc01390_at	*potB*	spermidine/putrescine ABC transporter, permease protein PotB	+2.02	0.014
	RCAP_rcc02185_at	*potI*	spermidine/putrescine ABC transporter, permease protein PotI	+2.12	0.004
	RCAP_rcc02186_at	*potF*	spermidine/putrescine ABC transporter, periplasmic spermidine/putrescine-binding protein PotF	+3.63	0.004

Table 3.7 (continued)

Transporters and Binding Proteins	RCAP_rcc02449_at	*potC*	spermidine/putrescine ABC transporter, permease protein PotC	+2.17	0.004
	RCAP_rcc02450_at	*potB*	spermidine/putrescine ABC transporter, permease protein PotB	+2.36	0.004
	RCAP_rcc02697_at	*thiB*	thiamine ABC transporter, periplasmic thiamin-binding protein	+2.40	0.005
	RCAP_rcc02698_at	*thiP*	thiamine ABC transporter, permease protein	+2.03	0.005
	RCAP_rcc03521_at	*fIiI*	flagellar protein export ATPase FliI	+2.34	0.003

2.2.5 Effect of Light on Central Metabolism

The extraordinary metabolic versatility of PNSB makes the bacteria switch between different metabolisms to maintain redox balance. Shift to the light period after a long dark period stimulated the synthesis of photosynthetic apparatus and led the production of reducing power. The excess electrons from the quinone pool must be eliminated for the maintenance of redox balance of the cell. For this, TCA cycle or NADH dehydrogenase function besides the Calvin cycle which fixes CO_2 to organic compounds. Calvin cycle utilizes most of the excess electrons via reduction of CO_2 into biosynthetic intermediate during the exponential growth. In this study, the growth of bacteria resumed in an exponential manner after the dark period (Figure 3.3). In addition, the Calvin cycle genes for fructose bisphosphate aldolase, ribulose bisphosphate carboxylase (RuBisCO) and hydrolase were up-regulated in this study (Table 3.8) which proves the activity of Calvin cycle upon entering light period. Moreover, glyoxylate reductase encoded by *gyaR* was down-regulated since it deactivates RuBisCO.

Bacteria respond to the incoming light in a mild intensity with a tactic behavior.

This behavior is called “energy taxis”. *R. capsulatus* has one flagellum located on the side of the cell body. This flagella rotates rapidly clockwise, causing propulsion of the cell, and reorients when it stops and coils up. *Rhodobacters* avoid dark and reverse their direction of swimming when they are out of a light area. (White, Drummond, & Fuqua, 2012). The flagellar genes were up regulated in this study with the genes for chemotaxis. The Che proteins are part of a signal transduction pathway between attractant or repellent and flagellar motor switch. CheA is a histidine kinase which transfers phosphoryl group to a response regulator protein. CheB and CheY are response regulator proteins which are phosphorylated and dephosphorylated. Methyl accepting chemotaxis proteins are chemoreceptor proteins in the cell membrane which bind to chemoeffectors and thus mediate the tactic behavior. These protein genes were also up-regulated in the presence of light after the dark period.

Phosphonate ABC transporter, phosphonates transport STP-binding protein and 4 other phosphonate metabolism genes encoded by *phn* operon were also up-regulated. Phosphonates are compounds that contain the chemically stable carbon–phosphorus bond (Villarreal-Chiu et al., 2012). *phn* operon encodes genes taking role in uptake and breakdown of phosphonates. This operon is stimulated by low inorganic phosphate condition; when supply of phosphate becomes limiting (White et al., 2012). For the cell growth phosphate is inevitable, since incorporates into nucleic acid structure and in almost every metabolism. One of the genes up-regulated in this study was for ribose 1,5-bisphosphokinase taking place in pentose phosphate pathway. This result is consistent with the cell growth in the light periods which is in need of phosphate molecules.

Down regulation of fatty acid oxidation complex together with propionyl-CoA carboxylase suggest that in light period, bacteria do not prefer beta oxidation of fatty acids for energy production, because energy can be produced by photosynthetic membrane system. This also means that in darkness bacteria can use beta oxidation of fatty acids to fulfill energy need.

The product of *phaZ* gene polyhydroxyalkalonate depolymerase was also down regulated. Polyhydroxyalkanoates are polyester polymers used by bacteria as storage

of carbon and energy (Jin & Nikolau, 2012). Bacteria used carbon storage materials for energy requirement during the darkness, and the need to use them was decreased by light energy.

Table 3. 8 Changes of important genes of the central metabolism by shift to light period

	Probe Set ID	Gene Symbol	Description	Fold Change	P value
Central Metabolism	RCAP_rcc01830_at	*fba*	fructose-bisphosphate aldolase	+4.02	0.002
	RCAP_rcc00579_at	*cbbL*	ribulose bisphosphate carboxylase, large subunit	+2.24	0.003
	RCAP_rcc01825_at	*cbbY*	hydrolase, HAD superfamily	+3.07	0.004
	RCAP_rcc00524_at	*gyaR*	glyoxylate reductase	-2.43	0.018
	RCAP_rcc03481_at	*fIiH*	flagellar biosynthesis/type III secretory pathway protein FliH	+2.27	0.009
	RCAP_rcc03483_at	*fliL*	flagellar basal body-associated protein FliL	+2.21	0.013
	RCAP_rcc03521_at	*fIiI*	flagellar protein export ATPase FliI	+2.34	0.003
	RCAP_rcc01185_at		methyl-accepting chemotaxis sensory transducer	+2.45	0.008
	RCAP_rcc01358_at	*cheB*	chemotaxis response regulator protein-glutamate methylesterase CheB	+3.34	0.002
	RCAP_rcc01726_at	*mcpH*	methyl-accepting chemotaxis protein McpH	+2.43	0.003
	RCAP_rcc01765_at	*cheA*	chemotaxis protein CheA	+2.30	0.004
	RCAP_rcc02611_at	*mcpA*	methyl-accepting chemotaxis protein McpA	+2.42	0.004
	RCAP_rcc03282_at	*apbE*	thiamin biosynthesis lipoprotein ApbE	+2.73	0.022

Table 3.8 (continued)

Central Metabolism	RCAP_rcc01188_at	*phnD*	phosphonate ABC transporter, periplasmic phosphonate-binding protein PhnD	+5.15	0.001
	RCAP_rcc01193_at	*phnG*	phosphonate metabolism protein PhnG	+2.09	0.001
	RCAP_rcc01194_at	*phnH*	phosphonate metabolism protein PhnH	+2.61	0.004
	RCAP_rcc01198_at	*phnK*	phosphonates transport ATP-binding protein PhnK	+2.03	0.005
	RCAP_rcc01200_at	*phnN*	ribose 1,5-bisphosphokinase (PRPP-forming)	+3.66	0.002
	RCAP_rcc01202_at	*phnM*	phosphonate metabolism protein PhnM	+2.98	0.004
	RCAP_rcc00518_at	*fadA*	fatty acid oxidation complex, beta subunit	-3.42	0.001
	RCAP_rcc00906_at	*pccB*	propionyl-CoA carboxylase, beta subunit	-5.20	0.001
	RCAP_rcc00911_at	*pccA*	propionyl-CoA carboxylase, alpha subunit	-7.28	0.002

2.2.6 Effect of Light on Protein Fate

Protein degradation machinery of *R. capsulatus* was significantly down regulated when bacteria enter the light period (Table 3.9). Down regulation of these genes under light condition also means increased transcription in dark period. Down-regulation of 27 genes for 30S and 50s ribosomal proteins and translation elongation factors (Appendix G) suggests intense transcription and translation processes in dark. Chaperons and chaperonins were down regulated in light, too. Molecular chaperons are involved in folding of proteins especially where high protein concentration

promote protein-protein interactions which result in significant protein denaturation (Hemmingsen et al., 1988). The result show that in a dark period, cold shock proteins (ATP-dependent proteases) and heat shock proteins (chaperons and chaperonins) were active. RNA chaperone Hfq was 6 fold down-regulated when exposed to light. In addition, RNA polymerase sigma factors σ^{70} and σ^{32} (heat shock sigma factor) were down regulated in the light period. σ^{70} is the primary sigma factor which transcribes essential genes and keeps essential pathways operating (Gruber & Gross, 2003). The relatively increased expression of these sigma factors in dark is a similar result of heat shock response in our previous study (Gürgan et al., 2015). In the future, the studies might focus on what happens in dark, rather than light in order to understand the metabolism and generate microorganisms for more efficient hydrogen production.

Table 3. 9 Changes of important genes of the protein fate by shift to light period

	Probe Set ID	Gene Symbol	Description	Fold change	P value
Protein Fate	RCAP_rcc00034_s_at	*hslU*	ATP-dependent hsl protease ATP-binding subunit hslU	-5.90	0.004
	RCAP_rcc00035_s_at	*hslV*	ATP-dependent protease HslV	-2.07	0.029
	RCAP_rcc00223_at	*dnaJ*	chaperone DnaJ	-4.87	0.009
	RCAP_rcc00224_at	*dnaK*	chaperone DnaK	-7.61	0.002
	RCAP_rcc02608_at	*clpX*	ATP-dependent Clp protease, ATP-binding subunit ClpX	-3.43	0.004
	RCAP_rcc02893_at	*cspA*	cold shock protein CspA	-2.37	0.016
	RCAP_rcc00607_at	*cspA*	cold shock protein CspA	-3.77	0.014
	RCAP_rcc03141_at	*cspD*	cold shock-like protein CspD	-2.27	0.014
	RCAP_rcc02977_at	*clpA*	ATP-dependent Clp protease, ATP-binding subunit ClpA	-6.36	0.039
	RCAP_rcc03406_at	*clpB*	chaperone ClpB	-26.92	0.001

Table 3.9 (continued)

Protein Fate	RCAP_rcc01167_at	*clpS*	ATP-dependent Clp protease adaptor protein ClpS	-3.54	0.016
	RCAP_rcc02609_at	*clpP*	ATP-dependent Clp protease, ATP-binding subunit ClpX	-4.30	0.003
	RCAP_rcc02399_at	*hflK*	HflK protein	-9.79	0.004
	RCAP_rcc02400_at	*hflC*	HflC protein	-21.52	0.002
	RCAP_rcc02477_at	*groS*	chaperonin GroS	-3.55	0.011
	RCAP_rcc02478_at	*groL*	chaperonin GroL	-5.24	0.036
	RCAP_rcc02818_at	*ibpA*	small heat shock protein IbpA	-4.19	0.013

3.3. Effect of High Light Intensity

Effect of light was studied by comparing the sample taken at the end of a dark period with the sample taken after 1 hour of 2000 lux light intensity. 2000 lux was a light intensity to which the bacteria were already acclimated. Effect of high light intensity was studied with a light intensity of 10,000 lux. High light intensity was applied to the bacteria at the 6^{th} hour of light period when bacteria were under 2000 lux light intensity. The shift to a 5 times more light intensity caused bacteria to boost the expressions of *nif* and *anf* genes (Table 3.10). This increase stimulated the need for ferrous ions for the structure of nitrogenase genes which can be seen by increased ferrous ion. Increasing light intensity means more electrons were excited at the photosynthetic reaction center. The cells should get rid of the excess electrons. For this purpose, hydrogen production is a very effective method. Therefore, by increasing the hydrogen production metabolism genes, the excess reducing power can efficiently be dissipated.

In a study by Muzziotti et al. (2016) 300W/m^2 light intensity increased hydrogen production rate and photosynthetic performance. In the physiological studies, we exposed bacteria to 7000 lux (400 W/m^2) and showed that this light intensity support photosynthetic activity and increase hydrogen production. We also showed that light intensity of 400 W/m^2 increase hydrogen production rate. We also showed that by low

light intensity after dark period, the photosynthetic reaction center genes and nitrogenase gene expression were stimulated, revealing that the photosynthetic activity and hydrogen production rate increases. Physiological data supported this, too. However, when we increase the high light intensity to 571 W/m^2, this might have caused saturation of the photosystem and bacteria decline the expression of photosystem genes (Table 3.10). Still, the quinone pool should have been over-reduced, therefore in order to dissipate the excess reducing power, nitrogenase genes' expressions were increased. Besides nitrogenase, gene expressions of electron transport complex and ferredoxins which carry electrons to nitrogenase increased (Table 3.12). Similarly, ferrous ion transport protein gene expression was stimulated parallel to increase in nitrogenase genes' expressions. Because of the limitations in the experimental circumstances, we could not keep the bacteria for long time under high light intensity without increase in the temperature of the culture. This much of light intensity can decline the hydrogen production in long term, as suggested in the literature (Androga et al., 2014). Decreased photosystem gene expression actually suggest that hydrogen production will decrease at this light intensity in the long term because of the saturation of photosynthetic apparatus (Hellingwerf et al., 1994). High light stress may also induce damage in the cell if light absorption exceeds the capacity of photosynthetic electron transport (Bruce & Vasil'ev, 2004).

Transcription process was significantly down regulated upon high light intensity. 29 genes belonging to 30 and 50 S ribosomal subunits were down regulated (Appendix H). However, heat shock sigma factor σ^E was about 3 fold up-regulated. It is induced upon unfolded outer membrane proteins or periplasmic proteins and thus protects the cell from extracytoplasmic stress. Accordingly, it regulates the transcription of genes for periplasmic folding catalysts, proteases, enzymes taking place in polysaccharide biosynthesis, and cell envelope proteins. This suggests that photosystem gene regulation upon high light intensity triggers σ^E since bacteria try to decreased the photosystem components.

Table 3. 10 Changes of important genes of nitrogen metabolism by high light intensity

	Probe Set ID	Gene Symbol	Description	Fold Change (HL/LL)	p value
Nitrogen Metabolism	RCAP_rcc00570_at	*nifK*	nitrogenase molybdenum-iron protein beta chain	+4.14	0.009
	RCAP_rcc00571_at	*nifD*	nitrogenase molybdenum-iron protein alpha chain	+2.68	0.022
	RCAP_rcc03263_at	*nifT*	NifT/FixU family protein	+5.12	0.0185
	RCAP_rcc03264_at	*nifZ*	NifZ family protein	+3.27	0.0281
	RCAP_rcc03268_at	*nifW*	nitrogen fixation protein NifW	+2.85	0.0219
	RCAP_rcc03269_at	*nifV*	homocitrate synthase	+2.60	0.0185
	RCAP_rcc03278_at	*nifX*	nitrogen fixation protein NifX	+3.45	0.0437
	RCAP_rcc00585_at	*anfH*	nitrogenase iron protein	+14.31	0.008
	RCAP_rcc00586_at	*anfD*	nitrogenase iron-iron protein, alpha subunit	+8.742	0.003
	RCAP_rcc00587_at	*anfG*	nitrogenase iron-iron protein, delta subunit	+14.53	0.002

Table 3.10 (continued)

Nitrogen Metabolism	RCAP_rcc00588_at	*anfK*	nitrogenase iron-iron protein, beta subunit	+5.21	0.001
	RCAP_rcc00589_at	*anfO*	nitrogenase iron-iron accessory protein AnfO	+5.92	0.003
Transporters and binding proteins	RCAP_rcc00091_s_at	*feoA2*	ferrous iron transport protein A	+2.88	0.001
	RCAP_rcc00092_at	*feoB*	ferrous iron transport protein B	+2.38	0.005
	RCAP_rcc02373_at		monosacharide ABC transporter, periplasmic monosacharide-binding protein	+2.07	0.006
Photosynthesis	RCAP_rcc00659_at	*puhA*	photosynthetic reaction center, H subunit	-4.74	1.7E+02
	RCAP_rcc00662_at	*bchL*	light-independent protochlorophyllide reductase, iron-sulfur ATP-binding protein	-2.95	1.0E-03
	RCAP_rcc00663_at	*bchH*	magnesium chelatase, H subunit	-2.48	6.9E-03
	RCAP_rcc00688_at	*bchY*	chlorophyllide reductase, BchY subunit	-2.41	1.4E-03
	RCAP_rcc00690_at	*pufQ*	cytochrome, subunit PufQ	-2.55	1.0E-03
	RCAP_rcc00691_at	*pufB*	light-harvesting protein B-870, beta subunit	-4.45	2.4E+03

Table 3.10 (continued)

Photosynthesis	RCAP_rcc00692_at	*pufA*	light-harvesting protein B-870, alpha subunit	-4.50	1.7E+02
	RCAP_rcc00693_at	*pufL*	photosynthetic reaction center, L subunit	-5.41	1.7E+02
	RCAP_rcc00694_at	*pufM*	photosynthetic reaction center, M subunit	-5.79	1.7E+02
	RCAP_rcc00695_at	*pufX*	intrinsic membrane protein PufX	-4.13	2.7E+03
	RCAP_rcc00736_at	*sdhB*	succinate dehydrogenase, iron-sulfur subunit	-2.23	4.0E-03
	RCAP_rcc02530_at	*pucB*	light-harvesting protein B-800/850, beta chain	-2.18	1.6E-03
	RCAP_rcc02531_at	*pucA*	light-harvesting protein B-800/850, alpha chain	-3.34	6.9E+01
	RCAP_rcc02532_at	*pucC*	protein PucC	-2.14	5.5E-03
	RCAP_rcc02533_at	*pucDE*	light-harvesting protein B-800/850, gamma chain	-3.85	3.6E+03
Electron transport	RCAP_rcc00573_at	*fdxD*	ferredoxin V	+4.30	0.013
	RCAP_rcc03284_at	*fdxN*	ferredoxin I	+2.83	0.030

Table 3.10 (continued)

Electron transport	RCAP_rcc03285_at	*fdxC*	ferredoxin IV	+2.02	0.027
	RCAP_rcc01421_at	*fldA*	flavodoxin	+3.09	0.008
	RCAP_rcc03289_at	*rnfC*	electron transport complex protein RnfC	+2.89	0.032
	RCAP_rcc03290_at	*rnfD*	electron transport complex protein RnfD	+4.54	0.015
	RCAP_rcc03291_at	*rnfG*	electron transport complex protein RnfG	+4.17	0.005
	RCAP_rcc03292_at	*rnfE*	electron transport complex protein RnfE	+3.08	0.030
	RCAP_rcc00767_at	*hupA*	hydrogenase, small subunit	+2.45	0.011

2.3.1 Microarray Validation

Real time quantitative PCR (RT-qPCR) is the gold standard allowing for a rapid, sensitive and easy confirmation for validation of microarray based gene expression (VanGuilder et al., 2008). Photosynthetic membrane components were expected to be up regulated by light, therefore 4 genes for photosystem components (*pucA*, *pufL*, *pufM*, *idi*), 1 gene for nitrogenase (*nifH*), 1 gene for electron transport from electron transport chain to the nitrogenase (*fxN*) and one ATP synthase subunit gene (*atpF*) were chosen for primer design. Beckman et al. (2004) states that the correlation between microarray and RT-qPCR results is much more higher when up-regulated genes were compared. Moreover, genes with more than 2.0 fold change are suggested to be selected for validation of microarray

results (Morey et al., 2006). Therefore, the up regulated genes after shift to light period (2000 lux) were used to validate microarray results. Figure 3.14 shows the comparison of fold changes and trends of differential expressions of genes with RT-qPCR and microarray. It is clear that the direction of regulation is same in both methods. Fold change values may differ between microarray and RT-qPCR since microarray is not as sensitive as RT-qPCR, but the important parameter is the direction of regulation. The custom designed *R. capsulatus* microarray chips used in this study were therefore successfully validated.

The expression of *pucA* gene was not found to significantly differ in light exposure, however, other *puc* genes, *pucC* and *pucDE* were significantly up regulated, this might also suggest that *pucA* gene might have up-regulated but maybe eliminated by fold change or downstream significance analysis. Similarly, *atpF* gene expression was not detected with microarray but it was found to be up-regulated by RT-qPCR.

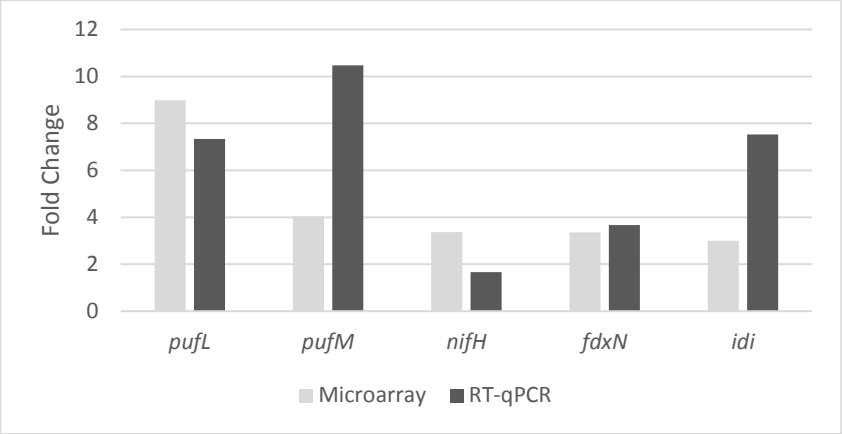

Figure 3. 14 Expression of genes by RT-qPCR and Microarray

CHAPTER 4

CONCLUSIONS

The effects of dark/light cycles, effect of shift to light and high light intensity on *R. capsulatus* were studied with physiological and transcriptomics approaches. Bacterial growth, pH, hydrogen production, bacteriochlorophyll a and organic acid profiles of wild type and *hup*$^-$ mutant of *R. capsulatus* were followed by samples at the end of each 12h light and 12h dark periods of both 2000 lux and 7000 lux light intensities.

Physiological studies revealed that bacterial growth ceased and even decreased in darkness and recovered in light. Concurrently, hydrogen production stopped in dark periods but resumed when light was available and even enhanced by 7000 lux light intensity. Both molar yield and hydrogen production rate increased for each bacterial strain. High light intensity also accelerated substrate consumption. Furthermore, bacteria shifted to fermentative mode and produced acetate in dark periods. High light intensity stimulated formate production of both bacterial strains. This study revealed that while a small amount of formate was produced and half of it was consumed by mutant strain, wild type *R. capsulatus* produced a significant amount of formate, especially under high light intensity by Wood-Ljungdhal pathway.

In order to learn the metabolic response of *R. capsulatus* microarray analysis were completed for the conditions of shift to light after a dark period, and exposure of bacteria to a stress causing high light intensity (10,000 lux). The results showed that shift to a light after a dark period stimulate expressions of photosynthetic apparatus, nitrogenase system and electron transport system genes. Photosynthetic reaction center genes, light harvesting complex genes and bacteriochlorophyll genes were triggered by light. The increased amount of excited electron from photosynthetic system and cyclic electron transfer chain must be dissipated, which was accomplished by increased *nif* and *anf* nitrogenase genes, and also CO_2 fixation by Calvin cycle genes. Electron transport to nitrogenase was also stimulated which was monitored by up-

regulation of ferredoxin and electron transport complex genes. Moreover, increased nitrogenase expression engendered need for molybdenum and iron and this stimulated iron and molybdenum biosynthesis proteins, transporters and binding proteins.

On the other hand, transcription processes were significantly down regulated by light which exhibits an intense transcription in darkness, which triggered stress response similar to temperature stress. This was identified by down-regulation of cold and heat shock protein chaperons, chaperonins and proteases, and also by sigma factor σ^{32} and σ^{70} in the light period.

High light intensity (10,000 lux) further enhanced nitrogenase and electron transport systems to dissipate excess electrons for redox balance, while down-regulated the photosystem genes in order to protect the photosynthetic membrane from damage.

Besides the effect of high light intensity stress, the processes in the darkness should be studied in further details. If the processes in darkness can be more enlightened, bacteria which speed up the energy metabolism in dark and can recover faster, more efficient hydrogen producers can be generated. In the future, for much better understanding of the metabolic relationships between the pathways and genes, gene map of *R. capsulatus* will be established.

In the future, proteome analysis of *R. capsulatus* under different conditions will be carried out. Data obtained from this study and future proteomics studies will be valuable to understand the changes in genetic regulations under light intensity stress and other stress conditions and may lead to genetic manipulations in the PNS bacteria for increased hydrogen yield in large scale industrial photobioreactors. The differentially expressed probes belonging to intergenic sequences from microarray analysis will contribute to complete the annotation of *R. capsulatus* genome. Moreover, the gene map of *R. capsulatus* will be generated with systems biology approaches.

REFERENCES

Adessi, A., & De Philippis, R. (2012). Hydrogen production: photofermentation. In P. C. Hallenbeck (Ed.), *Microbial technologies in advanced biofuels production* (pp. 53–75). New York: Springer.

Adessi, A., & De Philippis, R. (2013). Purple Bacteria: Electron Acceptors and Donors. In *Encyclopedia of Biological Chemistry* (Vol. 3, pp. 693–699).

Adessi, A., & De Philippis, R. (2014). Photobioreactor design and illumination systems for H_2 production with anoxygenic photosynthetic bacteria: A review. *International Journal of Hydrogen Energy*, *39*(7), 3127–3141.

Adessi, A., & Philippis, R. De. (2014). Photosynthesis and Hydrogen Production in Purple Non Sulfur Bacteria: Fundamental and Applied Aspects. In D. Zannoni & R. De Philippis (Eds.) (pp. 269–290). Springer Netherlands.

Afsar, N., Özgür, E., Gürgan, M., Akköse, S., Yücel, M., Gündüz, U., & Eroglu, I. (2011). Hydrogen productivity of photosynthetic bacteria on dark fermenter effluent of potato steam peels hydrolysate. *International Journal of Hydrogen Energy*, *36*(1), 432–438.

Afşar, N., Özgür, E., Gürgan, M., De Vrije, T., Yücel, M., Gündüz, U., & Eroglu, I. (2009). Hydrogen production by *R. capsulatus* on dark fermenter effluent of potato steam peel hydrolysate. *Chemical Engineering Transactions*, 18, S23-S28.

Akman, M. C., Erguder, T. H., Gunduz, U., & Eroglu, I. (2014). Investigation of the effects of initial substrate and biomass concentrations and light intensity on photofermentative hydrogen gas production by Response Surface Methodology. *International Journal of Hydrogen Energy*.

Allen, J. P., & Williams, J. C. (1998). Photosynthetic reaction centers. *FEBS Letters*, *438*(1), 5–9.

Allen, K. J., Lepp, D., McKellar, R. C., & Griffiths, M. W. (2010). Targeted microarray analysis of stationary phase *Escherichia coli* O157:H7 subjected to disparate nutrient conditions. *Journal of Applied Microbiology*, *109*(6), 2118–2127.

Androga, D. D., Özgür, E., Eroglu, I., Gündüz, U., & Yücel, M. (2012a). Amelioration of photofermentative hydrogen production from molasses dark fermenter effluent by zeolite-based removal of ammonium ion. *International Journal of Hydrogen Energy*, *37*(21), 16421–16429.

Androga, D. D., Özgür, E., Eroglu, I., Gündüz, U., & Yücel, M. (2012b). Photofermentative Hydrogen Production in Outdoor Conditions. In D. Minic (Ed.), *Hydrogen Energy - Challenges and perspectives* (pp. 77–120). InTech.

Androga, D. D., Sevinç, P., Koku, H., Yücel, M., Gündüz, U., & Eroglu, I. (2014). Optimization of temperature and light intensity for improved photofermentative hydrogen production using *Rhodobacter capsulatus* DSM 1710. *International Journal of Hydrogen Energy*, *39*(6), 2472–2480.

Argun, H., & Kargi, F. (2010). Effects of light source, intensity and lighting regime on bio-hydrogen production from ground wheat starch by combined dark and photo-fermentations. *International Journal of Hydrogen Energy*, *35*(4), 1604–1612.

Argun, H., Kargi, F., & Kapdan, I. K. (2009). Effects of the substrate and cell concentration on bio-hydrogen production from ground wheat by combined dark and photo-fermentation. *International Journal of Hydrogen Energy*, *34*(15), 6181–6188.

Arikawa, E., Sun, Y., Wang, J., Zhou, Q., Ning, B., Dial, S. L., Yang, J. (2008). Cross-platform comparison of SYBR Green real-time PCR with TaqMan PCR, microarrays and other gene expression measurement technologies evaluated in the MicroArray Quality Control (MAQC) study. *BMC Genomics*, *9*, 328.

Asada, Y., Ohsawa, M., Nagai, Y., Ishimi, K., Fukatsu, M., Hideno, A., Miyake, J. (2008). Re-evaluation of hydrogen productivity from acetate by some photosynthetic bacteria. *International Journal of Hydrogen Energy*, *33*(19), 5147–5150.

Avcioglu, S. G., Ozgur, E., Eroglu, I., Yucel, M., & Gunduz, U. (2011). Biohydrogen production in an outdoor panel photobioreactor on dark fermentation effluent of molasses. *International Journal of Hydrogen Energy*, *36*(17), 11360–11368.

Barbosa, M. J., Rocha, J. M. S., Tramper, J., & Wijffels, R. H. (2001). Acetate as a carbon source for hydrogen production by photosynthetic bacteria. *Journal of Biotechnology*, *85*(1), 25–33.

Basak, N., & Das, D. (2007). The prospect of purple non-sulfur (PNS) photosynthetic bacteria for hydrogen production: The present state of the art. *World Journal of Microbiology and Biotechnology*, *23*(1), 31–42.

Beckman, K. B., Lee, K. Y., Golden, T., & Melov, S. (2004). Gene expression profiling in mitochondrial disease: assessment of microarray accuracy by high-throughput Q-PCR. *Mitochondrion*, *4*(5–6), 453–470.

Benjamini, Y., & Hochberg, Y. (1995). Controlling the false discovery rate: a practical and powerful approach to multiple testing. *Journal of the Royal Statistical Society B*, *57*(1), 289–300.

Berghoff, B. A., & Klug, G. (2016). Stress and Environmental Regulation of Gene

Expression and Adaptation in Bacteria, 2 Volume Set. In F. J. de Bruijn (Ed.), *Stress and Environmental Regulation of Gene Expression and Adaptation in Bacteria* (1st ed., pp. 1–22). New Jersey: Wiley-Blackwell

Biebl, H., & Pfennig, B. (1981). Isolation of members of the family *Rhodospirillaceae*. In H. . Starr, M.P., Stolp, H., Trüper, H.G., Balows, A., Schlegel (Ed.), *The Prokaryotes* (pp. 267–273). New York: Springer.

Biegel, E., Schmidt, S., González, J. M., & Müller, V. (2011). Biochemistry, evolution and physiological function of the Rnf complex, a novel ion-motive electron transport complex in prokaryotes. *Cellular and Molecular Life Sciences*.

Blankenship, R. E. (2008). The Basic Principles of Photosynthetic Energy Storage. In *Molecular Mechanisms of Photosynthesis* (pp. 1–10). Oxford, UK: Blackwell Science Ltd.

Bock, A. K., Glasemacher, J., Schmidt, R., & Schönheit, P. (1999). Purification and characterization of two extremely thermostable enzymes, phosphate acetyltransferase and acetate kinase, from the hyperthermophilic eubacterium *Thermotoga maritima*. *Journal of Bacteriology*, *181*(6), 1861–7.

Boran, E., Özgür, E., Van Der Burg, J., Yücel, M., Gündüz, U., & Eroglu, I. (2010). Biological hydrogen production by *Rhodobacter capsulatus* in solar tubular photo bioreactor. *Journal of Cleaner Production*, *18*(SUPPL. 1).

Boran, E., Özgür, E., Yücel, M., Gündüz, U., & Eroglu, I. (2012a). Biohydrogen production by *Rhodobacter capsulatus hup*$^{-}$ mutant in pilot solar tubular photobioreactor. In *International Journal of Hydrogen Energy*, 37, 16437–16445.

Boran, E., Özgür, E., Yücel, M., Gündüz, U., & Eroglu, I. (2012b). Biohydrogen production by *Rhodobacter capsulatus* in solar tubular photobioreactor on thick juice dark fermenter effluent. *Journal of Cleaner Production*, *31*(August), 150–157.

Bruce, D., & Vasil'ev, S. (2004). Excess Light Stress: Multiple Dissipative Processes of Excess Excitation. In *Chlorophyll a Fluorescence* (pp. 497–523). Dordrecht: Springer Netherlands.

Chandrasekhar, K., Lee, Y.-J., & Lee, D.-W. (2015). Biohydrogen Production: Strategies to Improve Process Efficiency through Microbial Routes. *International Journal of Molecular Sciences*, *16*(4), 8266–8293.

Cheng, J., Poduska, B., Morton, R. A., & Finan, T. M. (2011). An ABC-type cobalt transport system is essential for growth of *Sinorhizobium meliloti* at trace metal concentrations. *Journal of Bacteriology*, *193*(17), 4405–16.

Chomczynski, P., & Sacchi, N. (1987). Single-step method of RNA isolation by acid guanidinium thiocyanate-phenol-chloroform extraction. *Analytical Biochemistry*, *162*(1), 156–159.

Claassen, P. A. M., de Vrije, T., Koukios, E., van Niel, E., Eroglu, I., Modigell, M., Ahrer, W. (2010). Non-thermal production of pure hydrogen from biomass: HYVOLUTION. *Journal of Cleaner Production*, *18*, S4–S8.

Colbeau, A., Richaud, P., Toussaint, B., Caballero, F. J., Elster, C., Delphin, C., Vignais, P. M. (1993). Organization of the genes necessary for hydrogenase expression in *Rhodobacter capsulatus*. Sequence analysis and identification of two hyp regulatory mutants. *Molecular Microbiology*, *8*(1), 15–29.

Crable, B. R., Plugge, C. M., McInerney, M. J., & Stams, A. J. M. (2011). Formate formation and formate conversion in biological fuels production. *Enzyme Research*, *2011*, 532–536.

Das, D., & Veziroglu, T. N. (2001). Hydrogen production by biological processes: a survey of literature. *International Journal of Hydrogen Energy*, *26*(1), 13–28.

Das, D., & Veziroglu, T. N. (2008). Advances in biological hydrogen production processes. *International Journal of Hydrogen Energy*, *33*(21), 6046–6057.

Dixon, R., & Kahn, D. (2004). Genetic regulation of biological nitrogen fixation. *Nature Reviews Microbiology*, *2*(8), 621–631.

Dumur, C. I., Nasim, S., Best, A. M., Archer, K. J., Ladd, A. C., Mas, V. R., Ferreira-Gonzalez, A. (2004). Evaluation of quality-control criteria for microarray gene expression analysis. *Clinical Chemistry*, *50*(11), 1994–2002.

Ehrenreich, A. (2006). DNA microarray technology for the microbiologist: an overview. *Applied Microbiology and Biotechnology*, *73*(2), 255–273.

Eroglu, I., Tabanoğlu, A., Gündüz, U., Eroğlu, E., & Yücel, M. (2008). Hydrogen production by *Rhodobacter sphaeroides* O.U.001 in a flat plate solar bioreactor. *International Journal of Hydrogen Energy*, *33*(2), 531–541.

Gerling, I. C., Ali, C., & Lenchik, N. (2003). Characterization of early developments in the splenic leukocyte transcriptome of NOD mice. In *Annals of the New York Academy of Sciences* (Vol. 1005, pp. 157–160). BioMed Central.

Gest, H., & Kamen, M. D. (1949). Photoproduction of Molecular Hydrogen by *Rhodospirillum rubrum*. *Science (New York, N.Y.)*, *109*(2840), 558–9.

Goldberg, I., Nadler, V., & Hochman, A. (1987). Mechanism of nitrogenase switch-off by oxygen. *Journal of Bacteriology*, *169*(2), 874–879.

Golomysova, A., Gomelsky, M., & Ivanov, P. S. (2010). Flux balance analysis of photoheterotrophic growth of purple nonsulfur bacteria relevant to biohydrogen production. *International Journal of Hydrogen Energy*, *35*(23), 12751–12760.

Gómez, X., Fernández, C., Fierro, J., Sánchez, M. E., Escapa, A., & Morán, A. (2011). Hydrogen production: Two stage processes for waste degradation. *Bioresource Technology*, *102*(18), 8621–8627.

Gruber, T. M., & Gross, C. A. (2003). Multiple Sigma Subunits and the Partitioning of Bacterial Transcription Space. *Annual Review of Microbiology*, *57*(1), 441–466.

Gürgan, M. (2011). *Microarray Analysis of the Effects of Heat and Cold Stress on Hydrogen Production Metabolism of Rhodobacter capsulatus*. Middle East Technical University. Retrieved from http://etd.lib.metu.edu.tr/upload/12613668/index.pdf

Gürgan, M., Erkal, N. A., Özgür, E., Gündüz, U., Eroglu, I., & Yücel, M. (2015). Transcriptional Profiling of Hydrogen Production Metabolism of *Rhodobacter capsulatus* under Temperature Stress by Microarray Analysis. *International Journal of Molecular Sciences*, *16*(6), 13781–97.

Hädicke, O., Grammel, H., & Klamt, S. (2011). Metabolic network modeling of redox balancing and biohydrogen production in purple nonsulfur bacteria. *BMC Systems Biology*, *5*, 150.

Hahn, F. ., Baker, J. ., & Poulter, C. (1996). Open reading frame 176 in the photosynthesis gene cluster of *Rhodobacter capsulatus* encodes idi, a gene for isopenthyl diphosphate isomerase. *Journal of Bacteriology*, *178*, 619–624.

Hallenbeck, P. C. (2011). Microbial paths to renewable hydrogen production. *Biofuels*, *2*(3), 285–302.

Hallenbeck, P. C. (2014). Bioenergy from Microorganisms: An Overview. In D. Zannoni & R. De Philippis (Eds.), *Microbial BioEnergy: Hydrogen Production*, *Advances in Photosynthesis and Respiration 38* (pp. 3–21). Springer Netherlands.

Hallenbeck, P. C., & Benemann, J. R. (2002). Biological hydrogen production; Fundamentals and limiting processes. In *International Journal of Hydrogen Energy* (Vol. 27, pp. 1185–1193).

Hartmann, T., & Leimkühler, S. (2013). The oxygen-tolerant and NAD^+-dependent formate dehydrogenase from *Rhodobacter capsulatus* is able to catalyze the reduction of CO_2 to formate. *FEBS Journal*, *280*(23), 6083–6096.

Hellingwerf, K. J., Crielaard, W., Hoff, W. D., Matthijs, H. C. P., Mur, L. R., & van Rotterdam, B. J. (1994). Photobiology of Bacteria. *Antonie van Leeuwenhoek*, *65*(4), 331–347.

Hemmingsen, S. M., Woolford, C., van der Vies, S. M., Tilly, K., Dennis, D. T., Georgopoulos, C. P., Ellis, R. J. (1988). Homologous plant and bacterial proteins chaperone oligomeric protein assembly. *Nature*, *333*(6171), 330–334.

Hillmer, P., & Gest, H. (1977). H_2 metabolism in the photosynthetic bacterium *Rhodopseudomonas capsulata*: H_2 production by growing cultures. *Journal of Bacteriology*, *129*(2), 724–31.

Hoekema, S., Douma, R. D., Janssen, M., Tramper, J., & Wijffels, R. H. (2006). Controlling light-use by continuous cultures in a flat panel photobioreactor. *Biotechnology and Bioengineering, Biotechnology and Bioengineering*, *95*(4), 613–626.

Holt, J. H., Krieg, N. R., Sneath, P. H. a., Staley, J. T., & Williams, S. T. (1994). Bergey's manual of determinative bacteriology ninth edition. *European Journal of Paediatric Neurology : EJPN : Official Journal of the European Paediatric Neurology Society*, *13*(6), 560.

Imhoff, J. F. (1995). Taxonomy and Physiology of Phototrophic Purple Bacteria and Green Sulfur Bacteria. In *Anoxygenic Photosynthetic Bacteria* (pp. 1–15). Dordrecht: Kluwer Academic Publishers.

Imhoff, J. F. (2006). The Phototrophic Alpha-Proteobacteria. In *The Prokaryotes* (pp. 41–64). New York, NY: Springer New York.

IPCC. (2006). 2006 IPCC Guidelines for National Greenhouse Gas Inventories. *2006 IPCC Guidelines for National Greenhouse Gas Inventories*, *3*(Chapter 2: Mineral Industry Emissions), 1–40.

Jeong, H. S., & Jouanneau, Y. (2000). Enhanced nitrogenase activity in strains of *Rhodobacter capsulatus* that overexpress the *rnf* genes. *Journal of Bacteriology*, *182*(5), 1208–14.

Jeremiasse, A. W., Hamelers, H. V. M., & Buisman, C. J. N. (2009). Microbial electrolysis cell with a microbial biocathode. *Bioelectrochemistry*, *78*, 39–43.

Jin, H., & Nikolau, B. J. (2012). Role of genetic redundancy in polyhydroxyalkanoate (PHA) polymerases in PHA biosynthesis in *Rhodospirillum rubrum*. *Journal of Bacteriology*, *194*(20), 5522–9.

Jouanneau, Y., Meyer, C., Naud, I., & Klipp, W. (1995). Characterization of an *fdxN* mutant of *Rhodobacter capsulatus* indicates that ferredoxin I serves as electron donor to nitrogenase. *Biochimica et Biophysica Acta (BBA) - Bioenergetics*, *1232*(1–2), 33–42.

Jouanneau, Y., Wong, B., & Vignais, P. M. (1985). Stimulation by light of nitrogenase synthesis in cells of *Rhodopseudomonas capsulata* growing in N-limited continuous cultures. *Biochimica et Biophysica Acta (BBA) - Bioenergetics*, *808*(1), 149–155.

Kappler, U., Huston, W. M., & Mcewan, A. G. (2002). Control of dimethylsulfoxide reductase expression in *Rhodobacter capsulatus* : the role of carbon metabolites and

the response regulators DorR and RegA. *Microbiology*, *148*, 605–614.

Kars, G., & Gündüz, U. (2010). Towards a super H_2 producer: Improvements in photofermentative biohydrogen production by genetic manipulations. *International Journal of Hydrogen Energy*, *35*(13), 6646–6656.

Kars, G., Gunduz, U., Rakhely, G., Yucel, M., Eroglu, I., & Kovacs, K. L. (2008). Improved hydrogen production by uptake hydrogenase deficient mutant strain of *Rhodobacter sphaeroide*s O.U.001. *International Journal of Hydrogen Energy*, *33*(12), 3056–3060. 37

Koku, H., Eroglu, I., Gündüz, U., Yücel, M., & Türker, L. (2002). Aspects of the metabolism of hydrogen production by *Rhodobacter sphaeroides*. *International Journal of Hydrogen Energy*, *27*(11–12), 1315–1329.

Kranz, R. G., Pace, V. M., & Caldicottt, I. M. (1990). Inactivation, Sequence, and *lacZ* Fusion Analysis of a Regulatory Locus Required for Repression of Nitrogen Fixation Genes in *Rhodobacter capsulatus*. *Journal of Bacteriology*, *172*(1), 53–62.

Kühlbrandt, W. (1995). Structure and function of bacterial light-harvesting complexes. *Structure*, *3*(6), 521–525.

Law, C. J., Roszak, A. W., Southall, J., Gardiner, A. T., Isaacs, N. W., & Cogdell, R. J. (2004). The structure and function of bacterial light-harvesting complexes. *Mol Membr Biol*, *21*(3), 183–191.

Levin, D. B., Pitt, L., & Love, M. (2004). Biohydrogen production: Prospects and limitations to practical application. *International Journal of Hydrogen Energy*, *29*(2), 173–185.

Li, X., Wang, Y., Zhang, S., Chu, J., Zhang, M., Huang, M., & Zhuang, Y. (2011). Effects of light/dark cycle, mixing pattern and partial pressure of H_2 on biohydrogen production by *Rhodobacter sphaeroides* ZX-5. *Bioresource Technology*, *102*(2), 1142–1148.

Liu, H., Grot, S., & Logan, B. E. (2005). Electrochemically assisted microbial production of hydrogen from acetate. *Environmental Science and Technology*, *39*(11), 4317–4320.

Livak, K. J., & Schmittgen, T. D. (2001). Analysis of Relative Gene Expression Data Using Real-Time Quantitative PCR and the $2^{-\Delta\Delta CT}$ Method. *Methods*, *25*(4), 402–408.

Madigan, M. T., & Jung, D. O. (2009). Chapter 01 - An Overview of Purple Bacteria: Systematics, Physiology, and Habitats. *The Purple Phototrophic Bacteria*, *28*, 1–15.

Masepohl, B., Kaiser, B., Isakovic, N., Richard, C. L., Kranz, R. G., & Klipp, W. (2001). Urea Utilization in the Phototrophic Bacterium *Rhodobacter capsulatus* Is Regulated by the Transcriptional Activator NtrC. *Journal of Bacteriology*, *183*(2), 637–643.

McEwan, A. G. (1994). Photosynthetic electron transport and anaerobic metabolism in purple non-sulfur phototrophic bacteria. *Antonie van Leeuwenhoek*, *66*(151), 151–164. R

McKinlay, J. B. (2014). Systems Biology of Photobiological Hydrogen Production by Purple Non-sulfur Bacteria (pp. 155–176). Springer Netherlands.

Meher Kotay, S., & Das, D. (2008). Biohydrogen as a renewable energy resource-Prospects and potentials. *International Journal of Hydrogen Energy*, *33*(1), 258–263.

Morey, J. S., Ryan, J. C., & Dolah, F. M. (2006). Microarray validation: factors influencing correlation between oligonucleotide microarrays and real-time PCR. *Biological Procedures Online*, *8*(1), 175–193.

Muzziotti, D., Adessi, A., Faraloni, C., Torzillo, G., & De Philippis, R. (2016). H2 production in *Rhodopseudomonas palustris* as a way to cope with high light intensities. *Research in Microbiology*, *167*(5), 350–356.

Oda, Y., Samanta, S. K., Rey, F. E., Wu, L., Liu, X., Yan, T., Harwood, C. S. (2005). Functional genomic analysis of three nitrogenase isozymes in the photosynthetic bacterium *Rhodopseudomonas palustris*. *Journal of Bacteriology*, *187*(22), 7784–7794.

Onder, O., Aygun-Sunar, S., Selamoglu, N., & Daldal, F. (2010). A glimpse into the proteome of phototrophic bacterium *Rhodobacter capsulatus*. *Advances in Experimental Medicine and Biology*, *675*, 179–209.

Oyedotun, K. S., & Lemire, B. D. (2004). The quaternary structure of the *Saccharomyces cerevisiae* succinate dehydrogenase. Homology modeling, cofactor docking, and molecular dynamics simulation studies. *The Journal of Biological Chemistry*, *279*(10), 9424–31.

Özgür, E., & Peksel, B. (2013). Biohydrogen production from barley straw hydrolysate through sequential dark and photofermentation. *Journal of Cleaner Production*, *52*, 14–20.

Özgür, E., Uyar, B., Öztürk, Y., Yücel, M., Gündüz, U., & Eroglu, I. (2010). Biohydrogen production by *Rhodobacter capsulatus* on acetate at fluctuating temperatures. *Resources, Conservation and Recycling*, *54*(5), 310–314.

Öztürk, Y. (2005). *Characterization of the genetically modified cytochrome systems and their application to biohydrogen production in Rhodobacter capsulatus*. Middle

East Technical University. Retrieved from http://etd.lib.metu.edu.tr/upload/3/12606961/index.pdf

Öztürk, Y., Gökçe, A., Peksel, B., Gürgan, M., Özgür, E., Gündüz, U., Yücel, M. (2012). Hydrogen production properties of *Rhodobacter capsulatus* with genetically modified redox balancing pathways. *International Journal of Hydrogen Energy*, *37*(2).

Ozturk, Y., Yucel, M., Daldal, F., Mandaci, S., Gunduz, U., Turker, L., & Eroglu, I. (2006). Hydrogen production by using *Rhodobacter capsulatus* mutants with genetically modified electron transfer chains. *International Journal of Hydrogen Energy*, *31*(11), 1545–1552.

Peters, J. W. (1995). Nitrogenase Structure and Function: A Biochemical-Genetic Perspective. *Annual Review of Microbiology*, *49*(1), 335–366.

Pfaffl, M. W., Collao, B., Molina-Quiroz, R. C., Pradenas, G. A., Saona, L. A., Durán-Toro, V., Zhang, J. (2001). A new mathematical model for relative quantification in real-time RT-PCR. *Nucleic Acids Research*, *29*(9), 45e–45.

Raina, A., & Jänne, J. (1975). Physiology of the natural polyamines putrescine, spermidine and spermine. *Medical Biology*, *53*(3), 121–47. Retrieved from

Rainbird, R. M., Atkins, C. A., & Pate, J. S. (1983). Effect of temperature on nitrogenase functioning in cowpea nodules. *Plant Physiology*, *73*(2), 392–4.

Rajeevan, M. S., Vernon, S. D., Taysavang, N., & Unger, E. R. (2001). Validation of array-based gene expression profiles by real-time (kinetic) RT-PCR. *The Journal of Molecular Diagnostics : JMD*, *3*(1), 26–31.

Ren, N., Guo, W., Liu, B., Cao, G., & Ding, J. (2011). Biological hydrogen production by dark fermentation: Challenges and prospects towards scaled-up production. *Current Opinion in Biotechnology*.

Rubio, L. M., & Ludden, P. W. (2008). Biosynthesis of the Iron-Molybdenum Cofactor of Nitrogenase. *Annual Review of Microbiology*, *62*(1), 93–111.

Sasikala, K., Ramana, C. V., & Raghuveer Rao, P. (1991). Environmental regulation for optimal biomass yield and photoproduction of hydrogen by *Rhodobacter sphaeroides* O.U. 001. *International Journal of Hydrogen Energy*, *16*(9), 597–601.

Schauer, K., Stolz, J., Scherer, S., & Fuchs, T. M. (2009). Both thiamine uptake and biosynthesis of thiamine precursors are required for intracellular replication of *Listeria monocytogenes*. *Journal of Bacteriology*, *191*(7), 2218–27.

Sevinç, P. (2010). *Kinetic Analyses of the Effects of Temperature and Light*. Middle East Technical University. Retrieved from http://etd.lib.metu.edu.tr/upload/12612195/index.pdf

Shi, L., Jones, W. D., Jensen, R. V, Harris, S. C., Perkins, R. G., Goodsaid, F. M., Tong, W. (2008). The balance of reproducibility, sensitivity, and specificity of lists of differentially expressed genes in microarray studies. *BMC Bioinformatics*, *9 Suppl 9*(Suppl 9), S10.

Simon, R., Lam, A., Li, M.-C., Ngan, M., Menenzes, S., & Zhao, Y. (2007). Analysis of gene expression data using BRB-ArrayTools. *Cancer Informatics*, *3*, 11–7.

Slonim, D. K., & Yanai, I. (2009). Getting started in gene expression microarray analysis. *PLoS Computational Biology*, *5*(10), e1000543.

Smyth, G. K. (2004). Linear Models and Empirical Bayes Methods for Assessing Differential Expression in Microarray Experiments. *Statistical Applications in Genetics and Molecular Biology*, *3*(1), 1–25.

Strnad, H., Lapidus, A., Paces, J., Ulbrich, P., Vlcek, C., Paces, V., & Haselkorn, R. (2010). Complete genome sequence of the photosynthetic purple nonsulfur bacterium *Rhodobacter capsulatus* SB 1003. *Journal of Bacteriology*, *192*(13), 3545–3546.

Tabor, C. W., & Tabor, H. (1976). 1,4-Diaminobutane (Putrescine), Spermidine, and Spermine. *Annual Review of Biochemistry*, *45*(1), 285–306.

Tellmann, G. (2006). The E-Method: a highly accurate technique for gene-expression analysis. *Nature Methods*, *3*(7), i–ii.

Tichi, M. A., & Tabita, F. R. (2000). Maintenance and control of redox poise in *Rhodobacter capsulatus* strains deficient in the Calvin-Benson-Bassham pathway. *Archives of Microbiology*, *174*(5), 322–333.

Trevino, V., Falciani, F., & Barrera-Saldaña, H. A. (2007). DNA microarrays: a powerful genomic tool for biomedical and clinical research. *Molecular Medicine (Cambridge, Mass.)*, *13*(9–10), 527–41.

Untergasser, A., Cutcutache, I., Koressaar, T., Ye, J., Faircloth, B. C., Remm, M., & Rozen, S. G. (2012). Primer3—new capabilities and interfaces. *Nucleic Acid Research*, *40*(15), 1–12.

Uyar, B. (2008). *Hydrogen production by microorganisms in solar bioreactor*. Middle East Technical University. Retrieved from http://etd.lib.metu.edu.tr/upload/2/12609252/index.pdf

Uyar, B., Eroglu, I., Yücel, M., Gündüz, U., & Türker, L. (2007). Effect of light intensity, wavelength and illumination protocol on hydrogen production in photobioreactors. *International Journal of Hydrogen Energy*, *32*(18), 4670–4677.

Uyar, B., Gürgan, M., Özgür, E., Gündüz, U., Yücel, M., & Eroglu, I. (2015). Hydrogen production by *hup*$^{-}$ mutant and wild-type strains of *Rhodobacter capsulatus*

from dark fermentation effluent of sugar beet thick juice in batch and continuous photobioreactors. *Bioprocess and Biosystems Engineering*, *38*(10).

Uyar, B., Gürgan, M., Özgür, E., Gündüz, U., Yücel, M., & Eroglu, I. (2015). Hydrogen production by hup- mutant and wild-type strains of *Rhodobacter capsulatus* from dark fermentation effluent of sugar beet thick juice in batch and continuous photobioreactors. *Bioprocess and Biosystems Engineering*, *38*(10), 1935–1942.

Uyar, B., Kars, G., Yücel, M., Gündüz, U., & Eroglu, I. (2012). Hydrogen Production via Photofermentation. In N. Azbar & D. B. Levin (Eds.), *State of the Art and Progress in Production of Biohydrogen* (pp. 54–77). BENTHAM SCIENCE PUBLISHERS.
VanGuilder, Heather D., Vrana, Kent E., Freeman, W. M. (2008). Twenty-five years of quantitative PCR for gene expression analysis. *BioTechniques*, *44*(5).

Villarreal-Chiu, J. F., Quinn, J. P., & McGrath, J. W. (2012). The genes and enzymes of phosphonate metabolism by bacteria, and their distribution in the marine environment. *Frontiers in Microbiology*, *3*, 19.

Wakayama, T., Nakada, E., Asada, Y., & Miyake, J. (2000). Effect of Light/Dark Cycle on Bacterial Hydrogen Production by *Rhodobacter sphaeroides* RV. *Applied Biochemistry and Biotechnology*, *84–86*(1–9), 431–440.

Weaver, P. F., Wall, J. D., & Gest, H. (1975). Characterization of *Rhodopseudomonas capsulata*. *Archives of Microbiology*, *105*(3), 207–16.

Wei, Y., Lee, J. M., Richmond, C., Blattner, F. R., Rafalski, J. A., & LaRossa, R. A. (2001). High-density microarray-mediated gene expression profiling of *Escherichia coli*. *Journal of Bacteriology*, *183*(2), 545–56. http://doi.org/10.1128/JB.183.2.545-556.2001

White, D., Drummond, J. (James T., & Fuqua, C. (2012). *The physiology and biochemistry of prokaryotes* (4th Editio). New York: Oxford University Press.

Wood, H. G., Ragsdale, S. W., & Pezacka, E. (1986). The acetyl-CoA pathway: a newly discovered pathway of autotrophic growth. *Trends in Biochemical Sciences*, *11*(1), 14–18. http://doi.org/10.1016/0968-0004(86)90223-9

Worden, C. R., Kovac, W. K., Dorn, L. A., & Sandrin, T. R. (2009). Environmental pH affects transcriptional responses to cadmium toxicity in *Escherichia coli* â€ƒK-12 (MG1655). *FEMS Microbiology Letters*, *293*(1), 58–64.

Yang, H., Zhang, J., Wang, X., Feng, J., Yan, W., & Guo, L. (2015). Coexpression of Mo- and Fe-nitrogenase in *Rhodobacter capsulatus* enhanced its photosynthetic hydrogen production. *International Journal of Hydrogen Energy*, *40*(2), 927–934.

Yilmaz, R., Yücel, M., & Oktem, H. A. (2008). Quality assessment of gene expression data for an affymetrix platform with the two sample t-tests statistical analysis.

International Journal of Biotechnology & Biochemistry, *4*, 101–108.

Ziegelhoffer, E. C., & Donohue, T. J. (2009). Bacterial responses to photo-oxidative stress. *Nature Reviews. Microbiology*, *7*(12), 856–63.

Zinchenko, V., Churin, Y., Shestopalov, V., & Shestakov, S. (1994). Nucleotide sequence and characterization of the *Rhodobacter sphaeroides glnB* and *glnA* genes. *Microbiology*, *140*(8), 2143–2151. http://doi.org/10.1099/13500872-140-8-2143

APPENDIX A

COMPOSITION OF THE GROWTH AND HYDROGEN PRODUCTION MEDIA

Table A. 1 The constituents of 1L MPYE medium

Medium composition	Amount
Bactopeptone	3 g
Yeast extract	3 g
$MgCl_2$	1.6 mL from 1M stock
$CaCl_2$	1 mL from 1M stock

The constituents are dissolved in distilled water; pH is adjusted to 7, and sterilized by autoclaving.

Table A. 2 The constituents of the growth and hydrogen production media per liter of solution

Medium composition	Growth medium 20/10 A/G	Hydrogen production medium 30/2 A/G
KH_2PO_4	3 g	3 g
$MgSO_4.7H_2O$	0.5 g	0.5 g
$CaCl_2.2H_2O$	0.05 g	0.05 g
Acetic acid	1.15 mL	2.29 mL
Na-Glutamate	1.85 g	0.36 g
Vitamin solution (10X)	0.1 mL	0.1 mL
Trace element solution (10X)	0.1 mL	0.1 mL
Fe-citrate solution (50X)	0.5 mL	0.5 mL

Vitamin solution, trace element solution and Fe-citrate solution are added after the other constituents are dissolved in distilled water and sterilized by autoclaving.

Table A. 3 The composition of 100 ml of 10x vitamin solution Composition

Composition	Amount
Thiamin Chloride Hydrochloride (B1)	500 mg
Niacin (Nicotinic acid)	500 mg
D + Biotin	15 mg

The constituents are dissolved in distilled water and sterilized by filtering

Table A. 4 The composition of 100 ml of 10x trace element solution

Composition	Amount
$ZnCl_2$	70 mg
$MnCl_2.4H_2O$	100 mg
H_3BO_3	60 mg
$CoCl_2.6H_2O$	200 mg
$CuCl_2.2H_2O$	20 mg
$NiCl_2.6H_2O$	20 mg
$NaMoO_4.2H_2O$	40 mg
HCl (25% v/v)	1 mL

The constituents are dissolved in distilled water and sterilized by autoclaving.

Ferric citrate solution: 5 g ferric citrate is dissolved in 100 ml distilled water and sterilized by autoclaving

APPENDIX B

OPTICAL DENSITY-DRY CELL WEIGHT CALIBRATION CURVES

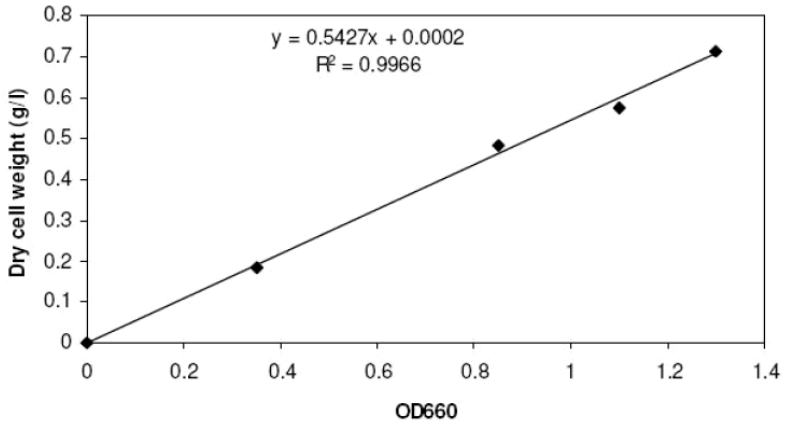

Figure B. 1 Calibration curve and the regression trend line for *Rhodobacter capsulatus* (DSM1710) dry cell weight vs OD660nm (Uyar, 2008)

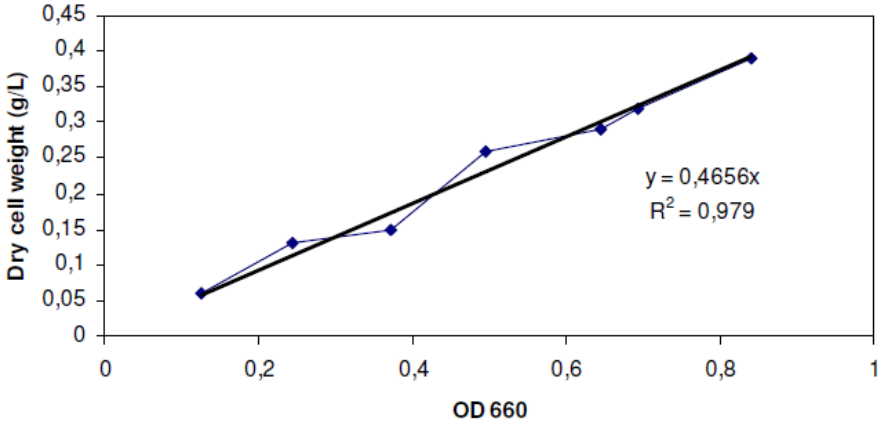

Figure B. 2 Calibration curve and the regression trend line for *Rhodobacter capsulatus* YO3 dry cell weight versus OD660 (Yavuz Öztürk, 2005)

APPENDIX C

SAMPLE GAS CHROMATOGRAM

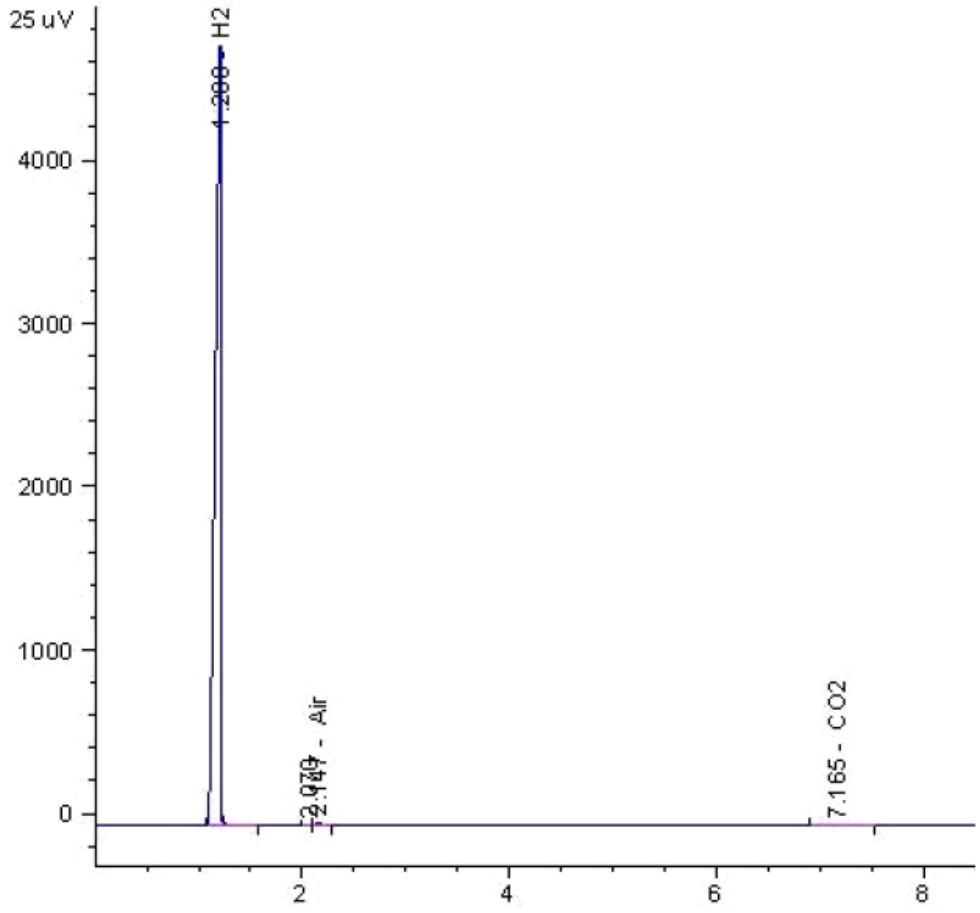

RetTime [min]	Type	Area [25 uV*s]	Amt/Area	Norm %	Grp	Name
1.208	BB	1.78157e4	5.36760e-3	92.790983		H2
2.147	VB	104.16668	4.30476e-2	4.351104		Air
7.165	BB	52.88443	5.56929e-2	2.857913		CO2
Totals :				100.000000		

Figure C. 1 A sample chromatogram for GC analysis of the produced gas

APPENDIX D

SAMPLE HPLC CHROMATOGRAPHY AND CALIBRATION CURVES

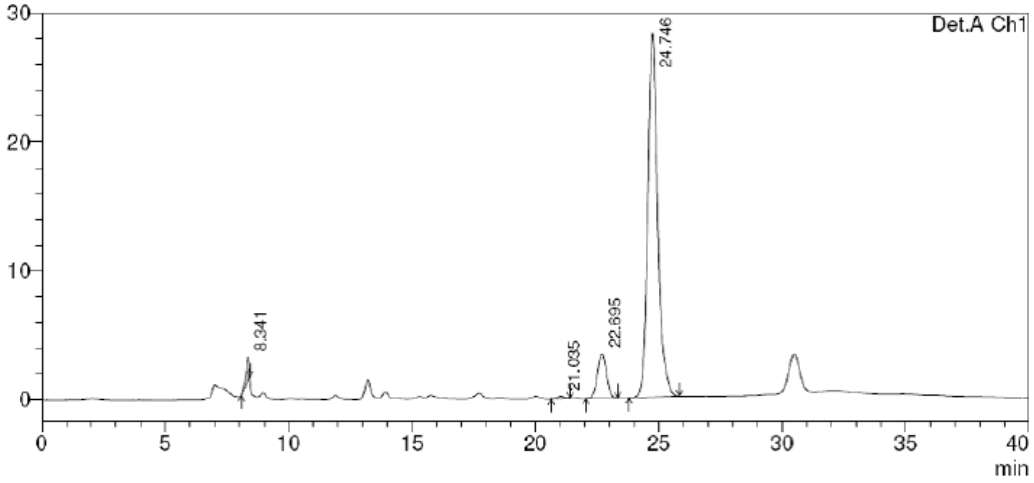

PeakTable

Detector A Ch1 210nm

Peak#	Ret. Time	Area	Height	Area %	Height %
1	8.341	14689	1859	1.654	5.516
2	21.035	3735	182	0.420	0.542
3	22.695	86422	3453	9.730	10.248
4	24.746	783359	28200	88.196	83.694
Total		888205	33695	100.000	100.000

Figure D. 1 A sample HPLC chromatogram for organic acids analysis. Peak 1 (mobile phase- H_2SO_4), Peak 2 (lactic acid), Peak 3 (formic acid) and Peak 4 (acetic acid)

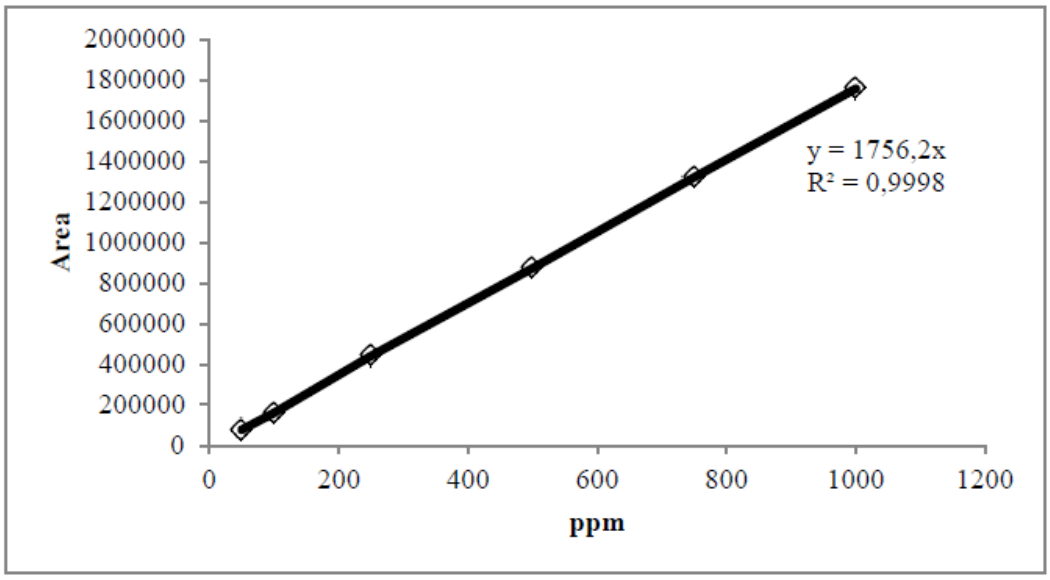

Figure D. 2 Standard HPLC calibration curve of acetic acid

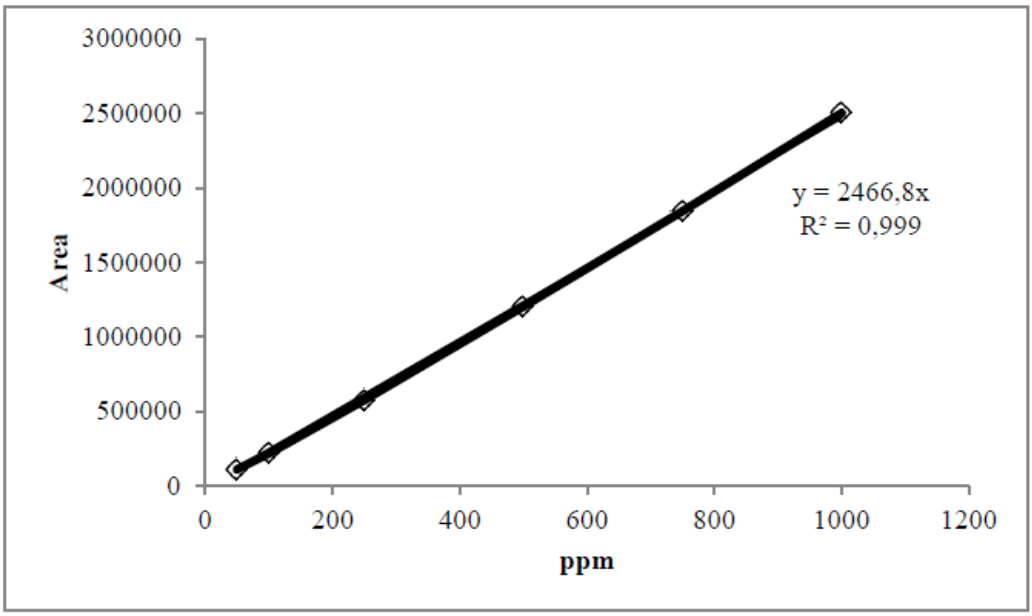

Figure D. 3 Standard HPLC calibration curve of formic acid

APPENDIX E

COMPOSITION OF TRIS EDTA BUFFER

1 M Tris-HCl (pH 7.5) stock solution: 157.6 g Tris-HCl is dissolved in 1 L of distilled water

1 mM EDTA (pH 8) stock solution: 186.1 g EDTA dissodium salt is dissolved in 700 ml distilled water, pH is adjudted to 8 by 5N NaOH, the volume is completed to 1 L.

Table E. 1 The constituents of TE buffer (10mM Tris, 1mM EDTA)

Composition	Amount
1 M Tris-HCl stock solution	1 mL
0.5 M EDTA stock solution	0.2 mL

The constituents are dissolved in 100 mL of distilled water and autoclaved.

APPENDIX F

SAMPLE BIOANALYZER GEL IMAGE AND ELECTROPHEROGRAM

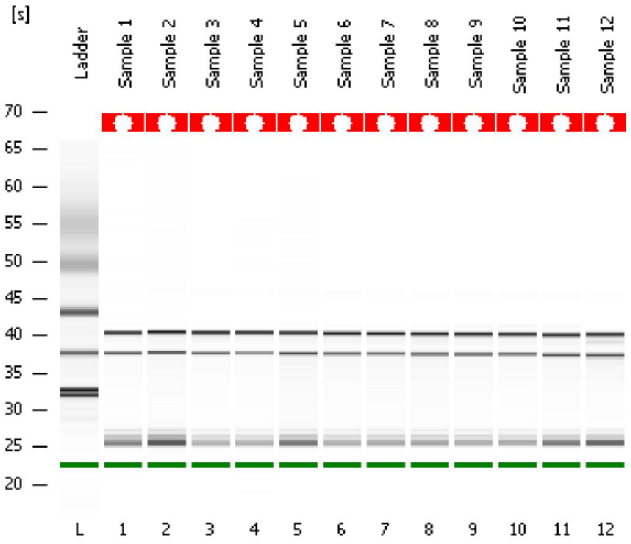

Figure F. 1 Bioanalyzer gel picture for total RNA of Rhodobacter capsulatus. Line at 25th s indicates 5S rRNA, line at 38th s indicates 16S rRNA and line at 40th s indicates 23S rRNA.

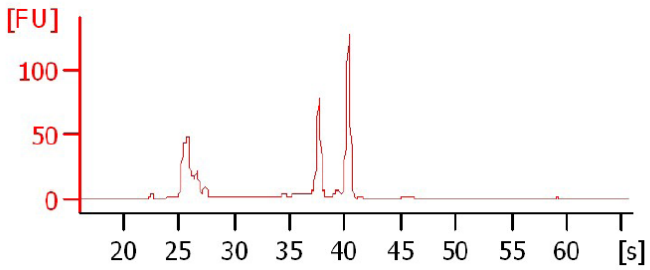

Figure F. 2 Bioanalyzer electropherogram for total RNA of Rhodobacter capsulatus. Peak at 25th s indicates 5S rRNA, peak at 38th s indicates 16S rRNA and peak at 40th s indicates 23S rRNA.

APPENDIX G

THE LISTS OF SIGNIFICANTLY CHANGED GENES OF *R. capsulatus* UPON LIGHT

Table G. 1 Differentially expressed after 15min of shift to light period

Probe Set ID	Gene Symbol	Description	Fold Change	P value
RCAP_rcc00014_at	*xylA*	xylose isomerase	+2.8855267	0.001
RCAP_rcc00021_at		cytochrome c peroxidase	+2.2540953	0.004
RCAP_rcc00058_at	*flhB*	flagellar biosynthetic protein FlhB	+2.0242705	0.007
RCAP_rcc00081_at	*leuC*	3-isopropylmalate dehydratase, large subunit	-2.197461	0.005
RCAP_rcc00085_at	*leuB*	3-isopropylmalate dehydrogenase	-2.2585752	0.025
RCAP_rcc00169_at	*kpsE*	capsule polysaccharide export protein	-2.2291992	0.004
RCAP_rcc00208_at	*argG*	argininosuccinate synthase	-2.1174877	0.023
RCAP_rcc00225_at	*alkB*	alpha-ketoglutarate-dependent dioxygenase AlkB	+2.297518	0.003
RCAP_rcc00242_at		conserved hypothetical protein 730	+2.0036824	0.005
RCAP_rcc00257_at	*leuS*	leucyl-tRNA synthetase	-2.4206676	0.012
RCAP_rcc00260_at		alanine racemase domain protein	-2.4170127	0.029
RCAP_rcc00277_at	*rbfA*	ribosome-binding factor A	-2.223494	0.003
RCAP_rcc00284_at	*pnp*	polyribonucleotide nucleotidyltransferase	-3.244937	0.011
RCAP_rcc00292_at	*rpoC*	DNA-directed RNA polymerase, beta' subunit	+2.179214	0.047
RCAP_rcc00295_at	*rpsG*	30S ribosomal protein S7	-2.080871	0.010
RCAP_rcc00303_at	*rpsS*	30S ribosomal protein S19	-2.6500282	0.050
RCAP_rcc00310_at	*rplN*	50S ribosomal protein L14	-3.7430341	0.0006
RCAP_rcc00313_at	*rpsN*	30S ribosomal protein S14	-4.0302405	0.002
RCAP_rcc00314_at	*rpsH*	30S ribosomal protein S8	-3.841806	0.003
RCAP_rcc00315_at	*rplF*	50S ribosomal protein L6	-3.5811226	0.012
RCAP_rcc00316_at	*rplR*	50S ribosomal protein L18	-3.4332538	0.026
RCAP_rcc00318_at	*rpmD*	50S ribosomal protein L30	-2.0230231	0.047
RCAP_rcc00326_at	*rpoA*	DNA-directed RNA polymerase, alpha subunit	-2.4294832	0.026
RCAP_rcc00345_at	*rpmH*	50S ribosomal protein L34	-2.0218978	0.021
RCAP_rcc00350_at	*rpmH*	50S ribosomal protein L34	-2.0948749	0.015

Table G.1 (continued)

RCAP_rcc00380_at		transglycosylase, Slt family	+2.0063636	0.005
RCAP_rcc00415_at		oxidoreductase, short-chain dehydrogenase/reductase family	-2.1248295	0.003
RCAP_rcc00456_at	*coaBC*	bifunctional phosphopantothenoylcysteine decarboxylase/phosphopantothenate--cysteine ligase	+2.1459103	0.004
RCAP_rcc00490_at	*metF*	5,10-methylenetetrahydrofolate reductase	-2.7756116	0.011
RCAP_rcc00513_at	*etfD*	electron transfer flavoprotein-ubiquinone oxidoreductase	-2.4202151	0.005
RCAP_rcc00571_at	*nifD*	nitrogenase molybdenum-iron protein alpha chain	+5.5405526	0.001
RCAP_rcc00585_at	*anfH*	nitrogenase iron protein	+3.828099	0.006
RCAP_rcc00587_at	*anfG*	nitrogenase iron-iron protein, delta subunit	+2.617207	0.007
RCAP_rcc00668_at	*ppsR*	transcriptional regulator PpsR	-2.3145025	0.002
RCAP_rcc00669_at	*bchE*	magnesium-protoporphyrin IX monomethyl ester anaerobic oxidative cyclase	+2.4713151	0.002
RCAP_rcc00692_at	*pufB*	light-harvesting protein B-870, beta subunit	-2.061075	0.021
RCAP_rcc00696_at	*dxS*	1-deoxy-D-xylulose-5-phosphate synthase	+2.2785316	0.004
RCAP_rcc00716_at	*pntB*	pyridine nucleotide transhydrogenase, beta subunit	-2.0786216	0.024
RCAP_rcc00728_at	*nurU*	NnrU family protein	-2.5939763	0.027
RCAP_rcc00742_at	*atpE*	ATP synthase F0, C subunit	-3.1818116	0.018
RCAP_rcc00744_at	*atpF*	ATP synthase F0, B subunit	-2.5000925	0.042
RCAP_rcc00773_at	*hupH*	hydrogenase expression/formation protein HupH	+2.0497026	0.012
RCAP_rcc00852_at	*srmB*	ATP-dependent RNA helicase SrmB	-2.0400355	0.010
RCAP_rcc00880_at		CHAP domain protein	-2.8268602	0.003
RCAP_rcc00889_at	*nosL*	NosL protein	+2.0480077	0.005
RCAP_rcc00975_at		cyclic nucleotide-binding domain protein	+2.0519924	0.004
RCAP_rcc00978_at		phage conserved hypothetical protein	+2.1168737	0.004
RCAP_rcc01021_at	*ugpC*	sn-glycerol-3-phosphate transport ATP-binding protein UgpC	+2.298864	0.004
RCAP_rcc01035_at		conserved domain protein	+2.9806807	0.014
RCAP_rcc01096_at	*abgB*	aminobenzoyl-glutamate utilization protein B	-2.080688	0.003
RCAP_rcc01141_at	*gltX*	glutamyl-tRNA synthetase	-2.2372918	0.009

Table G.1 (continued)

RCAP_rcc01155_at		conserved hypothetical protein	-2.0802288	0.025
RCAP_rcc01168_at		methyltransferase small domain protein	-2.2734516	0.002
RCAP_rcc01170_at		conserved hypothetical protein	+2.094454	0.010
RCAP_rcc01173_at	*hemC*	hydroxymethylbilane synthase	-2.0016975	0.004
RCAP_rcc01209_at		cell wall hydrolase, SleB	-2.2134097	0.010
RCAP_rcc01217_at	*ureD*	urease accessory protein UreD	+2.189577	0.004
RCAP_rcc01218_at	*ureA*	urease, gamma subunit	+2.0566754	0.004
RCAP_rcc01226_at	*urtB*	urea ABC transporter, urea binding protein UrtB	+3.7240293	0.0005
RCAP_rcc01264_at		reverse transcriptase family protein	-2.052706	0.007
RCAP_rcc01456_at		membrane protein, MarC family	-2.1563237	0.003
RCAP_rcc01568_at		RES domain family protein	+2.0677311	0.009
RCAP_rcc01580_at		conserved hypothetical protein	-2.118302	0.043
RCAP_rcc01603_at		hemolysin-III family protein	-2.207123	0.003
RCAP_rcc01643_at		transglutaminase-like family protein	+2.3096638	0.002
RCAP_rcc01670_at		conserved hypothetical protein	-2.1644404	0.014
RCAP_rcc01673_at	*glnB*	nitrogen regulatory protein P-II	+2.2845082	0.002
RCAP_rcc01689_at		phage conserved hypothetical protein	+2.0591354	0.016
RCAP_rcc01708_at	*pgk*	phosphoglycerate kinase	-2.1456397	0.011
RCAP_rcc01775_at	*aglK*	alpha-glucoside ABC transporter, ATP-binding protein	+2.1179426	0.006
RCAP_rcc01814_at		conserved hypothetical protein	-2.084963	0.003
RCAP_rcc01828_at	*rpe*	ribulose-phosphate 3-epimerase	+2.2404222	0.005
RCAP_rcc01829_at	*cbbM*	ribulose bisphosphate carboxylase, large subunit	+2.1305733	0.004
RCAP_rcc01844_at		sensor histidine kinase	-2.092591	0.003
RCAP_rcc01845_at		conserved domain protein	-2.027065	0.008
RCAP_rcc01867_at		protein of unknown function DUF853, NPT hydrolase putative	+2.3896708	0.005
RCAP_rcc01888_at		conserved hypothetical protein	-2.216299	0.006
RCAP_rcc01891_at	*emrE*	multidrug transporter EmrE	-2.46535	0.030
RCAP_rcc01932_at		glycosyl transferase, family 4	+2.1961799	0.010
RCAP_rcc01938_at		membrane protein, putative	+2.091956	0.008
RCAP_rcc01957_at		protein of unknown function DUF940	-2.065495	0.003
RCAP_rcc01963_at		conserved hypothetical protein	+2.0964184	0.016
RCAP_rcc01983_at		phage terminase, small subunit	+2.3499117	0.002
RCAP_rcc02009_at	*rplI*	50S ribosomal protein L9	-3.9577956	0.005
RCAP_rcc02010_at	*rpsR*	30S ribosomal protein S18	-3.8272128	0.003
RCAP_rcc02066_at		secretion protein, HlyD family	+2.2124162	0.003
RCAP_rcc02201_at	*adhE*	aldehyde-alcohol dehydrogenase	+2.2289975	0.004
RCAP_rcc02204_at		conserved hypothetical protein	+2.2018385	0.003

Table G.1 (continued)

RCAP_rcc02212_at		ThiJ/PfpI family protein	+2.237773	0.003
RCAP_rcc02277_at	*oppC*	oligopeptide ABC transporter, permease protein OppC	+2.1313572	0.003
RCAP_rcc02291_at			+2.0985022	0.034
RCAP_rcc02300_at	*rplU*	50S ribosomal protein L21	-2.1347718	0.004
RCAP_rcc02397_at		RNA polymerase sigma factor, sigma-70 family, ECF subfamily	-2.1359036	0.004
RCAP_rcc02463_at		hemolysin-type calcium-binding repeat family protein	+2.2720335	0.006
RCAP_rcc02497_at		ABC transporter, ATP-binding protein	+2.0186021	0.010
RCAP_rcc02507_at		membrane protein, putative	-2.1775577	0.004
RCAP_rcc02526_at	*amaB*	N-carbamoyl-L-amino acid amidohydrolase	+2.524248	0.007
RCAP_rcc02528_at		dihydropyrimidine dehydrogenase (NADP(+))	+2.1544664	0.047
RCAP_rcc02529_at		pyridine nucleotide-disulphide oxidoreductase family protein	+2.9771638	0.034
RCAP_rcc02550_at	*infA*	translation initiation factor IF-1	-2.129301	0.007
RCAP_rcc02604_at	*aat*	leucyl/phenylalanyl-tRNA--protein transferase	-2.0306551	0.008
RCAP_rcc02605_at		conserved hypothetical protein	-2.0267518	0.048
RCAP_rcc02628_at	*nadD*	nicotinate-nucleotide adenylyltransferase	+2.0235367	0.007
RCAP_rcc02665_at		hemolysin-type calcium-binding repeat family protein	-2.395194	0.002
RCAP_rcc02666_at		hydrolase, alpha/beta fold family	+2.391225	0.002
RCAP_rcc02850_at	*thiM*	hydroxyethylthiazole kinase	+2.3331964	0.006
RCAP_rcc02887_at		methyl-accepting chemotaxis sensory transducer	+2.4052284	0.007
RCAP_rcc02955_at	*cysK*	cysteine synthase	-2.0675507	0.004
RCAP_rcc02988_at		conserved hypothetical protein	-2.0037549	0.041
RCAP_rcc02990_at		YbaK/EbsC family protein	+2.1750796	0.003
RCAP_rcc03035_at	*fdhA*	NAD-dependent formate dehydrogenase, delta subunit	+2.046882	0.003
RCAP_rcc03049_at		major facilitator superfamily MFS_1	+2.1018968	0.003
RCAP_rcc03118_at		conserved hypothetical protein	+2.133378	0.003
RCAP_rcc03131_at		conserved hypothetical protein	-2.114857	0.004
RCAP_rcc03143_at		conserved hypothetical protein	+2.0181463	0.011
RCAP_rcc03165_at	*accA*	acetyl-CoA carboxylase, carboxyl transferase, alpha subunit	-2.1839275	0.004
RCAP_rcc03169_at		zinc finger domain protein	+2.0214763	0.005
RCAP_rcc03177_at		EAL domain protein	+2.1462715	0.005
RCAP_rcc03203_at	*glpD*	glycerol-3-phosphate dehydrogenase	+2.149975	0.003
RCAP_rcc03243_at	*ccrA*	crotonyl-CoA reductase	-2.5516217	0.012
RCAP_rcc03262_at		conserved hypothetical protein	+2.8307292	0.005
RCAP_rcc03263_at	*nifT*	NifT/FixU family protein	+6.3919196	0.0006
RCAP_rcc03264_at	*nifZ*	NifZ family protein	+8.053552	0.0003
RCAP_rcc03268_at	*nifW*	nitrogen fixation protein NifW	+2.0466754	0.005
RCAP_rcc03269_at	*nifV*	homocitrate synthase	+2.5697527	0.003

Table G.1 (continued)

RCAP_rcc03272_at		HesB/YadR/YfhF family protein	+4.6940136	0.004
RCAP_rcc03274_at	*nifQ*	NifQ family protein	+2.3479989	0.007
RCAP_rcc03278_at	*nifX*	nitrogen fixation protein NifX	+2.7890537	0.002
RCAP_rcc03279_at	*nifN*	nitrogenase molybdenum-iron cofactor biosynthesis protein NifN	+6.241855	0.0006
RCAP_rcc03290_at	*rnfD*	electron transport complex protein RnfD	+3.4525368	0.003
RCAP_rcc03294_at	*fccB*	FAD-dependent pyridine nucleotide-disulphide oxidoreductase	+3.131424	0.002
RCAP_rcc03364_at	*bioF*	8-amino-7-oxononanoate synthase	+2.0213513	0.010
RCAP_rcc03367_at		protein of unknown function DUF452	+2.1627913	0.003
RCAP_rcc03382_at	*tyrB*	aromatic-amino-acid aminotransferase	-2.1409314	0.016
RCAP_rcc03384_at	*emrA*	multidrug resistance protein A	-2.274516	0.002
RCAP_rcc03386_at	*amtB*	ammonium transporter	+2.8045292	0.003
RCAP_rcc03387_at	*glnB*	nitrogen regulatory protein P-II	+2.6052754	0.002
RCAP_rcc03448_at	*tyrB*	aromatic-amino-acid aminotransferase	-2.1440678	0.008
RCAP_rcc03490_at		VacJ family lipoprotein	-2.3002324	0.011
RCAP_rcc03494_at		conserved hypothetical protein	-2.2398152	0.006
RCAP_rcp00038_at		membrane protein, putative	+2.0166888	0.005
RCAP_rcp00060_s_at		TonB-dependent receptor	+2.3224344	0.013
RCAP_rcp00127_s_at	*mdcE*	malonate decarboxylase, gamma subunit	+2.0034118	0.006

Table G. 2 Differentially expressed genes of transcription, translation and nucleic acid metabolism by shift to light period

Probe Set ID	**Gene Symbol**	**Description**	**Fold Change**	**P value**
RCAP_rcc00001_at	*dnaA*	chromosomal replication initiator protein DnaA	-6.457041	0.002
RCAP_rcc00032_at		Smr protein/MutS2	-4.2309866	0.001
RCAP_rcc00060_s_at	*parB*	chromosome-partitioning protein ParB	-4.100369	0.001
RCAP_rcc00061_s_at	*parA*	chromosome-partitioning protein ParA	-2.4264703	0.004
RCAP_rcc00065_at	*rho*	transcription termination factor Rho	-4.84813	0.002
RCAP_rcc00079_at		iojap-related protein	-41.14032	3.04E-4
RCAP_rcc00118_at		sigma 54 modulation protein/ribosomal protein S30EA	-2.8285682	0.002
RCAP_rcc00146_at	*parC*	DNA topoisomerase IV, A subunit	+2.366674	0.004
RCAP_rcc00147_s_at	*tuf*	translation elongation factor Tu	-4.478977	0.005
RCAP_rcc00189_at	*cca*	CCA-adding enzyme	-2.367964	0.007

Table G.2 (continued)

RCAP_rcc00213_at	*nusA*	transcription elongation factor NusA	-2.4783478	0.004
RCAP_rcc00222_at	*radC*	DNA repair protein RadC	-2.6612475	0.009
RCAP_rcc00226_at	*mutY*	A/G-specific adenine glycosylase	+2.1248662	0.014
RCAP_rcc00251_at	*ade*	adenine deaminase	-2.462235	0.010
RCAP_rcc00263_at		two component transcriptional regulator, winged helix family	-3.657377	0.003
RCAP_rcc00265_at		RmuC domain protein	+2.4761314	0.004
RCAP_rcc00276_at	*rbfA*	ribosome-binding factor A	-2.8428707	0.005
RCAP_rcc00281_at	*rpsO*	30S ribosomal protein S15	-2.3587728	0.004
RCAP_rcc00286_at	*nusG*	transcription antitermination protein NusG	-3.5991642	0.002
RCAP_rcc00287_at	*rplK*	50S ribosomal protein L11	-2.8214972	0.005
RCAP_rcc00288_at	*rplA*	50S ribosomal protein L1	-4.292394	0.003
RCAP_rcc00289_at	*rplJ*	50S ribosomal protein L10	-5.1108856	0.009
RCAP_rcc00291_at	*rpoB*	DNA-directed RNA polymerase, beta subunit	-2.1589	0.033
RCAP_rcc00294_at	*rpsL*	30S ribosomal protein S12	-5.3850627	0.001
RCAP_rcc00296_at	*fusA*	translation elongation factor G	-4.0495796	0.011
RCAP_rcc00298_at	*rpsJ*	30S ribosomal protein S10	-8.676559	5.72E-4
RCAP_rcc00299_at	*rplC*	50S ribosomal protein L3	-2.339414	0.011
RCAP_rcc00300_at	*rplD*	50S ribosomal protein L4	-18.623388	568.851
RCAP_rcc00301_at	*rplW*	50S ribosomal protein L23	-2.9921262	0.013
RCAP_rcc00302_at	*rplB*	50S ribosomal protein L2	-2.1715627	0.044
RCAP_rcc00305_at	*rpsC*	30S ribosomal protein S3	-9.988032	0.005
RCAP_rcc00311_at	*rplX*	50S ribosomal protein L24	-2.7014205	0.016
RCAP_rcc00312_at	*rplE*	50S ribosomal protein L5	-3.1783473	0.022
RCAP_rcc00321_at	*rplO*	50S ribosomal protein L15	-2.4487922	0.003
RCAP_rcc00324_at	*rpsM*	30S ribosomal protein S13	-12.177331	8.77E-4
RCAP_rcc00325_at	*rpsK*	30S ribosomal protein S11	-4.978095	0.001
RCAP_rcc00327_at	*rplQ*	50S ribosomal protein L17	-5.6774487	0.009
RCAP_rcc00328_at		autoinducer-binding transcriptional regulator, LuxR family	-2.8978212	0.002
RCAP_rcc00355_at		S1 RNA binding domain protein	-2.1612236	0.008
RCAP_rcc00361_at	*rpmE*	50S ribosomal protein L31	-2.4142706	0.004
RCAP_rcc00364_at	*trmD*	tRNA (guanine-N1)-methyltransferase	+2.1290698	0.007
RCAP_rcc00418_at		transcriptional regulator, TetR family	+2.5580065	0.007
RCAP_rcc00458_at	*rpoH*	RNA polymerase sigma-32 factor	-4.3102703	0.003
RCAP_rcc00480_at	*rpsU*	30S ribosomal protein S21	-3.3140695	0.004
RCAP_rcc00483_at		transcriptional regulator, AsnC/Lrp family	+2.4610362	0.005
RCAP_rcc00494_at		transcriptional regulator, AsnC/Lrp family	+2.1312654	0.009
RCAP_rcc00532_at	*aspS*	aspartyl-tRNA synthetase	-2.9339716	0.004
RCAP_rcc00557_at	*metG*	methionyl-tRNA synthetase	-2.2572336	0.025
RCAP_rcc00623_at		transcriptional regulator, RpiR family	+2.586006	0.007

Table G.2 (continued)

RCAP_rcc00715_at	*pntA*	pyridine nucleotide transhydrogenase, alpha subunit	-2.6594875	0.008
RCAP_rcc00841_at	*gatB*	glutamyl-tRNA(Gln) amidotransferase, B subunit	+2.6601427	0.009
RCAP_rcc00864_at	*rpsI*	30S ribosomal protein S9	-2.7641537	0.047
RCAP_rcc00873_at		transcriptional regulator, XRE family	-2.0403523	0.022
RCAP_rcc01125_at	*rpsA*	30S ribosomal protein S1	-6.4450502	0.002
RCAP_rcc01134_at		transcriptional regulator, Fur family	-3.8618796	0.002
RCAP_rcc01171_at		ATP-dependent RNA helicase DbpA	-9.00551	8.77E-4
RCAP_rcc01205_at	*glyQ*	glycyl-tRNA synthetase, alpha subunit	-2.8611608	0.003
RCAP_rcc01236_at		transcriptional regulator, GntR family	-2.0420575	0.004
RCAP_rcc01270_at		transcriptional regulator, XRE family	+2.682348	0.004
RCAP_rcc01287_at	*mcrC*	McrBC restriction endonuclease system, McrC subunit	+2.7006147	0.002
RCAP_rcc01305_at		CRISPR-associated protein, Cas1 family	+2.015874	0.010
RCAP_rcc01308_at		transposase, IS66 family	+2.3141034	0.011
RCAP_rcc01340_at		transcriptional regulator, LysR family	+2.3377957	0.012
RCAP_rcc01347_at		pirin domain protein	+2.06408	0.005
RCAP_rcc01384_at	*uvrB*	UvrABC system protein B	-3.5229743	0.002
RCAP_rcc01499_at		DNA alkylation repair enzyme family protein	+2.2076066	0.004
RCAP_rcc01561_at		transcriptional regulator, Crp/Fnr family	-4.067068	0.001
RCAP_rcc01626_at	*frr*	ribosome recycling factor	-2.7591672	0.006
RCAP_rcc01661_at	*trmU*	tRNA (5-methylaminomethyl-2-thiouridylate)-methyltransferase	-2.3910108	0.009
RCAP_rcc01679_at	*ligT*	2'-5' RNA ligase	+2.5846722	0.003
RCAP_rcc01720_at	*ndk*	nucleoside diphosphate kinase	-3.1291277	0.044
RCAP_rcc01755_at	*cysS*	cysteinyl-tRNA synthetase	+2.1468756	0.017
RCAP_rcc01801_at	*hfq*	RNA chaperone Hfq	-6.0861073	0.002
RCAP_rcc01805_at	*ssb*	single-stranded DNA-binding protein	-2.8169546	0.007
RCAP_rcc01896_at		transcriptional regulator, GntR family	-3.2969882	0.003
RCAP_rcc01905_at		transposase, IS4 family	+2.0094163	0.005
RCAP_rcc01909_at	*rpmF*	50S ribosomal protein L32	-21.45179	4.70E-4
RCAP_rcc01912_at	*ihfA*	integration host factor, alpha subunit	-2.664493	0.002
RCAP_rcc01929_at	*hsdS*	type I restriction-modification system RcaSBIV, S subunit	+2.3231578	0.005
RCAP_rcc02011_at	*rpsF*	30S ribosomal protein S6	-5.56329	0.016
RCAP_rcc02021_at		transcriptional regulator, DeoR family	+2.5432162	0.002
RCAP_rcc02091_s_at		transposase, IS66 family	+4.9178085	8.77-E-4

Table G.2 (continued)

RCAP_rcc02103_at		transposase, IS3/IS911 family	+2.1380365	0.005
RCAP_rcc02195_at		HNH endonuclease family protein	-2.5995038	0.002
RCAP_rcc02299_at	*rpmA*	50S ribosomal protein L27	-2.7524788	0.002
RCAP_rcc02322_at	*prfC*	peptide chain release factor 3	-2.1355975	0.005
RCAP_rcc02361_at	*lexA*	LexA repressor	-3.3902903	0.003
RCAP_rcc02425_at	*surE*	5'-nucleotidase SurE	-2.6291988	0.007
RCAP_rcc02461_at	*thrS*	threonyl-tRNA synthetase	-2.0595784	0.010
RCAP_rcc02514_at	*dtd*	D-tyrosyl-tRNA(Tyr) deacylase	+2.464347	0.003
RCAP_rcc02515_at	*rhlE*	ATP-dependent RNA helicase RhlE	-6.3970904	0.003
RCAP_rcc02566_at		resolvase family protein	-3.8138843	0.004
RCAP_rcc02637_at		RNA polymerase sigma factor, sigma-70 family, ECF subfamily	-7.5107093	0.001
RCAP_rcc02759_at	*recR*	recombination protein RecR	-3.6199768	0.002
RCAP_rcc02811_at	*rpoH*	RNA polymerase sigma-32 factor	-3.0378351	0.004
RCAP_rcc03050_at	*rplY*	50S ribosomal protein L25	-4.377023	0.009
RCAP_rcc03054_at	*rpoD*	RNA polymerase sigma factor RpoD	-3.4139185	0.002
RCAP_rcc03081_at	*nrdR*	transcriptional regulator NrdR	-3.2873306	0.002
RCAP_rcc03132_at	*hrpB*	ATP-dependent RNA helicase HrpB	+2.0066082	0.005
RCAP_rcc03147_at		transcriptional regulator, MerR family	+2.053909	0.033
RCAP_rcc03154_at	*rplT*	50S ribosomal protein L20	-2.246937	0.009
RCAP_rcc03155_at	*rpmI*	50S ribosomal protein L35	-2.8737152	0.007
RCAP_rcc03321_at	*rluA*	ribosomal large subunit pseudouridine synthase A	+3.0611906	0.003
RCAP_rcc03325_at		hemimethylated DNA-binding protein family	-3.2146707	0.002
RCAP_rcc03383_at		transcriptional regulator, MarR family	-2.5682197	0.005
RCAP_rcc03404_at	*pyrF*	orotidine 5'-phosphate decarboxylase	-3.1902723	0.002
RCAP_rcc03421_at	*rnhA*	ribonuclease H	+2.64686	0.007
RCAP_rcc03434_at	*map*	methionine aminopeptidase	-2.4423792	0.003
RCAP_rcc03491_at		nucleoside-triphosphatase	-3.4807897	0.005
RCAP_rcc03492_at	*rph*	ribonuclease PH	-3.6219513	0.003
RCAP_rcc03493_at	*hrcA*	heat-inducible transcription repressor HrcA	-2.0315015	0.033
RCAP_rcp00053_s_at		transposase, IS4 family	-3.2665176	0.002
RCAP_rcp00054_s_at		transposase, IS4 family	-14.026845	6.26E-4
RCAP_rcp00064_at		prevent-host-death family protein	+2.254612	0.004
RCAP_rcp00096_at		transcriptional regulator, LysR family	-5.5285177	0.001
RCAP_rcp00107_at		transcriptional regulator, Crp/Fnr family	-3.50851	0.003
RCAP_rcp00107_s_at		transcriptional regulator, Crp/Fnr family	-3.1347408	0.005
RCAP_rcp00145_at		transposase, ISSpo9	+3.0760815	0.002
RCAP_rcc02590_at	*dksA*	DnaK suppressor protein	+2.0759714	0.041

APPENDIX H

THE LISTS OF SIGNIFICANTLY CHANGED GENES OF *R. capsulatus* UPON HIGH LIGHT INTENSTY

Table H. 1 Differentially expressed genes after 15 min of high light intensity application

Probe Set ID	Gene Symbol	Description	Fold Change	P value
RCAP_rcc00147_s_at	*tuf*	translation elongation factor Tu	-2.502	2.9E+03
RCAP_rcc00203_at		conserved domain protein	+2.59	3.0E+02
RCAP_rcc00290_at	*rplL*	50S ribosomal protein L7/L12	-2.50	9.8E+02
RCAP_rcc00296_at	*fusA*	translation elongation factor G	-2.74	1.2E+03
RCAP_rcc00301_at	*rplW*	50S ribosomal protein L23	-2.04	1.1E-03
RCAP_rcc00604_at		integral membrane protein, TerC family	+2.06	3.8E+03
RCAP_rcc00656_at		membrane protein, putative	-2.12	3.0E+03
RCAP_rcc00660_at	*pucC*	PucC protein	-2.01	2.2E-03
RCAP_rcc00661_at	*bchM*	magnesium-protoporphyrin O-methyltransferase	-2.27	3.1E+03
RCAP_rcc00669_at	*bchE*	magnesium-protoporphyrin IX monomethyl ester anaerobic oxidative cyclase	-2.71	9.1E+01
RCAP_rcc00670_at	*bchJ*	bacteriochlorophyll 4-vinyl reductase	-2.05	1.2E-03
RCAP_rcc00674_at	*idi*	isopentenyl-diphosphate delta-isomerase	-2.11	2.9E-03
RCAP_rcc00696_at	*dxS*	1-deoxy-D-xylulose-5-phosphate synthase	-2.36	1.2E+03
RCAP_rcc00737_at		hypothetical protein	+2.06	5.5E+02
RCAP_rcc00832_at	*pta*	phosphate acetyltransferase	-2.40	4.8E+03
RCAP_rcc00833_at	*ackA*	acetate kinase	-2.08	1.6E-03
RCAP_rcc00873_at		transcriptional regulator, XRE family	-2.14	2.1E-03
RCAP_rcc00901_at		conserved hypothetical protein	+2.192	2.8E+02
RCAP_rcc00906_at	*pccB*	propionyl-CoA carboxylase, beta subunit	-2.03	9.5E-03
RCAP_rcc01181_at		membrane protein, putative	+3.45	7.3E-01
RCAP_rcc01214_at	*iIvC*	ketol-acid reductoisomerase	-2.23	1.8E+03
RCAP_rcc01307_at		conserved hypothetical protein	+2.53	1.0E-03
RCAP_rcc01674_at	*glnA*	glutamine synthetase	-2.53	9.6E+01
RCAP_rcc01828_at	*rpe*	ribulose-phosphate 3-epimerase	-2.13	1.7E-03
RCAP_rcc01829_at	*cbbM*	ribulose bisphosphate carboxylase, large subunit	-2.36	3.4E+03
RCAP_rcc01831_at	*gap*	glyceraldehyde-3-phosphate dehydrogenase (phosphorylating)	-2.27	1.4E+03

Table H.1 (continued)

RCAP_rcc01832_at	*tkt*	transketolase	-2.04	7.3E+01
RCAP_rcc01888_at		conserved hypothetical protein	+3.00	3.9E+02
RCAP_rcc02277_at	*oppC*	oligopeptide ABC transporter, permease protein OppC	-2.08	3.3E+03
RCAP_rcc02390_at	*alkB*	alkane 1-monooxygenase	-3.92	2.1E+02
RCAP_rcc02515_at	*rhIE*	ATP-dependent RNA helicase RhlE	+2.25	1.6E+03
RCAP_rcc02521_at		pyrimidine ABC transporter, periplasmic pyrimidine-binding protein	+3.85	9.9E+00
RCAP_rcc02635_at	*cysT*	sulfate ABC transporter, permease protein CysT	-2.76	6.0E-03
RCAP_rcc02669_at	*fabA*	3-hydroxydecanoyl-[acyl-carrier-protein] dehydratase	-2.04	5.8E-03
RCAP_rcc02681_at		cytochrome b561 family protein	-2.25	8.7E+02
RCAP_rcc02682_at		cytochrome c'	-3.01	1.3E+03
RCAP_rcc02973_at	*atpA*	ATP synthase F1, alpha subunit	-2.20	5.5E+03
RCAP_rcc03406_at	*clpB*	chaperone ClpB	+2.09	6.1E+03
RCAP_rcp00121_at	*cbiO*	cobalt ABC transporter, ATP-binding protein CbiO	+2.09	3.1E+02

Table H. 2 Differentially expressed genes of transcription, translation and nucleic acid metabolism after 1h of high light intensity

Probe Set ID	**Gene Symbol**	**Description**	**Fold Change**	**P value**
RCAP_rcc00288_at	*rplA*	50S ribosomal protein L1	-2.07	0.012
RCAP_rcc00289_at	*rplJ*	50S ribosomal protein L10	-3.48	0.004
RCAP_rcc00291_at	*rpoB*	DNA-directed RNA polymerase, beta subunit	-2.04	0.007
RCAP_rcc00292_at	*rpoC*	DNA-directed RNA polymerase, beta' subunit	-2.28	0.001
RCAP_rcc00302_at	*rplB*	50S ribosomal protein L2	-2.62	0.008
RCAP_rcc00303_at	*rpsS*	30S ribosomal protein S19	-2.63	0.012
RCAP_rcc00304_at	*rplV*	50S ribosomal protein L22	-2.68	0.023
RCAP_rcc00305_at	*rpsC*	30S ribosomal protein S3	-2.78	0.009
RCAP_rcc00306_at	*rplP*	50S ribosomal protein L16	-2.17	0.009
RCAP_rcc00308_at	*rpmC*	50S ribosomal protein L29	-2.08	0.010
RCAP_rcc00310_at	*rplN*	50S ribosomal protein L14	-2.48	0.007
RCAP_rcc00311_at	*rplX*	50S ribosomal protein L24	-2.72	0.011
RCAP_rcc00312_at	*rplE*	50S ribosomal protein L5	-3.81	0.010
RCAP_rcc00313_at	*rpsN*	30S ribosomal protein S14	-3.47	0.019
RCAP_rcc00314_at	*rpsH*	30S ribosomal protein S8	-2.57	0.030
RCAP_rcc00316_at	*rplR*	50S ribosomal protein L18	-3.19	0.014

Table H.2 (continued)

RCAP_rcc00317_at	*rpsE*	30S ribosomal protein S5	-3.74	0.014
RCAP_rcc00324_at	*rpsM*	30S ribosomal protein S13	-2.36	0.005
RCAP_rcc00325_at	*rpsK*	30S ribosomal protein S11	-2.05	0.005
RCAP_rcc00326_at	*rpoA*	DNA-directed RNA polymerase, alpha subunit	-2.33	0.005
RCAP_rcc00327_at	*rplQ*	50S ribosomal protein L17	-2.12	0.002
RCAP_rcc00361_at	*rpmE*	50S ribosomal protein L31	-2.40	0.003
RCAP_rcc00362_at	*rplS*	50S ribosomal protein L19	-2.25	0.003
RCAP_rcc00367_at	*rpsP*	30S ribosomal protein S16	-2.19	0.009
RCAP_rcc00480_at	*rpsU*	30S ribosomal protein S21	-2.07	0.003
RCAP_rcc00863_at	*rplM*	50S ribosomal protein L13	-3.35	0.002
RCAP_rcc01663_at	*ctrA*	cell cycle transcriptional regulator CtrA	+2.17	0.040
RCAP_rcc01683_at		terminase-like family protein	+2.42	0.001
RCAP_rcc01821_at	*rpsB*	30S ribosomal protein S2	-2.46	0.002
RCAP_rcc01822_at	*tsf*	translation elongation factor Ts	-2.35	0.002
RCAP_rcc02009_at	*rplI*	50S ribosomal protein L9	-3.93	0.005
RCAP_rcc02010_at	*rpsR*	30S ribosomal protein S18	-3.42	0.006
RCAP_rcc02979_at	*rpsD*	30S ribosomal protein S4	-2.01	0.011
RCAP_rcc03050_at	*rplY*	50S ribosomal protein L25	-2.18	0.018
RCAP_rcc03154_at	*rplT*	50S ribosomal protein L20	-2.20	0.003
RCAP_rcc03283_at	*rseC*	sigma-E factor regulatory protein RseC	+2.94	0.011
RCAP_rcc00329_at		autoinducer synthesis protein	-2.00	0.003

CURRICULUM VITAE

PERSONAL INFORMATION

Name, Surname: Gürgan Eser, Muazzez

Birth: July 21, 1986, Ankara, Turkey

Citizen: Republic of Turkey

Phone: +90 312 256 18 41

Mobile: +90 505 774 68 24

email: muazzezgurgan@gmail.com

EDUCATION

2017	PhD, METU Department of Biology
2011	MSc, METU Department of Biology
2009	Minor Degree, METU Faculty of Education, Department of German Language
2008	BSc, METU Department of Biology

WORK EXPERIENCE

2008-2017	Research and Teaching Assistant, METU Department of Biological Science
2013	Researcher, Geo-Research Center, Potsdam, Germany

2006, 2007 Intern, Hacettepe University Medical School, Department of Metabolism, Molecular Genetics Lab

PUBLICATIONS

Ipekoglu EM, Gocmen K, Oz MT, **Gürgan M**, Yücel M. 2016. Cloning and heterologous expression of chlorophyll a synthase in *Rhodobacter sphaeroides*. Journal of Basic Microbiology, 57 (3), 238-244.

Gürgan M, Afşar Erkal N, Özgür E, Gündüz U, Eroglu, I, Yücel M. 2015. Transcriptional profiling of hydrogen production metabolism of *Rhodobacter capsulatus* under temperature stress by microarray analysis. International Journal of Molecular Sciences, 16, 13781-13797.

Uyar B, **Gürgan M**, Özgür E, Gündüz U, Yücel M, Eroglu, I. 2015. Hydrogen production by hup- mutant and wild-type strains of *Rhodobacter capsulatus* from dark fermentation effluent of sugar beet thick juice in batch and continuous photobioreactors. Bioprocess and Biosystems Engineering, 38, 1935-1942.

Öztürk Y, Gökçe A, Peksel B, **Gürgan M**, Özgür E, Gündüz U, Eroglu I, Yücel M. 2012. Hydrogen production properties of *Rhodobacter capsulatus* with genetically modified redox balancing pathways. International Journal of Hydrogen Energy, 37 (2), 2014-2020

Afsar N, Özgür E, **Gürgan M**, Akköse S, Yücel M, Gündüz U, Eroglu I. 2011. Hydrogen productivity of photosynthetic bacteria on dark fermenter effluent of potato steam peels hydrolysate. International Journal of Hydrogen Energy, 36 (1), 432-438.

Afşar N, Özgür E, **Gürgan M**, de Vrije T, Yücel M, Gündüz U, Eroğlu I. 2009. Hydrogen production by *R. capsulatus* on dark fermenter effluent of potato steam peel hydrolysate. Chemical Engineering Transactions, 18, 385-390.

PRESENTATIONS IN INTERNATIONAL CONFERENCES

Gürgan M, Koku H, Eroglu I, Yücel M. Hydrogen productivities of *Rhodobacter capsulatus* wild type and *hup*$^-$ mutant under low and high light intensity. Intenational Conference on Sustainable Development, Skopje, Macedonia, October 2016 - Oral Presentation

Ipekoglu E.M, Gocmen K, Öz M.T, **Gürgan M**, Yücel M. Biological Hydrogen Production by Pigment System Modified *Rhodobacter sphaeroides*. International Conference on Microalgae and Biodisel, Koç University, Istanbul, Turkey, July 2015 - Poster Presentation

Gürgan M, Afşar N, Özgür E, Eroglu I, Yücel M. Transcriptional Profiling of Hydrogen Production Metabolism of *Rhodobacter capsulatus* Under Temperature Stress by Microarray Analysis. *World Hydrogen Energy Congress,* Gwangju, South Korea, June 2014 - Poster Presentation

Gürgan M, Afşar N, Sevinç P, Özgür E, Gündüz U, Eroglu I, Yücel M. The effects of cold and heat stress on biohydrogen production by *Rhodobacter capsulatus. World Hydrogen Energy Congress*, Toronto, Canada, June 2012 – Oral Presentation

Afşar N, Özgür E, **Gürgan M**, Yücel M, Gündüz U, Eroglu I. Hydrogen productivity of different photosynthetic bacteria on dark fermenter effluents. 10th International Conference on Clean Energy, Famagusta, North Cyprus Turkish Republic, September 2010 – Oral Presentation

Özgür E, Uyar B, **Gürgan M**, Yücel M. Hydrogen production by hup- mutant and wild type strains of *Rhodobacter capsulatus* on dark fermenter effluent of sugar beet thick juice in batch and continuous photobioreactors. World Hydrogen Energy Congress, Essen, Germany, May 2010 – Oral Presentation

Öztürk Y, Gökçe A, **Gürgan M**, Yücel M. Improving hydrogen producing capacity of *Rhodobacter capsulatus* by genetically modifying redox balancing pathways. World Hydrogen Energy Congress, Essen, Germany, May 2010 – Oral Presentation

Afşar N, Özgür E, **Gürgan M**, de Vrije T, Yücel M, Gündüz U, Eroglu I. Hydrogen production by *Rhodobacter capsulatus* on dark fermenter effluent of potato steam peel hydrolysate. 12th International Conference on Process Integration, Modelling and Optimization for Energy Saving and Pollution Reduction, Rome, Italy, May 2009 – Oral Presentation

PROJECTS

METU Bap Project 07.02.2010.00.01.

METU Bap Project 07-02-2013-005.

MEMBERSHIPS

Türkiye Hidrojen Enerjisi Derneği

COMPUTER SKILLS

Microsoft Office Applications (Word, Excel, Powerpoint), Minitab, R, GCOS, GeneSpring, Internet Applications

LANGUAGES

Turkish: Native Language

English: Fluent

German: Medium